Investigation into the use of carbon nanotubes networks as gate electrodes in field-effect gas sensors with increased functionality

By

Xu Cao

A Thesis submitted in partial fulfilment of the requirements of the Degree of Doctor of Philosophy in School of Engineering and Materials Science, Queen Mary, University of London

September 2013

Declaration

I declare that the work presented in this thesis is my own and has not been submitted at another institution other than Queen Mary, University of London.

Xu Cao

Abstract

Gas sensors based on different principles have been developed for the applications of environmental monitoring, industrial processing, aerospace and the human body. Carbon nanotubes (CNTs) demonstrate a detectable electrical properties change upon gas molecules absorption. This has been extensively studied and used in chemiresistors and chemical field-effect transistors. Simultaneous response to different types of gases was reported. The aim of this study is to develop a new type of gas sensor by replacing the gate metal of a field-effect capacitor with a carbon nanotubes network. This novel sensor will combine resistivity measurements with potentiometric measurements, which should ideally lead to increased functionality and selectivity.

The substrates (Al/Si/SiO_2/Si_3N_4 or Al/Si/SiO_2/Si_3N_4/LaF_3) were fabricated with two gate electrode structures (interdigitated and two-line). CNTs in different solvents were drop or spray coated on to the substrates. Platinum coating on the CNTs was also introduced. The resistive measurements indicated an increase in the resistance of CNTs networks with increased oxygen concentration, and a decrease in the resistance of CNTs networks with increased hydrogen concentration with humidity interference. Evenly distributed CNTs film was achieved by spray coating which allowed the use of CNTs network as gate materials for potentiometric measurements. The potentiometric measurements suggested that the C-V curve shifted towards a lower voltage with an increased hydrogen concentration, and a higher voltage with an increased oxygen concentration. However, the response time was too long for practical applications. Pt deposition significantly improved the hydrogen response rate. A voltage shift of -450 mV with an equilibration time of 2 minutes was achieved when the hydrogen concentration increased from 1 to 100%. The C-V curve shifted by 500 mV with increased oxygen concentration (1-100%).

TABLE OF CONTENT

LIST OF TABLE

LIST OF FIGURES

Acknowledgements

I would like to thank my first supervisor Dr. S. Krause for her supervision and inspiration. Without her advice and guidance, the project would not have happened. Secondly, I would like to acknowledge my second supervisor Dr. M. Baxendale for his advice and providing the access to the facilities in Physics Department.

I am very grateful to Dr. C. J. Morgan in Physics Department for his assistance and cheerful collaboration. I would also like to express my acknowledgements to Dr. W. Moritz for his expertise on the LaF_3 coating. Acknowledgments were also addressed to Dr. Y. Zhou and Dr. L. Chen for their discussion on the project.

Finally, I would like to take this opportunity to thank my parents and my wife for their love and continuous support.

CHAPTER 1

INTRODUCTION AND HISTORY

Gas sensors are of tremendous interest in different fields for the detection of the presence of gases. Effectively sense gas molecules, such as oxygen (O_2), hydrogen (H_2) and carbon dioxide (CO_2) etc, and detect their level in the environment are crucial for pollutions level monitoring, industrial chemical processes control, space missions, agricultural and medical applications. The gas sensing process is normally achieved by the adsorption and desorption of gas molecules on a sensing materials. An ideal gas sensor should demonstrate high sensitivity and selectivity with reproducible results, fast response time (i.e., the time from sample introduction to signal stabilisation) and recovery time, low analyte consumption, low operating temperature and less temperature dependence (Wang and Yeow, 2009). Furthermore, a reduced dimension will also be beneficial in terms of portability. A wide range of materials have been investigated over the last two decades, however, limited sensitivity has been reported. Therefore, materials with high sensitivity and selectivity are highly demanded.

Hydrogen sensitive field-effect device research started in the 1970s (Lundström *et al.*, 1975). Discontinuous catalytic films showed response to CO, NO_x and NH_3 at elevated temperatures (Zubkans *et al.*, 1995, Spetz *et al.*, 2001). In these cases, the potential forming reaction took place at the three-phase boundary (metal-insulator-gas boundary). Adsorption and charge separation at the metal-insulator-gas interface led to concentration dependent potential changes. The morphology of the three-phase boundary and the catalytic activity of gate metal and underlying insulator have significant impacts on the gas sensor selectivity and the response kinetics. The introduction of porous metal gate on the gas sensitive field-effect device led to the possibility of detecting different gases (Zubkans *et al.*, 1995).

Carbon nanotubes (CNTs) discovered by Iijima (1991), have an unique geometry with a high aspect ratio. They are chiral in structure with either one single outer wall (named single-walled carbon nanotube, SWNT) (Iijima and Ichihashi, 1993) or multiple concentrically nestled walls (multi-walled carbon nanotube, MWNT) (Saito *et al.*, 1992) (Fig. 1). Compared with other gate metals, CNTs show a larger specific surface area, which allow the formation of a large and well defined three-phase-boundary. These properties are expected to result in a more stable and reproducible sensor signal and faster response of the structures to the target analytes.

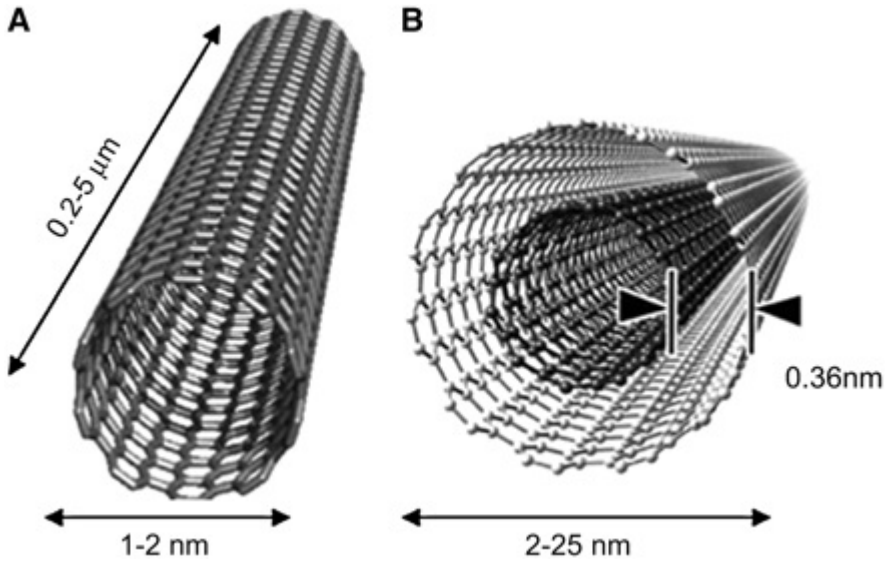

Fig. 1 Conceptual diagram of single wall carbon nanotube (SWCNT) (A) and multi-wall carbon nanotube (MWCNT) (B) (Hirsch, 2002, Iijima, 2002)

The first chemical sensor based on CNTs was invented by Kong (2000). When exposed to gas molecules, the resistance change of the sensors was attributed to the charge transfer between the molecules and the CNTs. For inert gases such as N_2 and He, where the charge transfer between molecules and the CNTs is negligible, the signals were considered to be attributed to the change in the electron and hole free carries lifetimes. CNT-based sensors are advantageous when compared with traditional sensors. It is well reported that CNT-based

sensors demonstrate effective analyte sensitivity at room temperature. They are therefore less temperature fluctuation dependent. The room temperature operation also leads to low power consumption of the device, and contributes to less sensitivity toward the thermally induced drift and longer sensor battery life.

The CNT-based sensors have been used for the detection of NO_2, NH_3 (Kong *et al.*, 2000), O_2 (Collins *et al.*, 2000), alcohol vapour (Someya *et al.*, 2003) and other gases. It was noticed that bare CNTs do not show appreciable sensitivity to H_2; therefore attempts were made to decorate the CNTs for improved sensor sensitivity and selectivity. Pt, Pd particles and metal oxide were employed to create a spillover effect at the metal nanoparticles. Some successful CNT-based sensors for environmental applications are summarised in Table 1. However, the selectivity is limited unless an array of CNTs with different compositions is used.

It is also noticed that CNT-based sensors are sensitive to water, and thus suffer from the potential interference from the relative humidity at room temperature. Different types of humidity CNT-based sensors were designed over the last few years.

Table 1: Summary of some successful CNT-based sensors and their sensing abilities

Analyte	Precaution Concentration	Current Successful Sensors	
		Sensor CNT Materials	Detection Limits
NO_2	21 ppb, long-term exposure may decrease lung function and increase the risk of respiratory symptoms	Bare CNTs	10 ppb (Santucci *et al.*, 2003)
		Metal decorated CNTs	100 ppb (Star *et al.*, 2006b)
		Metal oxide decorate CNTs	100 ppb (Sharma *et al.*, 2012)
NH_3	25 ppm, Health and Safety (HSE)	Bare CNTs	5 ppm (Quang *et al.*, 2006)
	Potential risk of lung damage and death when exposure to high concentration of NH_3.	Metal decorated CNTs	250 ppb (Lee *et al.*, 2013)
		Metal oxide decorated CNTs	5 ppm (Bittencourt *et al.*, 2006, Hoa *et al.*, 2007)
H_2	4% (LEL)	Pd-decorated CNTs	10 ppm (Star *et al.*, 2006b, Wong *et al.*, 2003b)
		Pt-decorated CNTs	0.4% (Kaniyoor *et al.*, 2009a)
CH_4	Lower Explosive limit (LEL) 5%	Metal-decorated CNTs	6 ppm (Star *et al.*, 2006b, Lu *et al.*, 2004b)
CO	30 ppm HSE	Bare CNTs	100 ppm
		Metal decorated CNTs	5 ppm (La *et al.*, 2011)
		Metal oxide decorated CNTs	10 ppm (Bittencourt *et al.*, 2006, Leghrib *et al.*, 2010b)
		Automatically doped CNTs	(Peng and Cho, 2003)
SO_2	5ppm, permissible exposure limit (PEL) by Occupational Safety and Health Administration (OSHA)	Bare CNTs	10 ppm (Goldoni *et al.*, 2003, Goldoni *et al.*, 2004)
H_2S	10 ppm PEL	Metal decorated CNTs	3 ppb (Mubeen *et al.*, 2009)
O_2	19.5-23.5%	CNT SAW sensor	1500 ppm (Chopra *et al.*, 2003, Picaud *et al.*, 2005)

Aims

The aim of the thesis was to develop a novel gas sensor which combines the field-effect gas sensor and carbon nanotubes gas sensor by replacing the gate metal of the field-effect gas sensor with carbon nanotubes networks.

Compared with other gate metals, carbon nanotubes networks could provide higher catalytic activity and a large specific surface area for the target gas sensor. The increased catalytic activity elevates the gas detection of the gas sensor, thus, more gases could be detected. The increased specific surface area could allow the formation of larger well defined three-phase-boundaries, which consequently reduce the response time and provide reliable signals. The different functionalities of both field-effect gas sensors and carbon nanotube gas sensor should provide a characteristic fingerprint response to target gases and potential interferents. The combination of these two measurement principles was expected to achieve a higher level of gas selectivity and sensitivity, which would otherwise not be achieved by a single sensor.

Two gold electrodes were patterned on the gate area of the field-effect capacitor (Fig. 2) to facilitate the resistance measurements. Carbon nanotubes were deposited on the substrate to bridge the two gold electrodes. In order to ensure that the potentiometric sensor response of the field-effect capacitor was dominated by the carbon nanotubes, the gold electrodes were designed to occupy a smaller proportion of the gate area compared with the carbon nanotubes network.

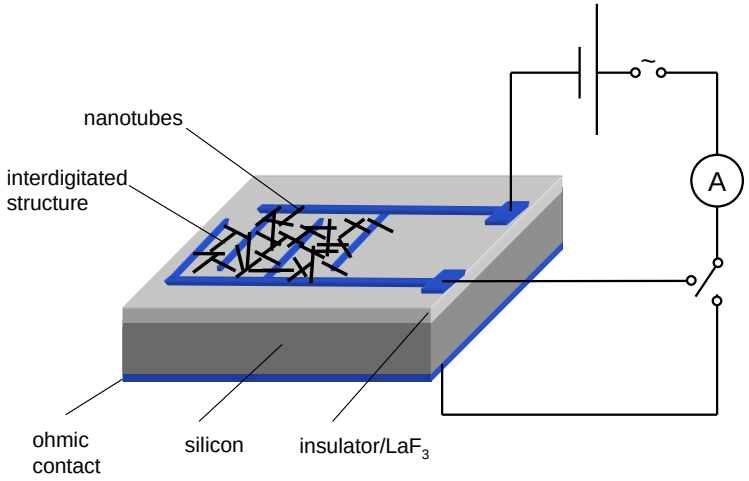

Fig. 2 Schematic of a gas sensor (combination of field effect gas sensor and carbon nanotube gas sensor)

Field-effect capacitors with $Si/SiO_2/Si_3N_4/CNTs$ and $Si/SiO_2/Si_3N_4/LaF_3/CNTs$ structures were fabricated. LaF_3 was previously used to enhance the response of field-effect capacitors. With the added catalytic activity of the ionic conductor LaF_3, the possibility of achieving faster response times and different sensitivities of the sensor structure to the target analytes was investigated. The sensitivity and selectivity can also be improved by modified CNTs surface. Pt was deposited on the CNTs to increase their affinity for the gases.

Structure of the Thesis

This thesis has been organised in a classical way. Chapter 1 gives a brief introduction and history of gas sensor, their current application and limitation, which leads to my aim of the thesis. Chapter 2 of my thesis focus on the literature review (the principle of field-effect capacitor, field-effect capacitor gas sensor applications, carbon nanobutes and the application of the carbon nanotubes gas sensors).

Silicon substrates with different gold electrode structures were prepared first. Based on the substrates, different types of carbon nanotubes, different coating methods, and different modifications of carbon nanotubes were investigated to explore the possibility of combining/creating a field-effect gas sensor and carbon nanotubes gas sensor.

Therefore, the experimental design, instrument and how the experimental specimen preparation was undertaken in Chapter 3. How the experiments were carried out is described in chapter 4 followed by the results and discussion. A summary of project conclusions are stated in Chapter 5. The future work of developing this field-effect capacitive gas sensor with CNTs as gate materials is talked about in Chapter 6. References used in this thesis were listed in Chapter 7 using Harvard reference style.

CHAPTER 2

LITERATURE REVIEW

2.1 Field-effect Capacitor

2.1.1 Structure of a Field-effect Capacitor

A field-effect capacitor is a capacitor in which the effective dielectric is a region of semiconductor material that has been depleted or inverted by a field-effect. It is based on a metal/insulator/semiconductor (MIS) structure, which represents a type of potentiometric sensor. The field-effect capacitors are promising since they can be used for arrays of sensors with different catalytic gate metals, different metal structures (porous or non-porous) and under different operation temperatures.

A typical field-effect capacitor consisting of a four layer sandwich structure: metal, insulator, semiconductor and ohmic contact as illustrated in Fig. 3. The metal on the top of the structure is the sensitive material in the gas sensing capacitive device. The sensitivity of the gas sensor depends on the activity of the metal. This gate material was first made with continuous Pd for hydrogen detection (Lundström et al., 1975). More choices of gate materials were developed with over the last 3 decades. $NaNO_2$-based solid electrolyte layer was selected as the gate material to detect NO_2 (Zamani et al., 2005). La_2O_3 was used to for a room temperature CO_2 sensor (Jinesh et al., 2011).

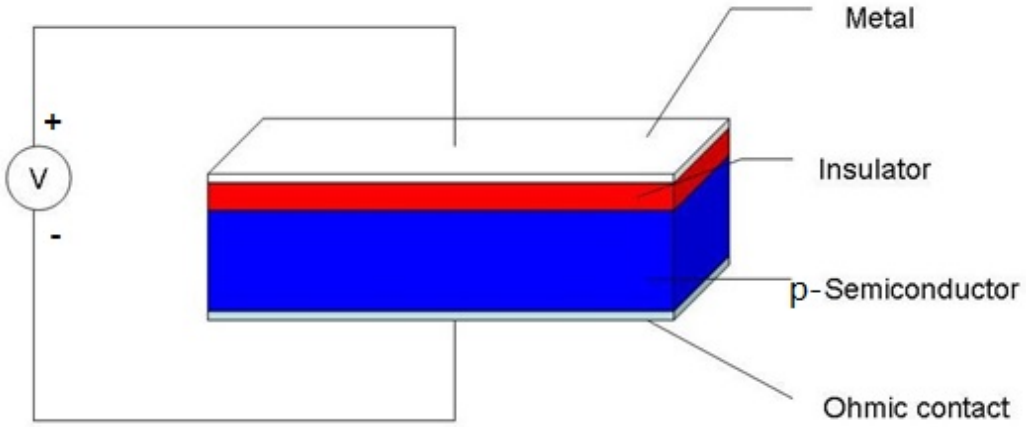

Fig. 3 Schematic of metal/insulator/semiconductor (MIS) structure

2.1.2 Principle of a Field-effect Capacitor

The properties of field-effect capacitors can be controlled via the DC voltage applied between metal gate and ohmic contact. There are three different modes in which the field-effect capacitors can be operated: accumulation, depletion and inversion.

Take a p-type semiconductor as an example (Fig. 4): Accumulation occurs when a voltage smaller than the flatband voltage is applied to the gate. Charge on the gate attracts holes from the substrate to the insulator-semiconductor interface. Depletion occurs when a more positive voltage than the flatband voltage is applied. Negative charge builds up in the semiconductor. The positive charge on the gate pushes the mobile holes into the substrate. Therefore, the semiconductor is depleted of mobile carriers at the interface. Due to the ionised acceptor ions, the negative charge is left in the space charge region. Inversion occurs when voltage applied is beyond the threshold voltage. In inversion, there

is a negatively charged inversion layer at the oxide-semiconductor interface in addition to the depletion layer. This inversion layer is due to minority carriers, which are attracted to the interface by the positive gate voltage.

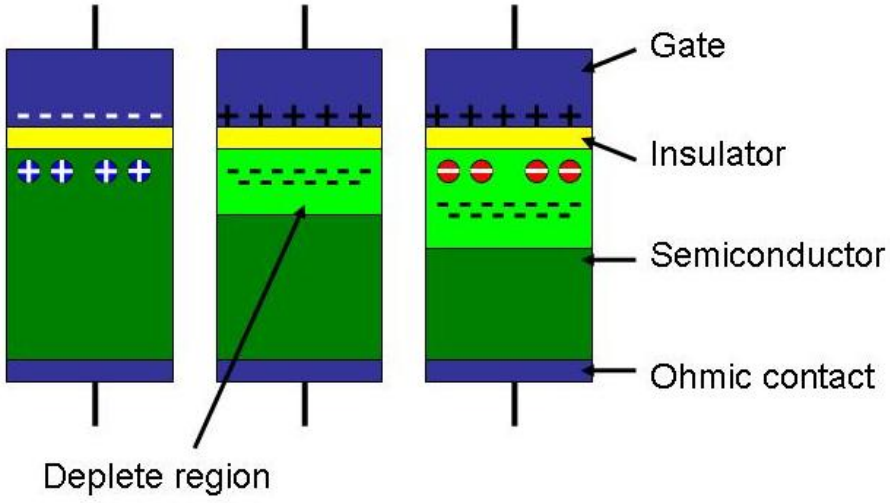

Fig. 4 Charges in a Metal-Oxide-Semiconductor structure under accumulation, depletion and inversion conditions

Capacitance voltage (C-V) measurements of MIS capacitors provide a wealth of information about the structure. C-V measurement is a frequency dependent measurement primarily in inversion because a certain time is required to generate the minority carriers in the inversion layer. The capacitance of the inversion region depends on the frequency of the applied signal. If the frequency is low enough, the electrons can therefore be generated by thermal generation and then the capacitance is very large. If the frequency is too high, the electron concentration might remain fixed at the average value, thereby, the capacitance depends on capacitance of depletion region. A typical high-frequency C-V curve is given in Fig. 5.

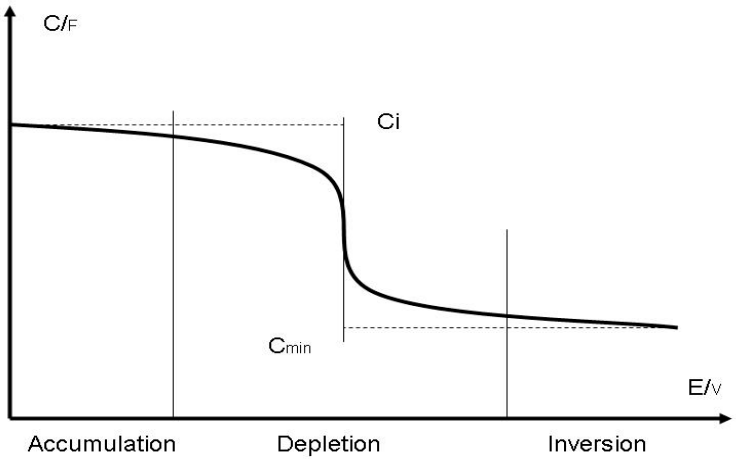

Fig. 5 High-frequency Capacitance-Voltage Curve

A MIS structure appears like two parallel-plate capacitors connected in series (Fig. 6): fixed capacitor (insulator related) and variable capacitor (applied signal related; space charge region). The capacitance can be calculated in accumulation, depletion and inversion modes with different equations.

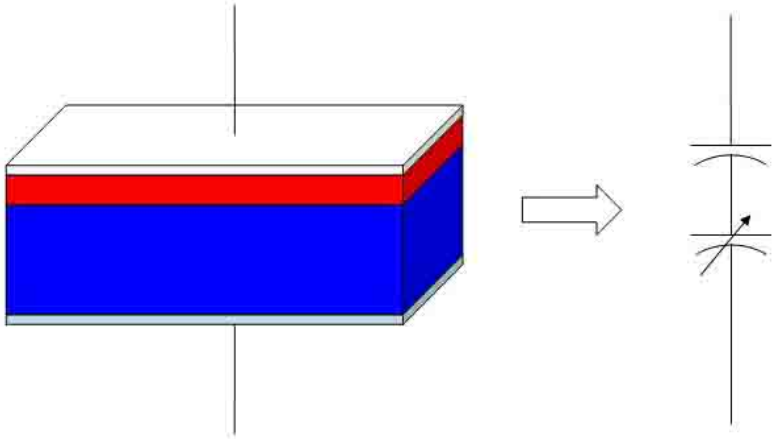

Fig. 6 MIS structure equals to two parallel-plate capacitors connected in series.

Accumulation

The MIS structure appears like a parallel plate capacitor. The properties are dominated by the insulator properties.

$$C = C_i = \frac{\varepsilon_i \times \varepsilon_0 \times A}{d} \tag{2.1}$$

Where C_i is the insulator capacitance (*Farad*), A is the area of capacitor area (cm^2), d is the thickness of the oxide layer (cm), ε_i is the dielectric constant of insulator and ε_0 is the permittivity in vacuum (F/cm).

Depletion

Positive voltage on the gate material pushes the mobile holes into the substrate. A depleted region left in the semiconductor next to the insulator which equals a variable capacitance C_d.

$$C_d = \frac{\varepsilon_s}{W_d} \tag{2.2}$$

Where ε_s is the semiconductor permittivity (F/cm), W_d is the width of the depletion layer (cm). The total capacitance can be expressed:

$$C = \frac{C_i \times C_d}{C_i + C_d} \tag{2.3}$$

Inversion

The depletion layer reaches a maximum width and remains constant for further increase in the applied bias voltage. The maximum depletion layer width can be calculated:

$$Wd_{\max} \approx \sqrt{\frac{4k_B T\varepsilon_s \ln(N_d/n_i)}{q^2 N_d}} \tag{2.4}$$

Where N_d is the donor impurity density (cm^{-3}), n_i is the intrinsic density (cm^{-3}) and T is the operation temperature (K). And the corresponding total capacitance is:

$$C_{\min} \approx \frac{\varepsilon_i}{d + (\varepsilon_i/\varepsilon_s)W_{d_{\max}}} \tag{2.5}$$

2.1.3 Applications of Field-effect Gas Sensors

Hydrogen sensitive Pd gate field-effect transistor was first reported by Lundstrom *et al.* (1975). Research on gas sensitive field-effect devices expanded in the 1980s. The principle, application and the characteristics of hydrogen sensitive Metal/Oxide/Semiconductor (MOS) structures were proposed by Lundstrom *et al.* (Lundstrom, 1981, Lundstrom and Soderberg, 1981). A dense catalytically active noble metal gate (Pd) could be used to detect hydrogen (Fig. 7). The hydrogen atoms emanated from dissociated hydrogen molecules on the Pd surface at an elevated temperature (around 150ºC). The atoms diffused through the Pd film and adsorbed at the Pd-SiO_2 interface to form a dipole layer. The dipole layer gave an abrupt potential change in the structure which is referred to a voltage change (ΔV) on the C-V curve.

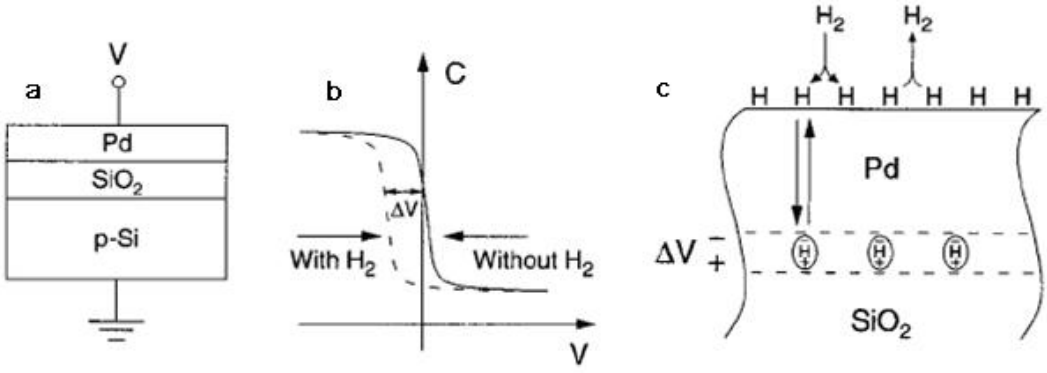

Fig. 7 (a), a Pd/SiO_2/p-Si field-effect structure, (b), a shift in voltage, ΔV, was observed in C-V curve when H_2 was present, (c), hydrogen atoms diffused through the Pd film and adsorbed at the Pd-SiO_2 interface (Lundstrom *et al.*, 1989).

Some other hydrogen-containing molecules (alcohols, hydrogen sulphide, ethylene and acetylene) can also be detected use the Pd-gate device. These molecules are dehydrogenated on the Pd surface in such a way that hydrogen atoms are released and transferred through the metal to the interface. The dehydrogenation is temperature dependent. When operating at different

temperatures, different molecules could be detected, which provides levels of selectivity of the device.

Ammonia was also successfully detected (Danielsson *et al.*, 1979). A large sensitivity was reported with a discontinuous thin (<10 nm) gate structure, but no sensitivity on a thick (>100 nm) gate structure (Winquist *et al.*, 1983, Spetz *et al.*, 1988) was reported. However, it was suggested that the detection of ammonia was based on a different mechanism. The molecules were dissociated at the borders between the catalytic gate and the insulator. Adsorption and charge separation at the gate-insulator-gas interface gave rise to concentration dependent potential changes. These thin discontinuous gates can detect all kinds of molecules that give rise to polarisation in the thin metal film.

Oxygen, fluorine and hydrogen fluoride were detected at room temperature by using a Pt/LaF_3/Si_3N_4/SiO_2/Si semiconductor field-effect structure (Miura *et al.*, 1989, Krause *et al.*, 1992, Moritz *et al.*, 1999). However, an ageing effect was observed a few days after the preparation of the Pt layer. The response rate was related to the age of the LaF_3 layer. A thermal treatment (above 160ºC) was proven to effectively reactivate the sensor (Moritz *et al.*, 2001). The mechanism of ageing and reactivation was investigated as well. It was shown that the adsorption and desorption of very small amounts of CO_2 determined the dynamic behaviour of the sensor.

A dual mode hydrogen sensor was developed by using Pd/AlN/SiC (Rahman *et al.*, 2008), which operated as a rectifying diode or a capacitor. This dual behaviour is attributed to the AlN layer which due to its large band gap value can act in a capacitive mode but also act in a diode current mode due to the presence of a small concentration of shallow donors.

2.1.4 Enhancement of Field-effect Capacitor Gas Sensor

The morphology of the three-phase boundary, the catalytic activity of gate materials, and underlying insulator are three key factors for sensor selectivity, sensitivity and the response time.

Morphology:

The dependence of the gas response on the morphology of the gate materials has been reported with the help of a scanning light pulse technique (SLPT) (Lofdahl *et al.*, 2001). The local gas response at different points of the gate area can be measured by SLPT. Only the surface layer is affected during the reactions, the sensitivity is therefore strongly dependent on the surface-to-volume ratio of the material used.

Catalytic activity of the gate materials:

The mechanism of the field-effect capacitor gas sensor is based on the reaction of the gate materials, gas and insulator. Therefore, the selection and the activity of the gate materials could have a direct impact on the sensitivity of the sensor. Different types of gate materials have been used in the literature for the detection of various gases. A brief summary was given out in Table 2.

Table 2: Gate materials use in field-effect capacitor gas sensors

Gate Materials	Application	Detection Limit
Pt	CO (Samman *et al.*, 2000).	100 ppm
Pt-SnO_x	O_2 and CO gases was also reported (Kang and Kim, 1994)	
Ir/Pd	NH_3 (Winquist *et al.*, 1984)	1 ppm
Pd	H_2 (Lundström *et al.*, 1975)	10 ppm
Ru/RuO_2	H_2,CO,C_3H_6 and NH_3 (A. Salomonsson, 2005)	

Underlying insulator:

Sensitivities for different gases and short response times at room temperature were achieved by introducing the ion conductor LaF_3 into field-effect capacitors (Krause *et al.*, 1992). $Si/SiO_2/Si_3N_4/LaF_3$/metal structures were found to be responsive to oxygen, hydrogen, hydrofluoric acid and fluorine. The increased activity of the LaF_3-metal-gas boundary is caused by the ability of LaF_3 to absorb and therefore stabilise a variety of oxygen and fluorine containing species such as hydroxide ions, peroxide, fluoride ions and carbon dioxide. This would allow the gas sensor operate with a low energy cost, and also reduce the size of the device.

2.2 Carbon Nanotubes

2.2.1 Fundamentals of Carbon Nanotubes

C_{60} and other fullerenes have stimulated intense interest in the structures accessible to graphitic carbon sheets (Kroto *et al.*, 1985). The earliest reports of tubular carbon structures was published in 1955 (Hofer *et al.*). CNTs were imaged even earlier during studying deposits in blast furnaces in the Potteries (Davis *et al.*, 1953), however they were recognised as carbon vermicules instead of tubular. Clear images of pristine carbon nanotubes (CNTs) were first published by Oberlin *et al.,* (1976) as shown in Fig. 8. Despite the early knowledge of CNTs, the interest of CNTs was exploded after the Nature paper by Lijima (1991). CNTs were discovered from a cathode by a carbon-arc discharge method similar to the one used for fullerenes preparation.

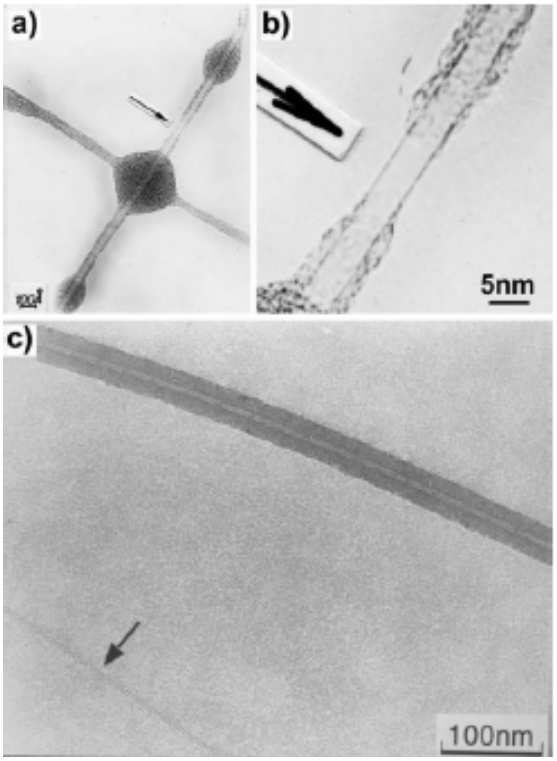

Fig. 8 Carbon nanotubes imaged in 1976 (Oberlin *et al.*)

The structure of CNT is cylindrical rolled hexagonal carbon network with two ends capped with pentagonal carbon structures (Fig. 9). CNTs are allotropes of carbon with a nanostructure that can have a length-to-diameter ratio greater than 10,000,000 and as high as 132,000,000 (Wang *et al.*, 2009). There are two types of carbon nanotubes named after their structure, single-walled and multi-walled. The structure of a single-walled carbon nanotube (SWNT) can be conceptualised by wrapping one layer of graphite into a cylinder. Multi-walled nanotubes (MWNTs) consist of multiple layers of graphite. Two different models are commonly used to describe the structures of multi-walled nanotubes. In the Russian Doll model, sheets of graphite are arranged in concentric cylinders. In the Parchment model, a single sheet of graphite is rolled in around itself.

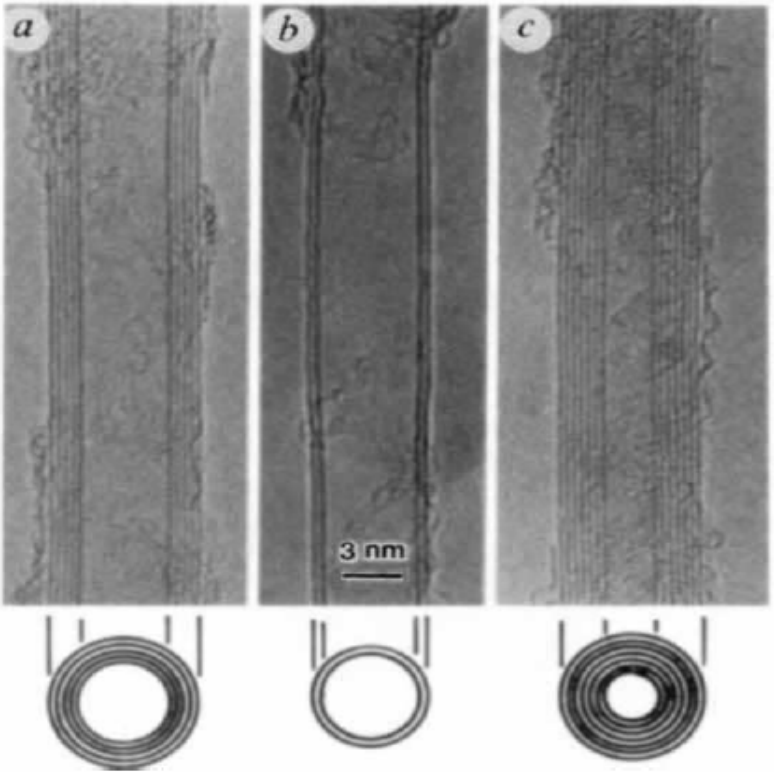

Fig. 9 (a). Tube consisting of five graphitic sheets, diameter 6.7 nm. (b). Two-sheet tube, diameter 5.5 nm. (c). Seven-sheet tube, diameter 6.5 nm, diameter 2.2 nm (Iijima, 1991)

Single-walled carbon nanotube (SWNTs) is normally a few nanometres in diameter, and could be up to several centimetres in length (Kanzow *et al.*, 2001). In contrast, the multi-walled carbon nanotubes have a relative larger diameter (10 - 40 nm) (Chopra *et al.*, 2002). The bonding of CNTs is composed of sp^2 bonds. This bonding structure provides the molecules with a unique strength. CNTs are the strongest and stiffest materials yet discovered in terms of tensile strength and elastic modulus. A Young's modulus of 1.47 TPa and a tensile strength of SWNT of 100 GPa were reported (Peng *et al.*, 2008, Wong *et al.*, 1997, Falvo *et al.*, 1997, Krishnan *et al.*, 1997, Demczyk *et al.*, 2002). Nanotubes naturally align themselves into "ropes" by Van der Waals forces. Under high pressure, nanotubes can merge together, trading some sp^2 bonds for sp^3 bonds. This makes it very difficult to separate CNTs to individual tubes.

Because of the symmetry and unique electronic structure of graphene, the structure of a SWNT has a strong influence on its electrical properties. The electronic properties of carbon nanotubes depend on their diameter and helicity (Saito *et al.*, 1992). The chirality and the fibre diameter are uniquely specified by the vector c_h.

$$c_h = na_1 + ma_2 \tag{2.6}$$

Where n and m are integer; a_1 and a_2 are the unit vectors of graphite as shown in Fig. 10. Carbon nanotube with given n and m value, the nanotube is metallic when $2n + m = 3q$ (where q is an integer); otherwise, the nanotube is a semiconductor. Therefore, all armchair nanotubes ($n = m$) are metallic, and nanotubes (5, 0), (6, 4), (9, 1) etc. are semiconducting. Alternatively, this could be described as the SWNT is metallic when ($(n - m)/3$ = integer. Theoretically,

metallic nanotubes can have an electrical current density more than 1,000 times stronger than metals such as silver and copper.

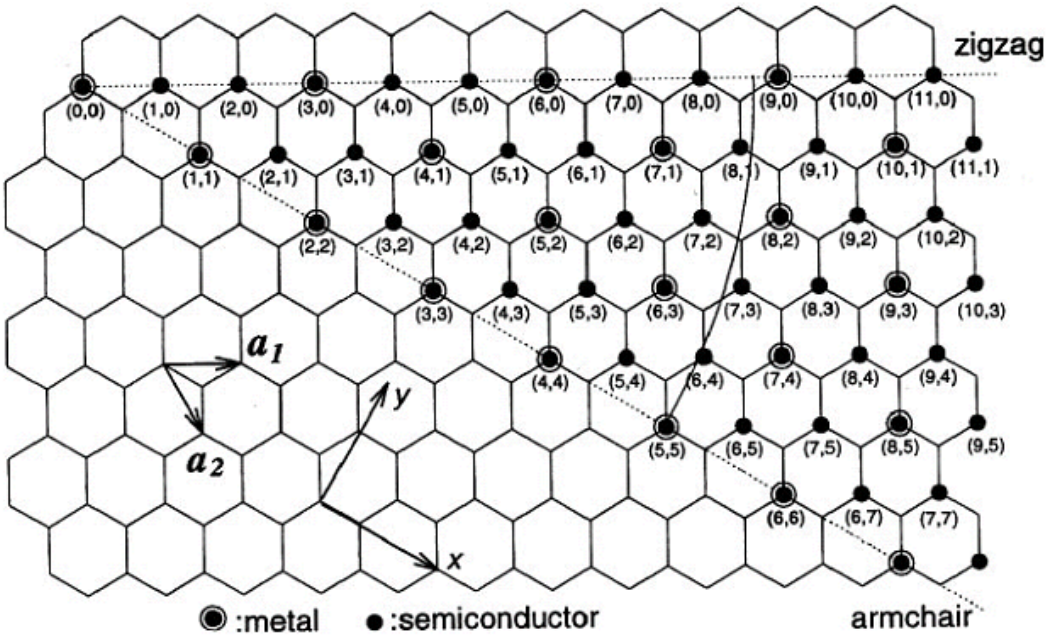

Fig. 10 Schematic of the electrical properties estimation on graphite cylinder (Dresselhaus *et al.*, 1992)

Graphite tubules appear like cylinders which were rolled from a graphite sheet. The tubules can be identified by their lattice vectors c_h. The chiral angle is denoted by θ, while a_1 and a_2, denote the unit vectors of graphite. Possible vectors for chiral fibres. The circled dots and dots, respectively, denote metallic and semiconducting behaviour for each fibre. Measurements of conductivities in nanotubes also showed p-type (hole conducting) behaviour in semiconducting nanotubes. This was attributed to Shottky barriers with metallic contacts or adsorption of oxygen onto the tube walls or the junctions with the contacts (Tans *et al.*, 1998, Martel *et al.*, 1998).

2.2.2 Synthesis of Carbon Nanotubes

High-energy lasers (Guo *et al.*, 1995b), arc-discharge (Iijima, 1991) and chemical vapour deposition (Joseyacaman *et al.*, 1993) were widely used for carbon nanotubes synthesis.

High-energy laser

A high power laser (YAG type) has been used to vaporise the pure graphite targets at 1200ºC in an argon atmosphere (Fig. 11). The multi-walled carbon nanotubes can be produced in a cooled collector (Guo *et al.*, 1995a). The single wall carbon nanotubes can also be produced by adding some metal particles as catalysts (Thess *et al.*, 1996).

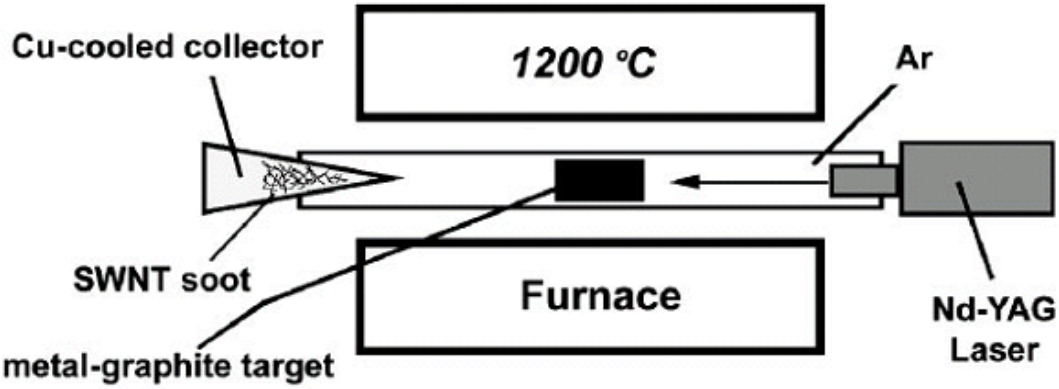

Fig. 11 The production of single wall carbon nanotubes using laser technique (Terrones, 2003)

Arc-discharge

Two high-purity graphite electrodes were kept apart with a distance of 1-2 mm. The arc was produced by passing a direct current (80-100 A) in a He atmosphere. Deposit formed at a rate of 1 mm/min on the cathode and the anode was consumed during arcing. Multi-walled carbon nanotubes were produced in the deposit (Ebbesen and Ajayan, 1992). Just one year later, single wall carbon nanotubes was produced by arcing graphite electrodes with metal

catalyst in the methane and argon atmosphere (Iijima and Ichihashi, 1993). Nowadays single wall carbon nanotubes can also be produced by different metals catalyst such as Gd (Subramoney *et al.*, 1993), Co-Pt (Lambert *et al.*, 1994), Co-Ru (Lambert *et al.*, 1994), Co (Ajayan *et al.*, 1993), Ni-Y (Journet *et al.*, 1997), Ph-Pt (Saito *et al.*, 1998b) and Co-Ni-Fe-Ce (Huang *et al.*, 2001).

Chemical vapour deposition

The growth mechanism of carbon nanotubes by the chemical vapour deposition technique is still not clear. The decomposition of C_2H_2 on the top of the catalytic surface creates H and C species. Three possible mechanisms have been reported:

1. Top carbon diffusion through catalytic particles (Baker and Chludzinski, 1980)

2. Top carbon diffusion on catalytic particles (Baird *et al.*, 1974)

3. Bottom carbon diffusion through catalytic particles (Baker *et al.*, 1973)

In general, chemical vapour deposition (CVD) results in MWNTs or poor quality SWNTs. The SWNTs produced with CVD have a large diameter range, which was difficult to control. But on the other hand, this method is very easy to scale up, which favours commercial production.

2.2.3 Reactivity of Carbon Nanotubes

Consider the interrelation between the two most stable fullerenes C_{60} and C_{70}. C_{70} is made of C_{60} by adding one row of five armchair hexagons along the equator normal to a fivefold axis. This suggests adding instead j such rows of armchair hexagons to obtain a C_{60} + 10j molecule which would be in the form of a monolayer graphite tubule. Similarly, by cutting the C_{60} molecule in half, normal to a threefold axis along the zigzag edges, a perfect fit can be made to a one-atom-thick cylindrical sheath consisting of j rows of nine zigzag hexagons (zigzag fibre).

So the chemical reactivity of carbon nanotubes is in reality similar to that graphite tubule and fullerenes caps. Graphite tubule walls are not reactive, but their two fullerene caps are reactive. Some of functional groups such as -COOH, -OH and -C=O can be attached on the two caps of the carbon nanotubes. These groups are responsible for some chemical properties of the carbon nanotubes (Lin *et al.*, 2003, Wong *et al.*, 1998, Dai *et al.*, 2003).

There are some weak interactions between the graphite tubule such as hydrogen bonding, π-π stacking, electrostatic force, Van der Waals forces and hydrophobic interactions. They allow the walls of carbon nanotube to catch small molecules or bio chemically active molecules (Chen *et al.*, 2001). These kinds of abilities make carbon nanotubes available for wide range of sensor area such as gas sensors, electrochemical detectors and biosensors with immobilised biomolecules (Liu *et al.*, 2000).

2.2.4 Applications of Carbon Nanotubes Gas Sensors

Carbon nanotubes have been used in different areas including field emission sources (Saito *et al.*, 1998a, Baughman *et al.*, 2002, Sugie *et al.*, 2001, Yue *et al.*, 2002, Lee *et al.*, 2001, Zhao *et al.*, 2013), Li ion batteries (Zhao *et al.*, 2005a, Yoon and Park, 2013), electrochemical devices (He *et al.*, 2013), molecular sensors (Hilder *et al.*, 2012), hydrogen storage (Li *et al.*, 2011), scanning probe tips (Lee *et al.*, 2008a) and remove heavy metal from the waste water (Mubarak *et al.*, 2014).

The first gas sensor based on carbon nanotubes was invented by Kong *et al.,* (Kong *et al.*, 2000). A p-type transistor was built by using a semiconducting SWNT to bridge the two metal contacts on a SiO_2/Si substrate (Fig. 12). The conductance of p-type semiconducting SWNT was observed increased when exposed to NO_2 and decreased with exposure to NH_3 with air as the carrier gas. Exposure to NO_2 resulted in a shift of the SWNT Fermi level towards the valence band, which created more conducting mobile holes. The increase of conducting mobile holes could therefore improve the conductance of SWNT. For the case of NH_3, exposed to NH_3 shifted the valence band of the nanotube away from the Fermi level, resulting in hole depletion and reduced conductance. The gas molecular sensing mechanisms for SWNTs also have been investigated by a number of experimental and theoretical groups (Peng and Cho, 2000, Chang *et al.*, 2001, Mercuri *et al.*, 2005, Zhang *et al.*, 2006a).

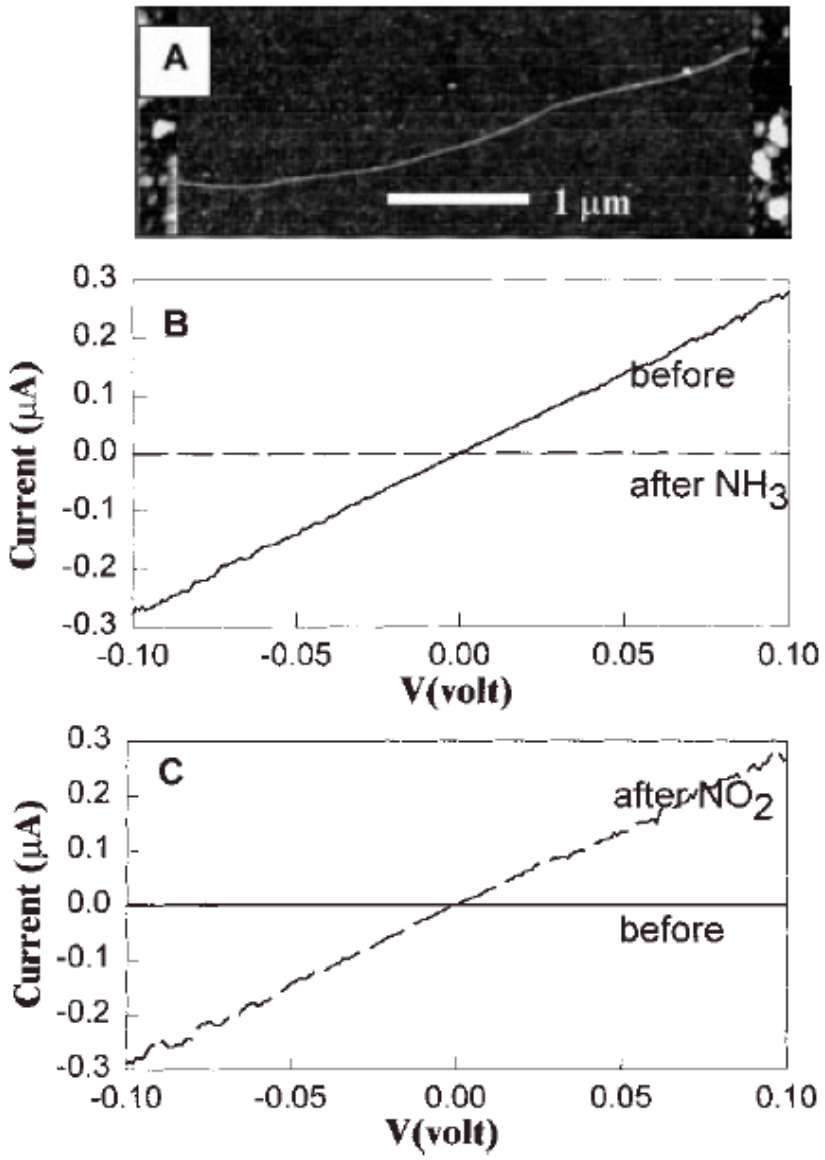

Fig. 12 Changes of electrical characteristics of a semiconducting SWNT in chemical environments. (A) Atomic force microscopy image of a metal/S-SWNT/metal sample used for the experiments. Nanotube diameter is 1.8 nm. The metal electrodes consist of 20 nm thick Ni, with 60 nm thick Au on top. (B) Current versus voltage curves recorded before and after exposure to NH_3. (C) Current versus voltage curves recorded under Vg= +4 V, before and after NO_2 exposure (Kong *et al.*, 2000).

The conductance of the SWNT sample increased sharply by about three orders of magnitude after 200 ppm of NO_2 was introduced. The response time increased when the NO_2 concentration was reduced, where 0.5 to 1 minute was

reported for 20 ppm NO_2 and 5 minutes for 2 ppm NO_2. When exposed to 1% NH_3, the conductance of the SWNT was observed to decrease 100-fold with a response time of 1 to 2 minutes. An increase response time of 10 minutes was noticed when the NH_3 concentration was reduced to 0.1%. Therefore, the sensing limit for this SWNT gas sensor within a 10 minutes detection time is 2 ppm for NO_2 and 0.1% for NH_3. Long-term exposure to NO_2 at concentration above 21 ppb or NH_3 at concentration above 25 ppm may decrease lung function and increase the risk of respiratory symptoms. Therefore, the improvement of sensitivity of the SWNT gas sensor was needed.

The change of the resistance of carbon nanotubes thin films was reported when exposed to NO_2 at an operating temperature of around 165 °C (Cantalini *et al.*, 2003, Valentini *et al.*, 2003). The detection limit was improved to around 10 ppb with this elevated operating temperature (Fig. 13). The thin films of carbon nanotubes prepared by plasma enhanced chemical vapour deposition indicated the potential of using CNTs as a material for NO_2 detection for environmental application.

The effect of contaminations of the carbon nanotubes has also been studied (Goldoni *et al.*, 2003). The experimental results indicated that the gas sensing property of CNTs were severely compromised by the presence of catalyst particles, contaminants, and defects coming from the purification procedure. The cleaned CNTs could be used as a gas sensing material capable of measuring environmentally significant levels of toxic molecules (<100 ppb) such as SO_2, NH_3, and NO_2.

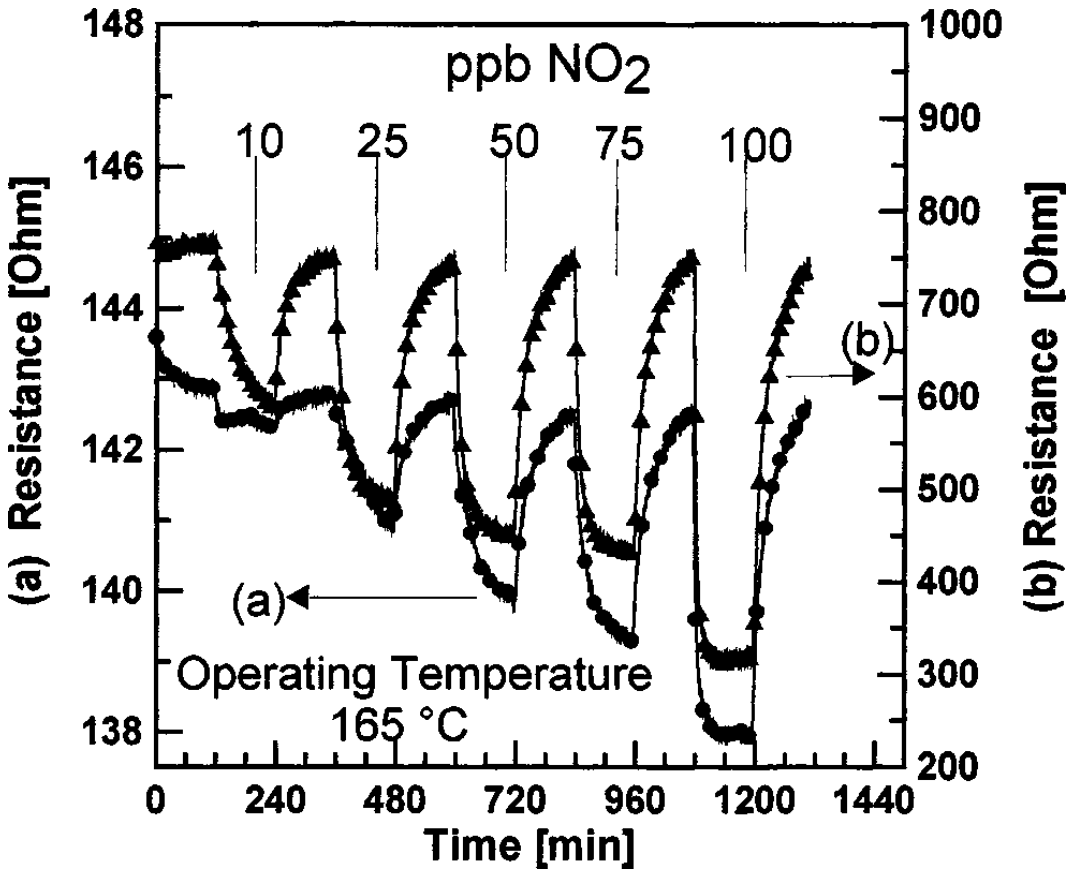

Fig. 13 Resistance changes at an operating temperature of 165°C and NO_2 concentrations ranging from 10 to 100 ppb. (a) resistance change of the film after the first thermal treatment; (b) resistance change of the film after the second thermal treatment (Cantalini *et al.*, 2003).

The sensitivity of bare SWNTs network was increased by heat treatment (Quang *et al.*, 2006). The sample was soaked in N_2 ambient for two hours with a temperature of 300 °C before the measurements. After saturated with N_2, the sample was cool down to room temperature, and exposed to NH_3 with N_2 as the carrier gas. The detection limit was improved to 5 ppm. The response of the sensor to NH_3 exposure was depicted in Fig. 14. The improved NH_3 sensor has a good detection limit (5 ppm) and responds time of 10 minutes. However, the activation procures for this improvement was not practical.

A MWNTs network based NH_3 gas sensor was fabricated by using positive DEP on a microelectrode array by Junta (Junya *et al.*, 2003). The proposed sensor achieved a rapid ppm level of sensitivity by impedance spectroscopy.

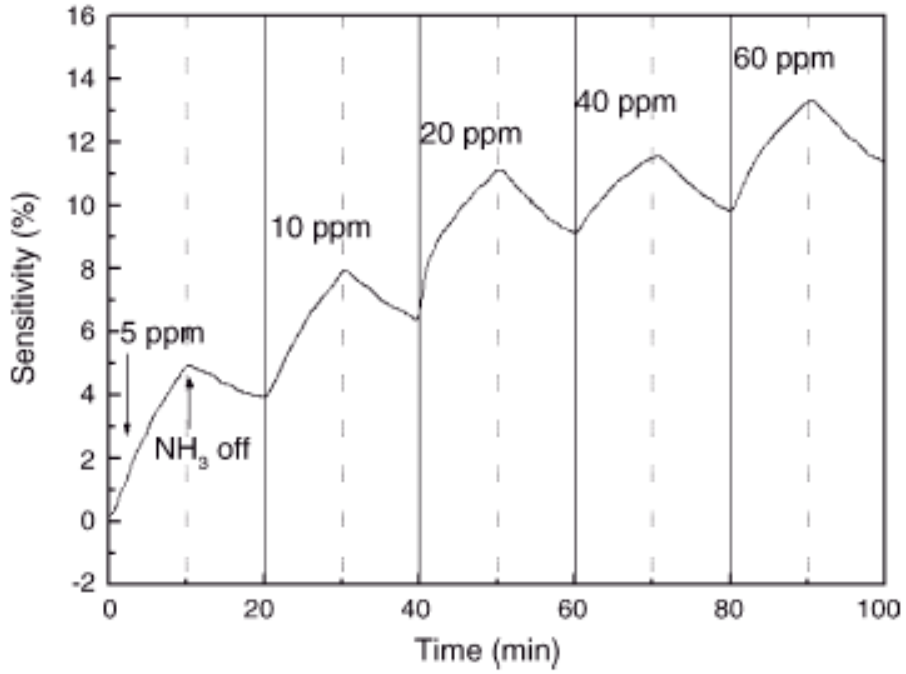

Fig. 14 Responds of SWNT sensor to various NH_3 concentrations at room temperature. At the concentration of 40 ppm, the sensor sensitivity seems smaller than the expected value (Quang *et al.*, 2006).

As a general comparison, conventional solid-state sensors for NO_2 and NH_3 operate at temperatures over 426.85 °C (Qin *et al.*, 2000, Sharma *et al.*, 1998), and polymer sensors have poor sensitivities and slow (10 minutes) response times (Miasik *et al.*, 1986). The resistive measurements of an individual CNT or CNTs network provide a better choice over metal-oxide sensors and polymer sensor.

The changes in the resistance of the CNTs network were also used for the detection of O_2 (Collins *et al.*, 2000, Huang *et al.*, 2009), SO2, NO (Goldoni *et al.*, 2004), organic vapour (Li *et al.*, 2003, Someya *et al.*, 2003) and inorganic vapour (Valentini et al., 2004).

Some functional materials were applied to the CNTs gas sensor in order to improve the sensitivity and selectivity. The materials were organic polymers,

bio-molecules or catalytic metal, metal-oxide and nanoparticles attached to the CNT sidewalls. These functional groups serve as sensing elements, exhibiting a broad range of electronic, chemical, physical and biological recognition properties that are often highly sensitive to changes in their chemical environment. CNTs are the support that is physically responsive to stimuli from the molecular world around these functional materials.

Modify CNTs with polymers and molecules

Polymer material is often used to improve the sensitivity and selectivity for the CNTs sensors. A high NO_2 sensitive SWNTs based gas sensor was fabricated (Qi *et al.*, 2003). SWNTs were synthesised by chemical vapour deposition (CVD) between metal electrodes of preformed metal (Mo) electrodes from patterned catalyst on a Si/SiO_2 substrate. Polyethyleneimine was applied onto SWNTs with immersion in a 20 wt % PEI/methanol solution for 2 hours. The functionalised CNTs based gas sensor responds to as low as 100 ppt of NO_2 at room temperature. The PEI coated CNTs based gas sensor showed no response when exposed to NH_3, which provide the ability to detect NO_2 without the interference of NH_3. They also demonstrated selective detection of NH_3 by using Nafion, which blocks certain types of molecules (NO_2) from reaching nanotubes.

The success of PEI coated CNTs draw some more interest to the modification of CNTs with gas sensing polymer to improve the sensitivity of the CNTs based gas sensor. The selectivity of CNTs based sensor can also be improved by using polymer to block the toxic gas under certain condition.

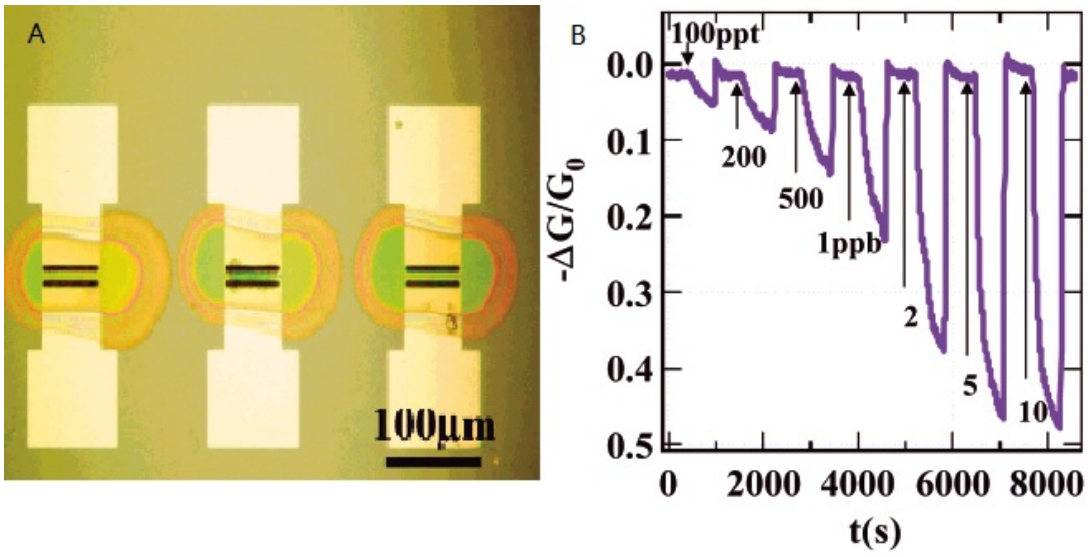

Fig. 15 A, Optical image CNTs based gas sensor. B, Change in conductance for the PEI functionalised device exposed to various concentrations of NO_2 gas.

Polyaniline (PANI) was widely used to improve the NH_3 sensitivity on CNTs based gas sensor (Zhang *et al.*, 2006b, He *et al.*, 2009, Chen *et al.*, 2012, Yoo *et al.*, 2009). A good detection limit as low as 50 ppb NH_3 was achieved by using polyaniline to functionalise the CNTs, which is the lowest NH_3 concentration yet detected at room temperature. Good reproducibility was also demonstrated.

The sensing properties of CNTs–porphyrin films were investigated (Penza *et al.*, 2011a). The presence of the porphyrin films increased the sensitivity of the CNTs based gas sensor to volatile compounds (acetone, methanol, ethyl acetate and tetrahydrofurane). Poly(o-anisidine) was deposited onto CNTs to detect inorganic vapour, charge was transferred with electron hopping, which affected the inter-tube conductivity through physically adsorbed polymers (Valentini *et al.*, 2004) and also resulted in increased sensitivity.

A gas sensor was synthesised through dielectrophoretic assembly of nanostructured layer of poly(3,4-ethylenedioxythiophene)/poly(styrenesulfonate) (PEDOT/PSS) matrix and O_2 plasma-treated SWNTs (Jian *et al.*, 2013). The gas

sensor showed high sensitive, selective, rapid, stable and reversible responses for detection of 2-300 ppm NH_3 and 6-1000 ppb trimethylamine gases at room temperature, suggesting its potential for assessing fish freshness in the fishery chain.

A room temperature CO_2 sensor was also proposed based on clad-etched Fiber Bragg Grating (FBG) with polyallylamine-amino-CNTs (Shivananju *et al.*, 2013). The detection range is between 1000 ppm and 4000 ppm with a limit of 75 ppm.

The application of polymer on the CNTs improved the gas sensitivity of CNTs based gas sensor. Furthermore, the selectivity of CNTs based sensor can be designed by appling different kind of polymer according to the testing eniorment. It gives the opportunity to detect the gases without some interference. However, the polymer coating applied on CNTs cannot operate at elevated temperature. The polymer coating was therefore unable be used under some harsh conditions.

Modify CNTs with metal

A lot work has been done to discover the sensing mechanism of the CNTs based gas sensor. Both theoretical (Zhao *et al.*, 2005b, Yeung *et al.*, 2008b) and experimental works (Larciprete *et al.*, 2007, Sayago *et al.*, 2007, Jennifer *et al.*, 2005, Kumar and Ramaprabhu, 2006, Mubeen *et al.*, 2007, Sun and Wang, 2007a, Lu *et al.*, 2004a, Young *et al.*, 2005, Star *et al.*, 2006a, Male *et al.*, 2004) indicated the molecule absorption ability of CNTs was linked to the metal elements in the CNTs. Compared with polymer modified CNTs gas sensor, the metal particles modified CNTs gas sensor are more stable. They could be used under harsher conditions.

Pd-functionalised SWNTs were studied as a gas sensor by several groups (Wong *et al.*, 2003a, Sayago *et al.*, 2007, Mubeen *et al.*, 2007). The gas sensor based on Pd/CNTs/n-Si was fabricated (Wong *et al.*, 2003a). MWNTs were grown on the highly doped n-Si substrate by MPECVD (Plasma-enhanced chemical vapour deposition). A thin film of palladium was selectively sputtered on the surface with a patterning mask (Fig. 16). They study showed that the H_2 sensing ability with the Pd decorated CNTs under wide operating temperature. However, they only demonstrated the H_2 sensitivity at a concentration of 100%.

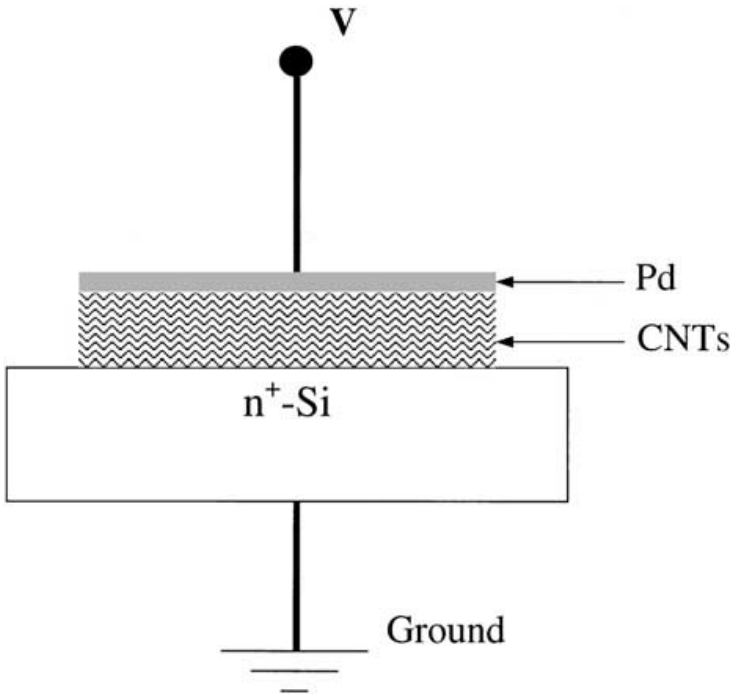

Fig. 16 Schematic diagram of the Pd/CNTs based gas sensor (Wong *et al.*, 2003b).

Pd nanoparticles were also used to functionalise CNTs to detect CH_4 (Lu *et al.*, 2004b). The Pd nanoparticles were sputtered on CNTs. The Pd loaded CNTs (1% wt) were then dispersed into solvent, and drop coated on the interdigitated electrodes. The CH_4 concentrations between 6 to 100 ppm were successfully detected at the room temperature. The hydrogen sensitivity of raw CNTs and Pd

sputtered CNTs (Fig. 17) was compared (Sayago *et al.*, 2005). Pd sputtered CNTs showed H_2 sensitivity (concentrations from 0.5% to 3 %) at room temperature. The temperature dependence on H_2 detection for raw SWNT sensor indicates H_2 sensing activity at temperatures higher than 200 °C.

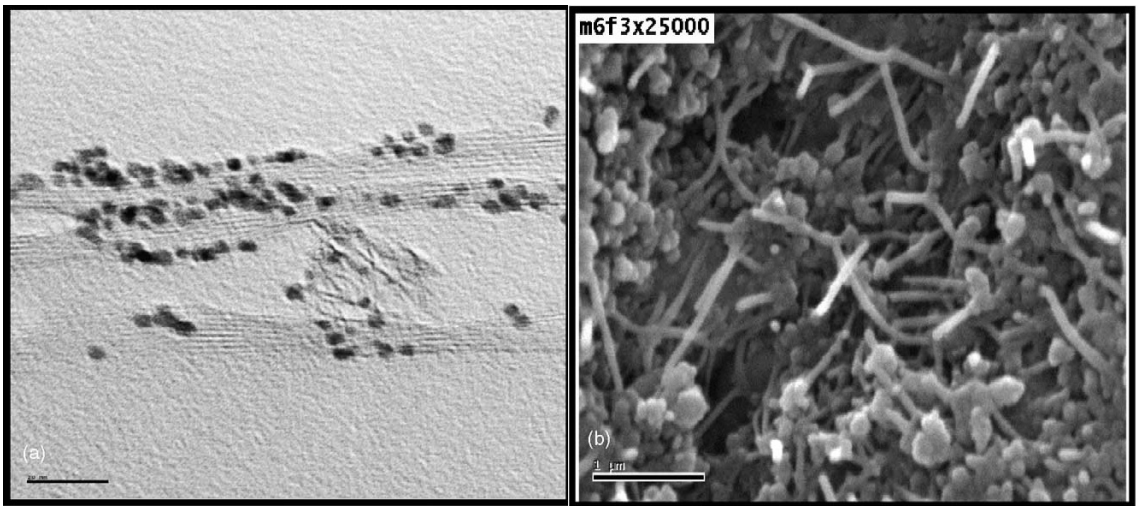

Fig. 17 (a) Transmission electron microscopy image of the SWNTs functionalised with Pd nanoparticles (scale bar 20 nm) and (b) scanning electron microscopy image of the SWNTs as-grown film prepared by the airbrush method (Sayago *et al.*, 2005).

Pd functionalised CNTs were prepared by sputter and thermal evaporation (Jennifer *et al.*, 2005). Both cases had good sensitivity to H_2 but the evaporated films exhibited a more rapid response and recovery. The thermal evaporation loaded sample could detect H_2 to a level of 10 ppm at room temperature. The responses time was less than 1 minute and recovery less than 30 seconds when exposed to air. This indicated that the sputter deposition might damage the CNTs while thermal evaporation did not.

SWNTs network was also modified by Pd nanoparticles using an electrochemical method (Schlecht *et al.*, 2007). The Pd decorated CNTs function as effective H_2 sensors enabling the detection of H_2 concentrations as low as 10 ppm at room temperature. The Pd/CNTs could also be deposited on poly(ethylene terephthalate) sheets serve as building blocks for the fabrication of

mechanically flexible hydrogen sensors with excellent sensing performance (Sun and Wang, 2007b).

The Pd decorated CNTs enable the detection of H_2 as low as 10 ppm with a short response time and recovery time at room temperature, which raw CNTs is not capable. The lower detection limit and response time of Pd/CNTs gas sensor were good for the practical use.

Pt nanoparticles were also used to decorate the CNTs for hydrogen sensor at room temperature (Kumar and Ramaprabhu, 2006). CNTs were loaded with Pt particles in the solvent while stirring Fig. 18. The Pt functionalised MWNTs gas sensor was tested to 4 % H_2. The results showed the Pt/ MWNTs gas sensor was a good hydrogen sensor with high sensitivity and reversibility at room temperature. The Pd/CNTs gas sensor was also fabricated by the Kumar to compare the gas sensitivity with Pt/CNTs gas sensor. The Pd decoration was proved to be a better choice for a H_2 sensor compared with Pt. The conclusion was also confirmed by the later study with Kaniyoor *et al.,* (Kaniyoor *et al.*, 2009b).

The adsorption of small molecules on a transition-metal doped SWNT has been studied within density functional theory (Yeung *et al.*, 2008a). By replacing a C atom with a Pt atom on the SWNT, the study has shown that the adsorption of gases was favourable and resulted in a charge-transfer event that modified the conductance of the nanotube as a whole.

CNTs gas sensor with and without Pt modification was measured for the gas (NO_2, NH_3, CO_2, CH_4, CO and C_2H_5OH) sensitivity (Penza *et al.*, 2011b). The functionalised CNTs with sputtered Pt catalyst loadings of 8, 15 and 30 nm performed an enhanced gas sensitivity operating at a temperature of 120 °C. A detection of 50 ppb NO_2 has been sensed at 120 °C. The maximum NO_2 gas

sensitivity has been measured by the Pt modified CNT gas sensor with a loading of 8 nm. The results demonstrated that the highest NO_2 gas sensitivity has been achieved up to one higher order of magnitude compared to other tested gasses (NH_3, CO_2, CH_4, and CO).

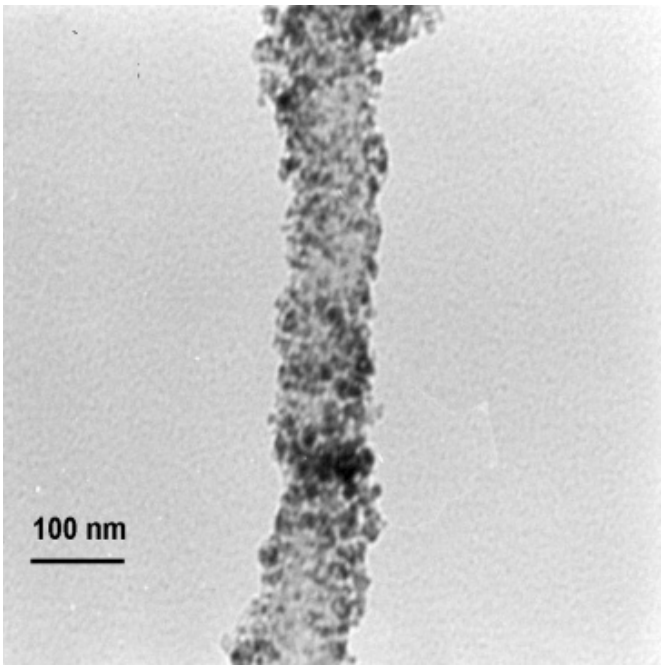

Fig. 18 TEM image of Pt dispersed MWNT.

Several works about Rh decorated CNTs have been published (Larciprete *et al.*, 2007) (Leghrib *et al.*, 2010a) (Leghrib and Llobet, 2011). The possibility of detecting ppb level of NO_2 at room temperature was reported. Pt, Rh and Ag decorated CNTs was fabricated to compare with raw CNTs (Penza *et al.*, 2009). The gas (NO_2, H_2, ethanol and toluene) sensitivity was tested at room temperature. Metal functionalised with CNTs performed to remarkably enhanced NO_2 gas sensitivity. The presence of 1 ppm NO_2 has been sensed at room temperature. Smaller concentration of NO_2 (0.1 ppm) has been sensed at 150 °C by the functionalised CNTs sensors. Compared to raw CNTs, the increasing temperature improved the NO_2 sensitivity of the raw CNTs. The

elevated temperature reduced the catalytic efficiency in the gas detection for the functionalised CNTs.

SWNTs doped with alkanethiol monolayer protected gold clusters have been investigated for ultra high sensitivity detection of NO_2 (Young *et al.*, 2005). The response to NO_2 of the Au/CNTs increased with the amount of Au until a threshold loading level was achieved, after which no further enhancement of sensor response is observed. The detection limit for NO_2 has been improved to 4.6 ppb at room temperature.

Ag nanoparticles decorated SWNTs, which is selective to H_2S at room temperature, has also been fabricated (Fam *et al.*, 2009). It seems therefore that the presence of different metal particles functionalising the CNT walls make the CNTs sensitive to several gases at room temperature. It has been proposed that to use a gas sensor array, which contains different the metal particles to decorate CNTs such as Pd, Pt, Au, Ag, Rh and Al. The sensor array should make the CNTs based gas sensor more robust and suitable for real life applications.

Au and Pt particles have been used at the same time to functionalise CNTs (Penza *et al.*, 2007). The gas (NO_2 and NH_3) sensitivity improved one order of magnitude with Au/Pt/MWNTs based gas sensor operated at high temperatures (400-500 K).

Modify CNTs with Metal-oxide Clusters

Many metal oxides are suitable for detecting combustible, reducing, or oxidizing gases by conductive measurements. The following oxides show a gas response in their conductivity: Cr_2O_3, Mn_2O_3, Co_3O_4, NiO, CuO, SrO, In_2O_3, WO_3, TiO_2, V_2O_3, Fe_2O_3, GeO_2, Nb_2O_5, MoO_3, Ta_2O_5, La_2O_3,CeO_2, Nd_2O_3 (Kanazawa *et al.*,

2001). The conductivity response is generally determined by the efficiency of catalytic reactions with detected gas participation, taking place at the surface of gas sensing material. Therefore, the control of catalytic activity of gas sensor material is one of the most commonly used means to enhance the performances of gas sensors. For example, the pure SnO_2 thin film without any catalyst exhibits very poor gas sensitivity. Noble metals (Au, Ag, Pt and Pd) are high-effective oxidation catalysts and this ability can be used to enhance the reactions on gas sensor surfaces (Wang *et al.*, 2008, Haridas *et al.*, 2008, Shimizu *et al.*, 2001, Lu *et al.*, 2004a).

The novel hybrid type of gas sensor could be fabricated by using CNTs or metal/CNTs as the catalysts on metal oxide type of gas sensor. The CNTs could be used as the guide for the nanoparticle metal-oxide film growing and this allows the coating of the inner and outer surface of the CNTs with a highly conformal film of controllable thickness.

A hybrid SWNTs/SnO_2 gas sensor was developed to detect NO_2 at room temperature (Wei *et al.*, 2004). SWNTs were added and dispersed in the organometallic (Sn [OOCCH (C_2H_5) C_4H_9]$_2$) solutions. The solution was spin coated on the interdigitated part of the sample, and heated to dry (Fig. 19). The coating layers were sintered at 500 °C in a fast-fire gas-tight furnace to decompose the coating materials, and obtain SnO_2 gas-sensing films. The CNTs was wrapped in the SnO_2 after the sintering (Fig. 20). Therefore, a model was presented to relate potential barriers to electronic conduction in the hybrid material. This model indicated that the high sensitivity was associated with the stretching of the depletion layers at the grain boundaries of SnO_2 and the SWNTs/SnO_2 interfaces when detected gases were adsorbed.

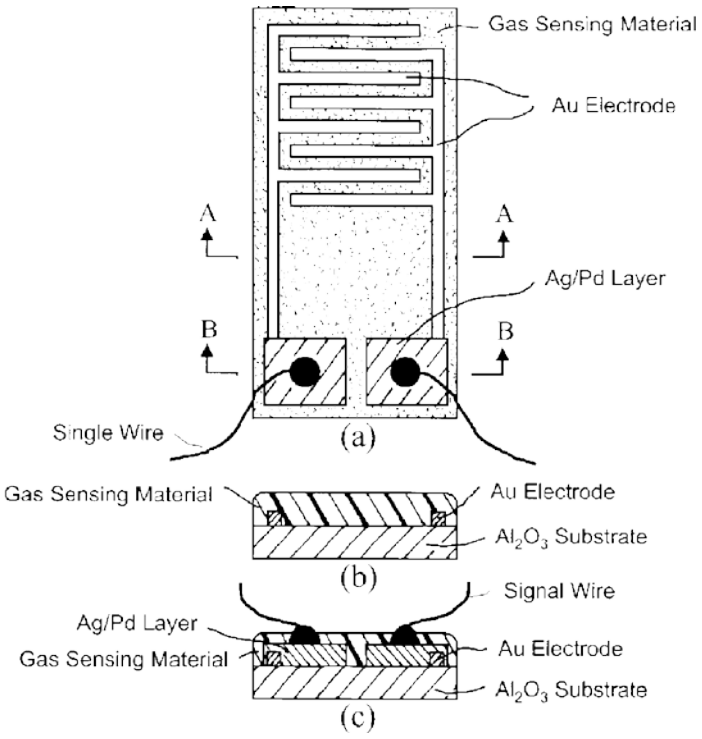

Fig. 19 Schematic of SWNTs/SnO_2 based gas sensors. (a) top view; (b) cross-section along line A–A in the top view, and (c) cross-section taken along line B–B in the top view (Wei *et al.*, 2004).

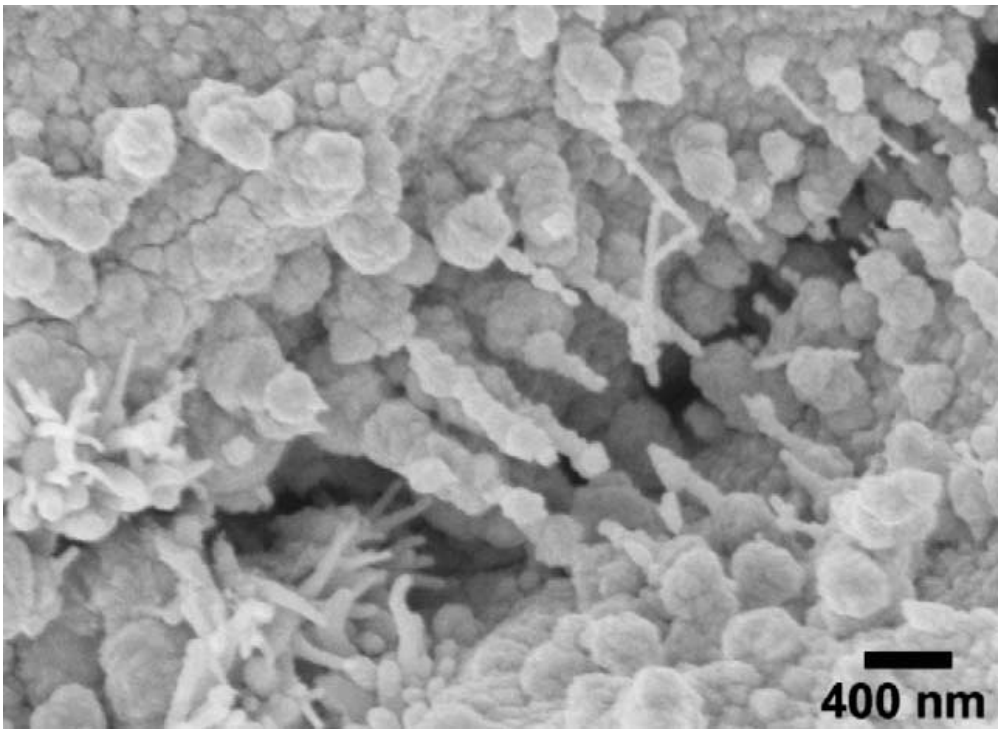

Fig. 20 FE-SEM micrograph of hybrid SWNTs/SnO_2 sensor (Wei *et al.*, 2004).

This hybrid gas sensor solved the problems of conventional SnO_2 sensors that cannot detect NO_2 at room temperature. However, the lowest concentration of NO_2 measured was 200 ppm, which is not good enough for the practical use. The MWNTs/SnO_2 was also investigated (Liang *et al.*, 2004). The detection limit was tested as 2 ppm for NO and NO_2 and 10 ppm for ethanol and acetylene.

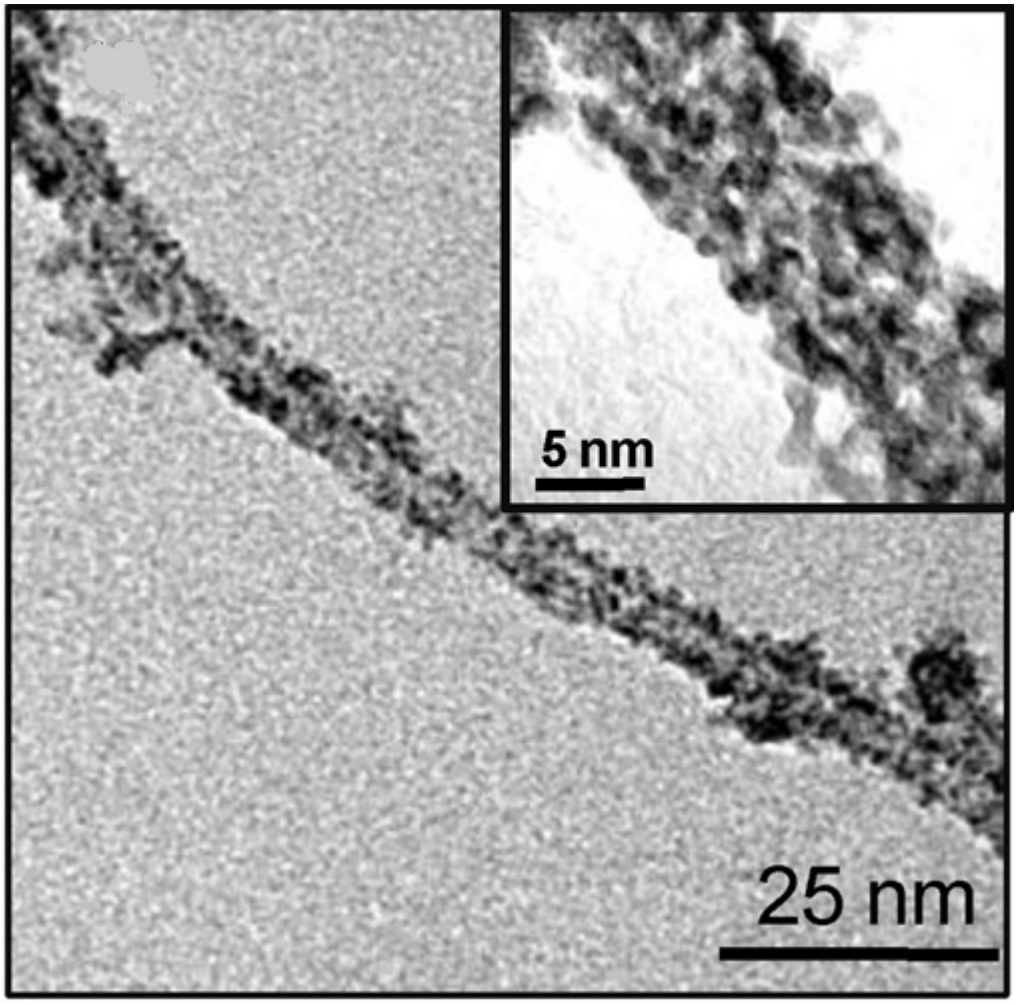

Fig. 21 TEM image of SWNT coated with tin oxide (Mubeen et al., 2013).

A electrochemical functionalization method was utilized to decorate SWNTs with SnO (Mubeen et al., 2013). The gas (NH_3, NO_2, H_2, H_2S, acetone, and water vapour) sensing performance was evaluated at room temperature. SnO was site

specifically precipitated on the surface of SWNTs because of an increase in local pH during electrochemical reduction of nitrate to nitrite ions. By adjusting the amount of charge passed during deposition, the amount of tin oxide deposited on SWNTs was controlled, which altered the electronic and gas sensing properties of the nanostructures. The resulting hybrid nanostructures showed excellent sensitivities. The detection limit was 25 ppb for NO_2 and 10 ppm for H_2 at room temperature. The enhanced sensing performance was due to the charge transfer at the interface of SnO nanoparticles and CNTs.

Improved gas sensitivity was reported by controlled the particles size of metal-oxide applied on CNTs. It indicates the importance of size of reaction site, which guides the path for decoration materials applied on CNTs.

Systems such as Au/CNT/SnO_2, Nb–Pt co-doped/CNT/TiO_2, Sb/CNT/SnO_2 etc were applied to the identification of CO, NH_3, ethanol, formaldehyde, toluene, NO_2, C_6H_6 and O_2. The hybrid material sensors improved the gas sensing performance by factors of 2-5 compared to that of the sensor without CNTs. It also gives the ability to detect gases at a relatively low operating temperature (<335 °C) (Llobet *et al.*, 2008). The metal-oxide gas sensor operates stable at high temperature. The metal-oxide/CNTs gas sensors therefore could also used at relative higher temperature compared to polymer decorated CNTs gas sensor.

CHAPTER 3

MATERIALS AND METHODS

3.1 Structure of the Experiments

Gas sensor samples investigated in the present thesis were made from two main components: field-effect capacitor devices and carbon nanotube network which bridges the two gate electrodes.

This chapter outlines the test sample preparation including the preparation of p-type silicon wafers and gold electrodes fabrication of the filed-effect devices, carbon nanotube dispersion and coating, Pt particle deposition. Details of the experimental set up were also been described.

After the sample preparation, substrate structure characterisation, capacitance-Voltage (C-V) measurements and gas sensitivities and selectivity were tested. Due to the nature of the project, how those measurements were completed will be reviewed in the results and discussion chapter.

3.2 Preparation of the Field-effect Capacitor

3.2.1 Substrate Preparation

P-type silicon wafers (500 ± 5 um thickness, 150 mm diameter, <100> 20-30 Ω/cm, Si-Mat, Germany, Fig. 22) with 20 nm thermally grown oxide (SiO_2) and 30 nm CVD nitride (Si_3N_4) were used for the present study. The wafers were purchased with insulator on both sides. The substrate preparation was carried out as illustrated in Fig. 23.

The insulator was removed from one side for the ohmic contact before cutting into small pieces. A wafer was placed on a flat clean surface. Concentrated hydrofluoric acid (HF, 48%, Sigma-Aldrich, UK) was dropped on the wafer surface by a plastic disposable pipette (1.5 ml, extended fine tip with small bulb,

VWR, UK). The etching process was completed when the hydrophilic wafer changed to hydrophobic. In order to prevent damage of the insulator on the reverse side, the HF solution was kept away from the edge of the wafer. After etching, the etched wafer was rinsed using distilled water and blown dry with nitrogen.

Fig. 22 P-type silicon wafer with a diameter of 15 mm, purchased form Si-Mat, Germany

An aluminium ohmic contact with a thickness of 100 nm was coated on the silicon side of the wafer by a thermal evaporator (Edwards Coating System E306A, Crawley, UK, Fig. 24). The etched wafer was placed on the specimen stage of the thermal evaporator where the silicon side faced down. A tungsten filament with coating material was used and the thermal vacuum evaporator was heated. The coating material first melted and then evaporated into vapour with further continuous heating. The evaporated material particles travelled in straight lines and condensed on the cold substrate surface and on the vacuum chamber walls. A low pressure of $5x10^{-5}$ Torr was used to avoid reaction between the vapour and atmosphere.

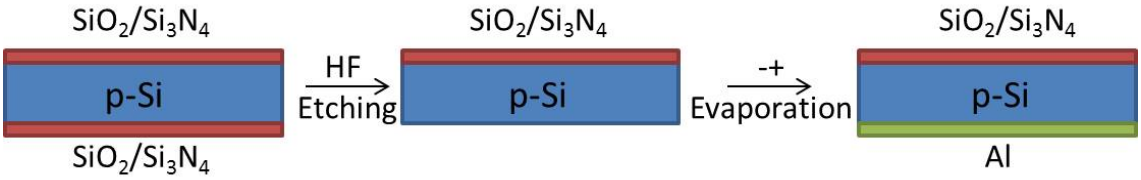

Fig. 23 Schematic showing the substrate preparation, where the p-type silicon wafer was first etched with HF on one side to remove the insulator, and then coated with aluminium ohmic contact by thermal evaporation.

Lanthanum fluoride has been used as an ion conductor on selected samples to improve the gas sensitivity. The working principle was explained as the movement of F^- ion conduction (Miura *et al.*, 1989). An ion conductor (LaF_3) layer (around 5 µm) was sputtered coated on the top of Si_3N_4 by Dr. W. Moritz (Chemie an der, Humboldt-Universität).

Fig. 24 Thermal Vacuum Evaporator (Edwards Coating System E306A, Crawley, UK)

3.2.2 Gate Structures

The wafer was then directly placed on a clean hotplate (Magnetic stirrer hotplate CD162, Stuart, UK), heated at 360°C for 15 minutes to improve the connection between the silicon substrate and the aluminium ohmic contact. The gate structures were prepared by lift-off through photolithography and thermal evaporation through a nickel mask. Photolithography was used to make micro-size interdigitated electrodes.

Compared with the carbon nanotubes network, the gold strips between the electrodes were designed to occupy a smaller proportion of the gate area in order to ensure that the carbon nanotubes network dominated the potentiometric sensor response of the host field-effect capacitor. These gate electrodes structures were further simplified to two metal lines (Fig 10). Thermal evaporation through a nickel mask was used to make larger electrode structures (the two-line structure).

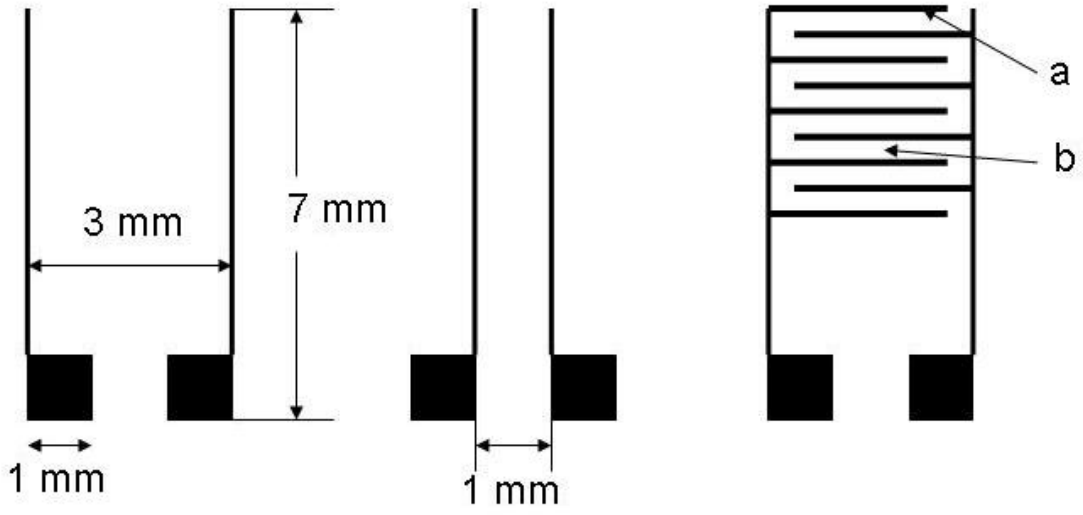

Fig. 25: Schematic of the interdigitated structure sample and two lines sample

For the interdigitated structure, the width of the metal finger was designated as a, and the gap space between the metal fingers was b (Fig. 25). A selection of gate structures with different metal finger width and gap space (Table 3) was prepared for current project.

Table 3: The metal finger and gap size of interdigitated structures (unit: μm):

Metal finger width, a	3	6	10	50	10	100
Gap space between the metal fingers, b	10	30	100	150	10	100

3.2.2.1 Lift-off through Photolithography

Photolithography was completed by the following steps: wafer cleaning, photoresist application, soft baking, exposure, curing, development, evaporation of metal contact and lift-off.

1. Wafer Cleaning

The etched wafers were cut into square pieces with a dimension of 2 cm x 2 cm. These square pieces were soaked in acetone (179124, Sigma-Aldrich, UK) and then ethanol in an ultrasonic bath (KC3 Ultrasonic bath, Kerry, UK) for 15 minutes respectively, so as to remove particulate matter on the substrate surface and any traces of organic, ionic, and metallic impurities. The substrates were then blow-dried and dehydrated by hard baking at 140ºC for 20 minutes in succession.

2. Photoresist Application

A positive photoresist (S1813, MICROPOSIT, Shipley Company, USA) was spin-coated onto the silicon substrate surface at a rate of 5000 rpm for 1 minute using spin coater (KW48, Chemat Technology). The coating process produced a thin (1.3 μm) uniform layer of photoresist on the substrate surface.

3. Soft baking

The wafer was soft baked on a hotplate at 100°C for 1 minute. The soft baking was used to remove the solvent from the photoresist and improve the connection between photoresist and the silicon substrate.

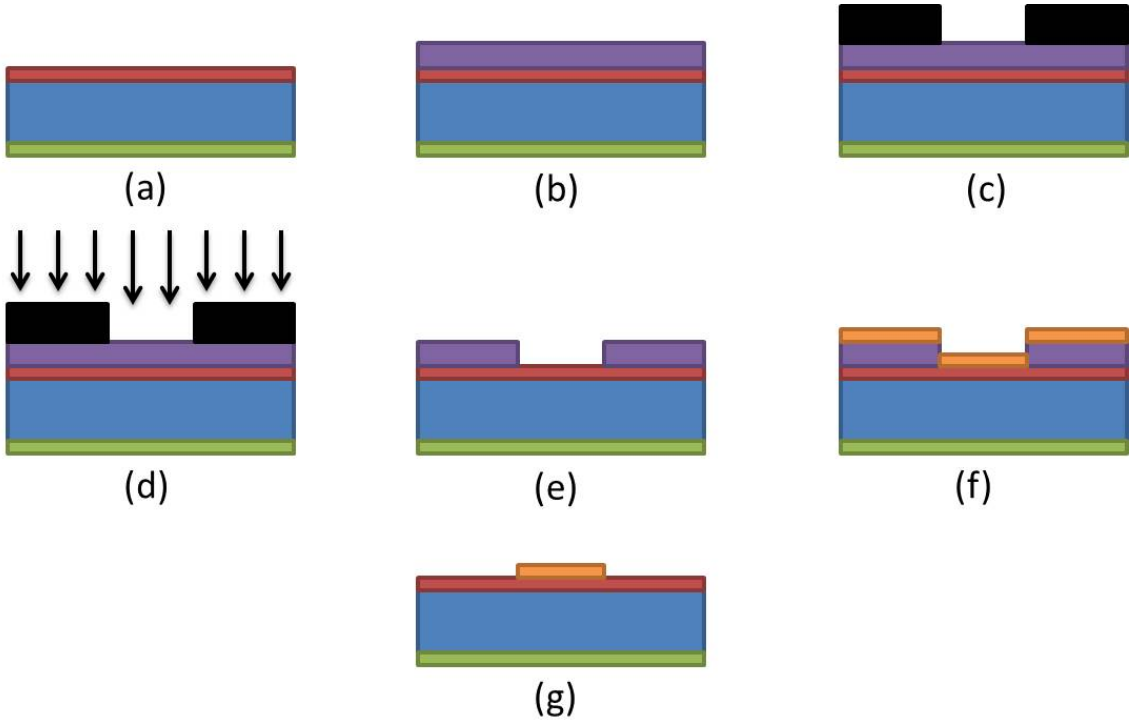

Fig. 26 Schematic showing the preparation of the top gate electrodes though lift-off process. A cleaned prepared substrate (a) was spin coated with photoresist S1813, and heated on a hotplate at 100°C for 1 minute, (b). The sample was placed under a mask with design pattern. UV light was applied on the sample with the mask, (d). The sample was then soaked in chlorobenzene for 10 minutes, followed by 5 minutes heating at 85°C. The UV exposed part of photoresist was washed off during the development, (e). Cr (20 nm) and Au (80 nm) was thermal evaporated respectively (f). The rest of photoresist was then washed off by placed the sample in an ultrasonic bath for approximate 5 minutes. The design pattern was fabricated on the substrate (g).

4. Exposure

The photoresist was exposed to UV light in order to remove the underlying material. The exposure to the UV light changed the chemical structure of the

photoresist. Consequently, it became more soluble in developer. A Karl Suss mask aligner (MJB 3 UV400, Karl Suss America Inc., USA) was used to expose the photoresist. Contact model was used to get a higher resolution. The silicon substrates were exposed to UV light for 20 seconds at an intensity of 22.4 mW/cm^2 with a wavelength of 275 nm.

5. Curing

The silicon substrates were dipped in chlorobenzene for 10 minutes so as to create an undercut in the photoresist profile during development. The substrates were then baked for another 5 minutes at 85°C using a hotplate.

6. Development

Developer prepared by mixing one part of Microposit 351 (MICROPOSIT, Shipley) with three parts of distilled water was used for the wafer development. The silicon substrates were placed into the developer for 40 seconds to allow development. After removal, the substrates were rinsed with deionised water immediately and then blown dry.

7. Evaporation of metal contact

A 20 nm chromium layer and 80 nm gold layer were coated onto the silicon substrates by thermal vacuum evaporation.

8. Lift-off

These silicon substrates were placed in a beaker in an ultrasonic bath approximate 5 minutes until the pattern was completed and then blown dry.

3.2.2.2 Thermal Evaporation through a Nickel Mask

Thermal evaporation through a nickel mask was used to prepare the two-line structure. A nickel film (0.5 mm in thickness) was cut into square pieces (5 X 5 cm) and stuck to a hard board with adhesive tape. Positive photoresist (S1813) was spin coated onto the nickel film surface at a rate of 1000 rpm for 1 minute. The nickel film was then soft baked at 90°C for 10 minutes. A transparent projection slide with the computer designed pattern structure was printed out. The nickel film was subsequently placed under the patterned transparency for 1 minute UV exposure (20 W) before dipped in a developer prepared by mixing one part of Microposit 351 (Shipley) and 3 parts of distilled water. Specimen was withdrawn after 30 seconds, rinsed with deionised water immediately and blown dry.

An acid mixture were prepared by mixing 5 parts of HNO_3 (70.5%, Sigma-Aldrich, UK) with 5 parts CH_3COOH (99%, Sigma-Aldrich, UK) and 2 parts H_2SO_4 (98.07%, Sigma-Aldrich, UK). One part of the resulting acid mixture was diluted by a factor of 28 with distilled water. The resultant solution was used as etching solution. The nickel film was soaked in the etching solution and the etching rate was 0.25 μm/min. The nickel mask was taken out when the pattern became visible. It was then rinsed using water to remove any residual etching solution. The gate electrodes were then thermally evaporated through this nickel mask.

3.3 Carbon Nanotubes Coating

Multi-walled carbon nanotubes (NC7000 Series, Nanocyl, Belgium) and single-walled carbon nanotubes (HiPco, Carbon Nano-technologies Incorporated, USA) were used for coating in this project. Both drop coating and spray coating technique were carried out.

3.3.1 Drop Coating

Carbon nanotubes (1.7 g) were weighed by an analytical balance (Mettler AE 200, Mettler Instruments Ltd, UK) with an accuracy of 0.0001g. CNTs were then suspended in 7 ml methanol in an ultrasonic bath (KC3 Ultrasonic bath, Kerry, UK) for 10 minutes. One millilitre of the resultant suspension was diluted by a factor of 7 in methanol accordingly, followed by a 1 hour ultrasonic treatment.

The carbon nanotubes in the suspension had a tendency to agglomerate into ropes and bundles due to the van der Waals inter-atomic forces. It was noticed that the carbon nanotubes started to sediment after 30 minutes. Therefore, the suspension is prepared fresh every time and used as soon as it came out of the ultrasonic bath.

A syringe (1 ml, single-use insulin syringe, 613-2041, VWR, UK) was used for drop coating experiments in the present study. The drop coating method tended to form an uneven carbon nanotubes network.

3.3.2 Spray Coating

Spray coating was claimed to provide an improvement of CNTs coating compared with drop coating, and was therefore adopted in the present project. Two different CNTs suspensions were prepared by different methods in order to provide stable CNTs suspensions for spray coating.

3.3.2.1 Aqueous SDS/SWNTs Suspension

An aqueous solution containing 0.44 wt% single-walled carbon nanotubes (SWNTs) with 1 wt% sodium dodecyl sulphate (SDS, CH_3 $(CH_2)_{11}OSO_3Na$, Sigma-Aldrich) was prepared. SDS has a tail of 12 carbon atoms, attached to a sulfate group, which gives the molecule amphiphilic properties. It could attach and surround the carbon nanotubes surface under ultrasonic treatment (as shown in Fig. 27). SDS was used herein to stabilise the carbon nanotube suspension (Strano *et al.*, 2003).

The SWNTs/SDS solution was subjected to mild probe sonication (Ultrasonic Processor SOVC505-00, Geneq, Canada) with a power of 100 W and a frequency of 20 kHz for 90 minutes. Two hours centrifugation at 3000 rpm/min was carried out to separate higher density contaminants from the dispersed SWNTs. The SWNT supernatant was then extracted and dispersed. The carbon nanotubes should remain dispersed in the suspension for a long period.

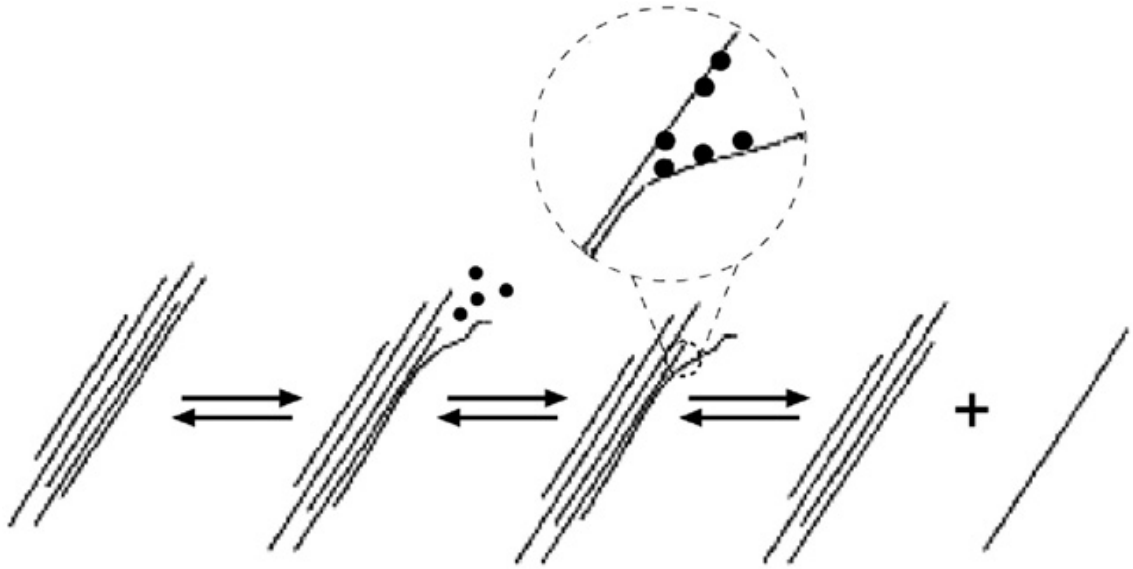

Fig. 27 Mechanism of nanotube isolation from bundle by ultrasonication and surfactant stabilisation (Strano *et al.*, 2003)

The solution was then diluted with water by a factor of 100 before deposition. The sprayed samples both before and after washing with de-ionised water were characterised using atomic force microscopy (AFM). The AFM images (Fig. 28) indicated that the excess SDS was washed away.

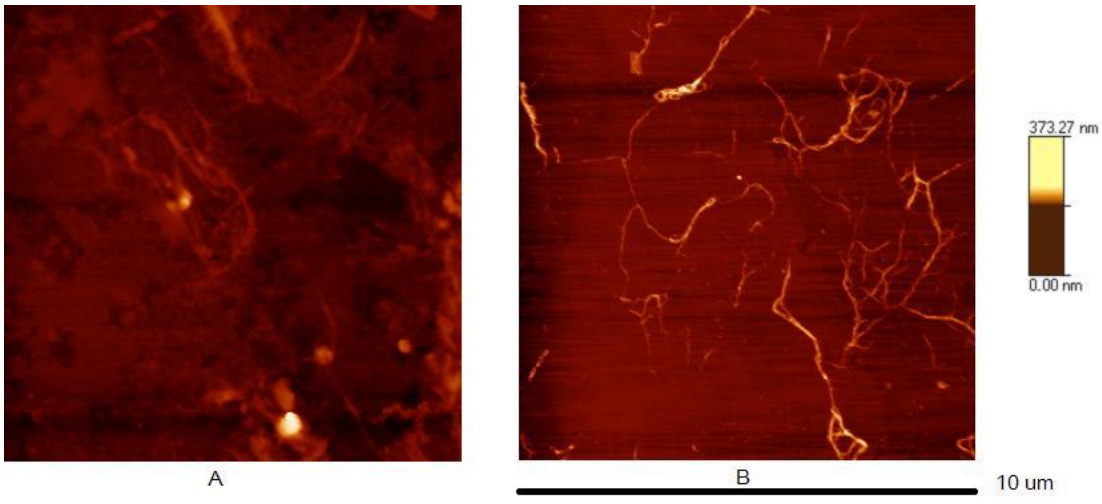

Fig. 28 AFM images of the sample A, before SDS was washed away and B, after SDS was washed away (provided by C. J. Morgan)

3.3.2.2 N, N-dimethylformamide (DMF) carbon nanotube suspension

The strategies for the dissolution of SWNTs have involved complexation of the CNTs walls with surfactants (SDS). Those molecules attached to the CNTs walls were difficult to remove, which altered the physical and chemical properties of the SWNTs. Furtado *et al.,* proposed an effective chemical process to obtain clean, individual single-walled carbon nanotubes in a stable solution in 2004 (Furtado *et al.*). The process included dry oxidation, acid reflux, neutralisation, ultrasonic disperion and centrifugation.

A similar process was used in current study to get individual SWNTs. The carbon nanotubes were baked at 365°C for 90 minutes in air. It was required to achieve selective oxidation of the amorphous carbon and minimise nanotube mass loss. If dry oxidation is completed carefully, only 10% of the SWNTs will be lost during this step. Importantly, the carbon coating on the metal particles is also weakened during this step (Harutyunyan *et al.*, 2002).

The metal particles were then removed by a reflux in acid solution, using a strongly oxidising HNO_3 solution (3 M) for 16 hours. The solution was filtered with a 5 μm pore size filter paper (Grade 595, 5 μm, Whatman Inc, UK) through vacuum. The solid residues were washed with deionised water (around 2 liters). After washing, a small amount of sodium hydroxide solution (NaOH, pH=10) was used to neutralise the acidity of the residual and followed by 50 ml of hot deionised water. Litmus paper was used to check the pH value in the funnel. The NaOH wash and pH check were repeated until the pH value reached 7.

Ultrasound was then applied to disperse and debundle the purified SWNTs bundles in DMF solvents. Ultrasonic dispersion was carried out for 4 hours in a bath. After ultrasonic dispersion, the solution (1 ml) was then immediately centrifuged using a Eppendorf microcentrifuges (5417C, Eppendorf Scientific,

Germany) at a rate of 14,000 rpm for 30 seconds. The supernatant liquid on the top containing the debundled SWNTs was withdrawn for later use (Fig. 29).

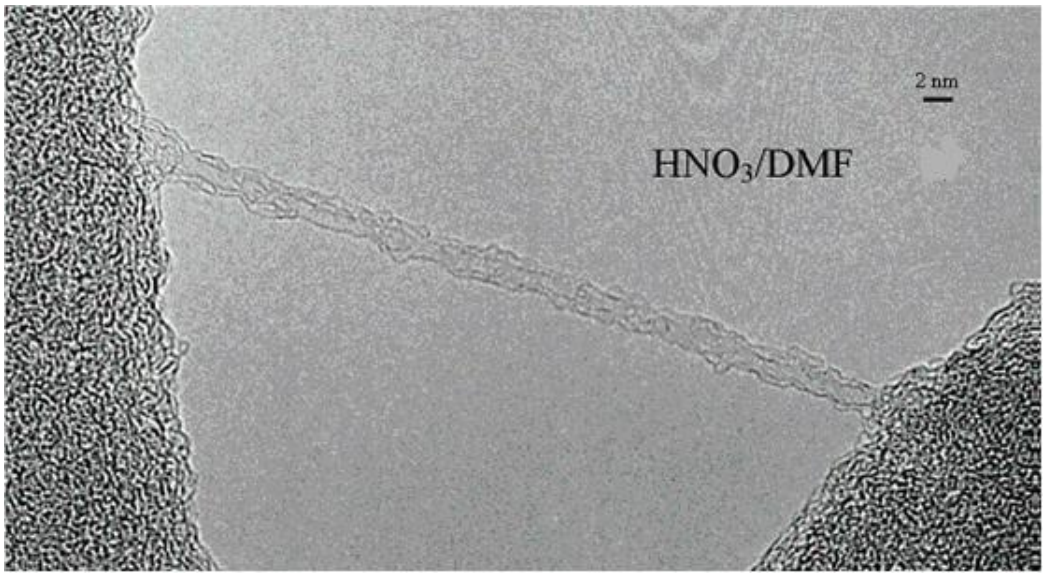

Fig. 29 TEM image of debundled SWNTs dispersed in DMF after HNO_3-reflux (Furtado *et al.*, 2004)

3.3.2.3 Spray Coating Process

SWNTs networks were airbrushed (AB-135A, Everythingairbrush, UK) onto the substrates through an o-ring sealed mechanical compression mask of aperture with a diameter of 4 mm (Fig. 30). The silicon substrate was placed in the centre of the two plates where an O-ring was placed on top of the substrate to insulate the coating area from the edge of the substrate. Therefore, the carbon nanotubes mats were only formed inside of the O-ring. This mask setup provides a thick CNTs network layer without short circuit between the gate and ohmic contract.

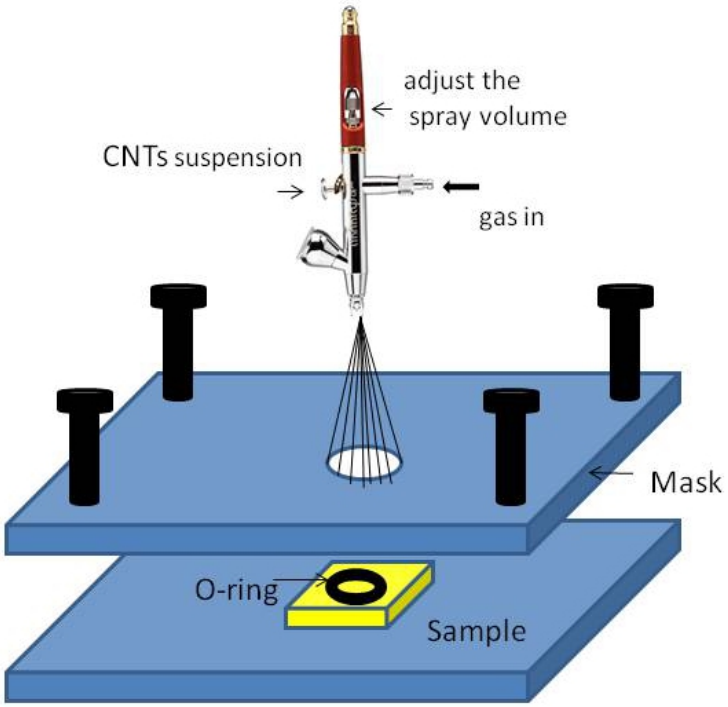

Fig. 30 Schematic of the device used for spray coating (with mask)

The airbrush was pressurised with filtered compressed air and held approximately 5 cm above the substrate. Single sweep brush strokes were applied, where a second brush strokes could only be applied when the previous one was dried.

3.4 Pt particles Deposition

Pt particles decorated CNTs have been proved to improve the H_2 sensitivity compared to raw CNTs. The Pt functionalised CNTs were fabricated in this study. Electrochemical deposition was chosen because of the advantage of decorating the CNTs after the CNTs have been sprayed on the sample. It was easy to compare the gas sensitivity difference between before and after Pt decoration.

The electrodeposition and characterisation of Pt particles have been reported (Day *et al.*, 2005). The solution for Pt deposition contained 2 mM potassium hexachloroplatinate (K_2PtCl_6, Sigma-Aldrich, UK). Perchloric acid (0.5 M) was used as a supporting electrolyte. The deposition was carried out with three electrodes system as illustrated in Fig. 31 (autolab pgstat30, Metrohm Autolab, The Netherlands). The interdigitated part of sample was immersed into the solution. An O-ring was used to seal the solution. The two top gold electrodes and CNTs network were used as working electrode. Ag/AgCl wire and Pt were used as reference and counter electrode. A deposition potential of -0.4 V (versus Ag/AgCl) was used.

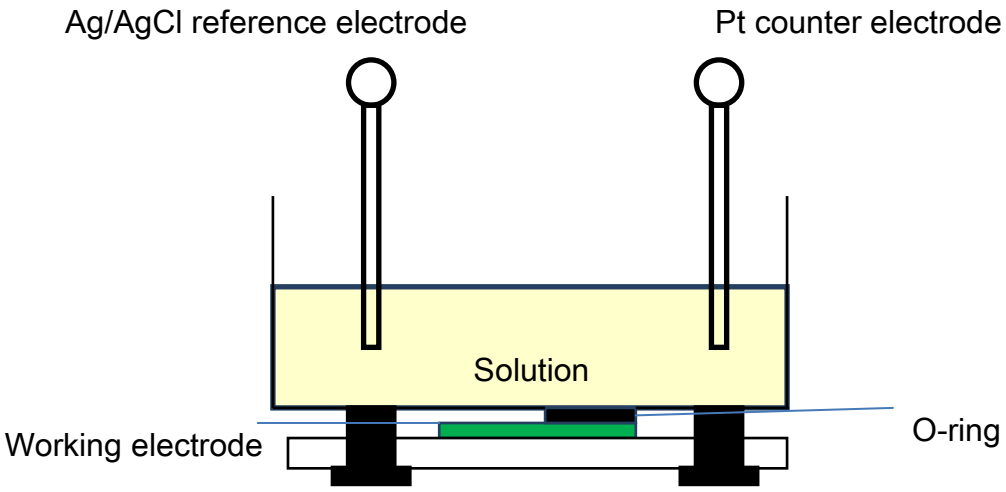

Fig. 31 Schematic of setup used for Pt electrodeposition

3.5 Experimental Setup

3.5.1 Gas Sensing by Gas Flow Setup

A multi-functional setup was designed to achieve both potentiometric and resistive measurements. The setup was built by five main parts: gas cylinders array, mass flow control system, humidity mix system, measurement system and computer (Fig. 32).

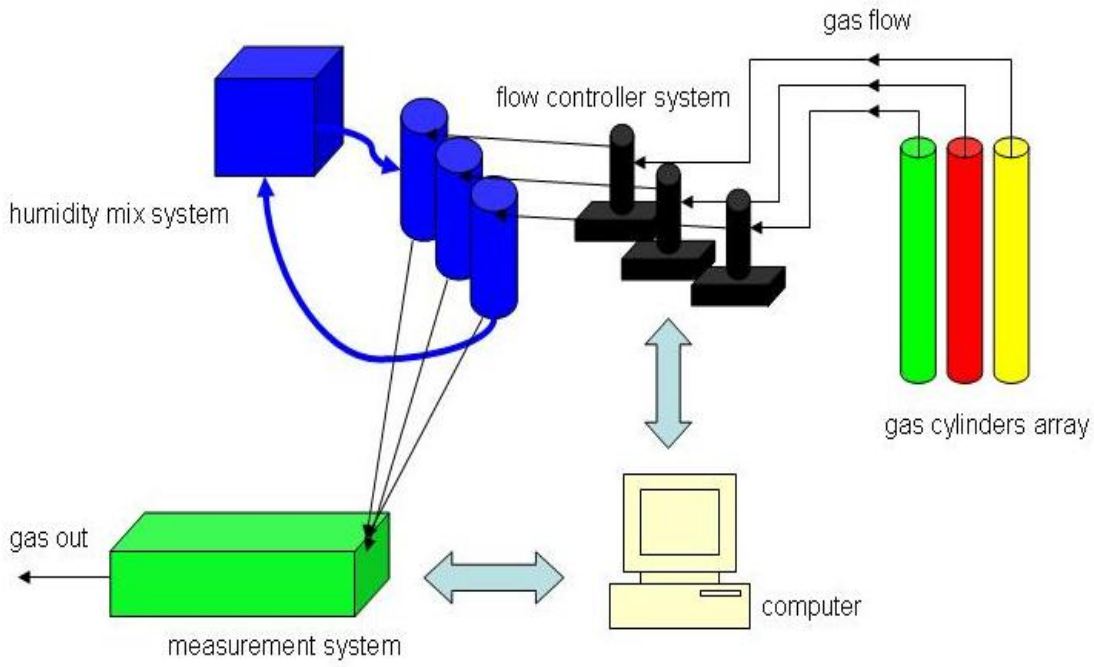

Fig. 32 Schematic of the experimental setup

Gas cylinders array

The gas cylinders were purchased from BOC gas (UK). The gas flow through the regulator was set to 1 bar. All gases were delivered using 6 mm outer diameter (OD) tubes. Swagelok stainless steel tube fitting were used to ensure the whole setup was gas tight and contaminations free.

Flow control system

Three mass flow controllers (Brooks, UK) were used to control the gas flow concentration. The mass flow controllers were powered via 0154 read out (Brooks) and connected to a RS-485 network. The flow conditions were monitored on the display of 0154. The RS-485 network was connected to a computer via an isolated RS-232/422/485 converter (4WSD9OTB, B&B Electronics, USA). Smart DDE software (v 1.2, Brooks) was run in the background to achieve a handshake between the computer and mass flow controllers. A custom-compiled Labview (v 8.0, National Instruments) program was used for the operation. The gas flow concentration and the flowing time can be controlled by the computer within a delay of 0.2 second.

Humidity mix system

Humidity mix system was made up of a water chiller and three custom-made bubblers as shown in Fig. 33.

Humidity is defined as the amount of water vapour in the air, which could be expressed in two different ways including relative humidity and absolute humidity. It is temperature dependent. The quantity of water in a particular volume of air is designated as absolute humidity. At various temperatures, the absolute humidity is given in Table 2. The humidity of the test gases was adjusted by bubbling them through water at different temperatures.

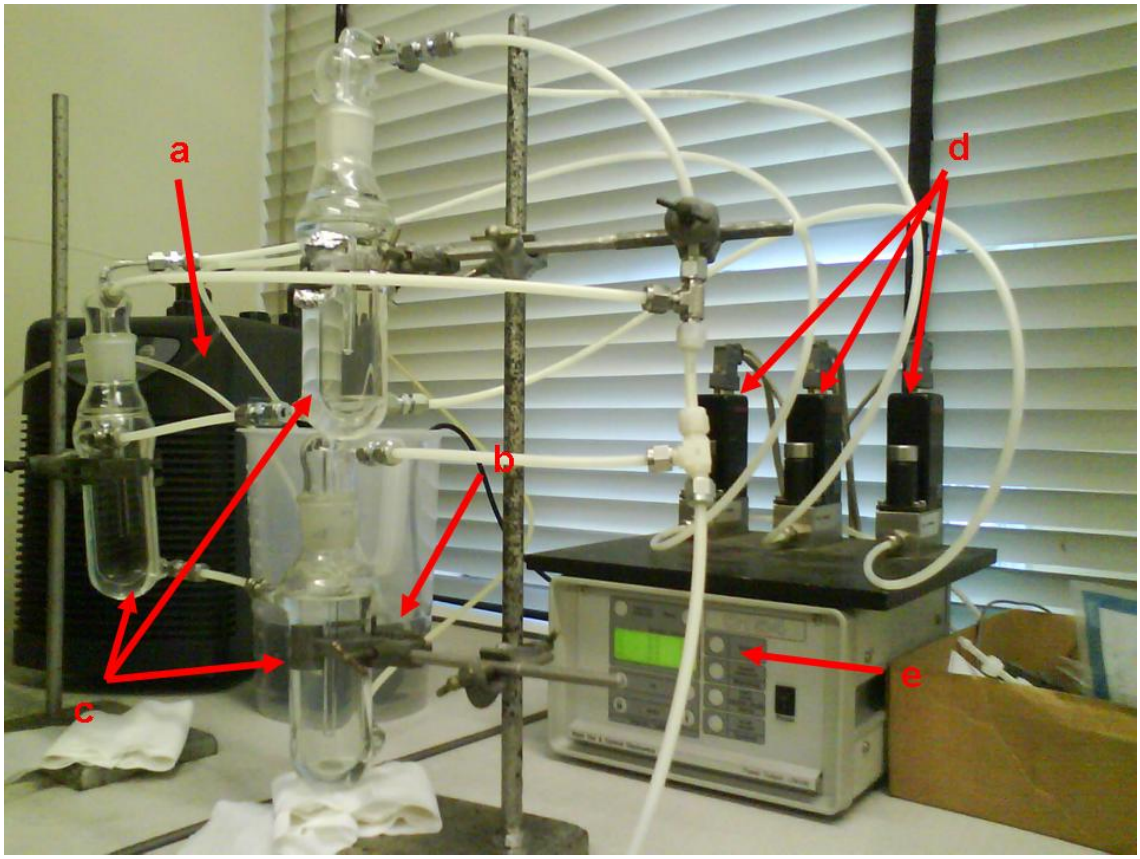

Fig. 33 Gas flow system and humidity mix system: (a), water chiller; (b), water pump; (c), glass container for humidity mix; (d), mass flow controllers and (e), 0154 read out

Table 4: the absolute humidity value at various temperatures

Temperature (°C)	Absolute humidity (g/m^3)	Percentage In the air (%)
-5	3.3	0.33
0	4.8	0.48
5	6.8	0.68
10	9.4	0.94
15	12.8	1.28
20	17.3	1.73
25	23.0	2.3
30	30.4	3.04
35	39.6	3.96
40	51.1	5.11

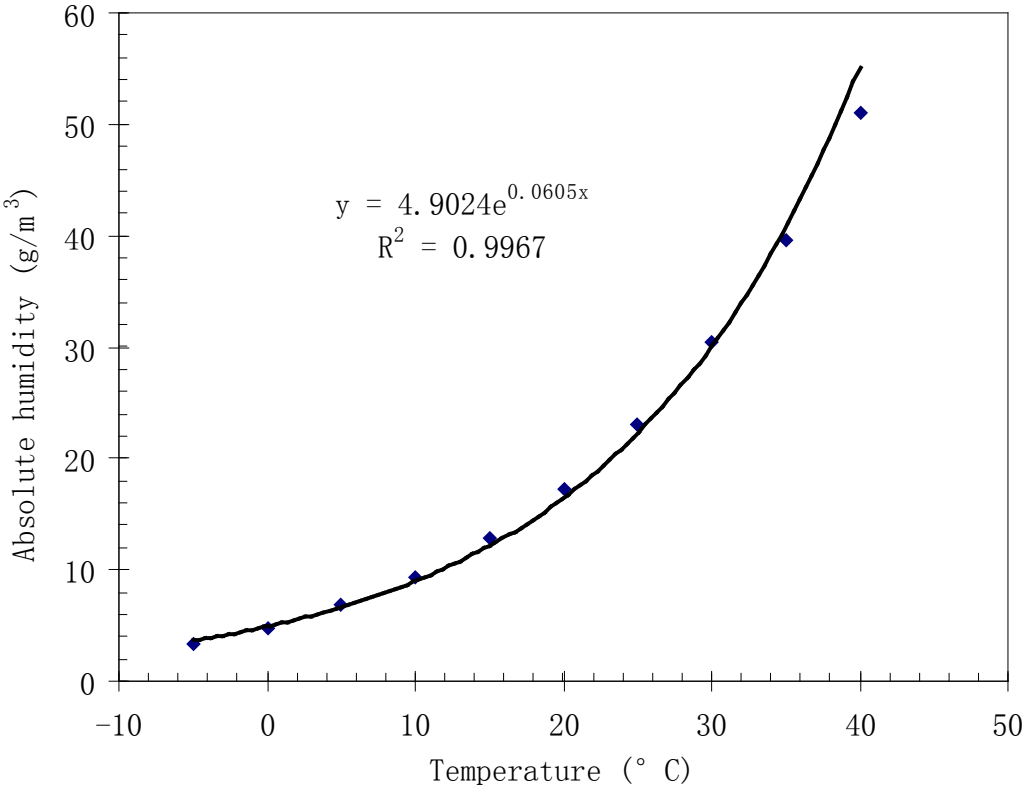

Fig. 34 Relationship between absolute humidity and temperature

The absolute humidity was plotted against temperature, a clear relationship can be established and expressed as $y=4.9024e^{0.0605x}$, with a R^2 value of 0.9967; where y is the absolute humidity and x is the temperature (Fig. 34).

Measurement system

A Teflon gas tight cell with an interior dimension of 8 cm x 5 cm x 2 cm was designed together with the supporting engineers in the school of Engineering and Materials Science in Queen Mary. As illustrated in Fig. 35, the cell could host up to 4 samples together along the direction of gas flow. During experiment, gas sensor sample was placed in the cell. The ohmic contact was connected to the connection c, and the two top gate electrodes were connected to a and b. The connections a and b were then connected to a multi-channel potentiometer

(VMP2, Biologic science instrument, France) for the resistive measurement of the CNTs network. Connections a, b and c were connected to the potential meter for the potentiometric measurement.

A custom-compiled Labview program was used to control the operation. Life-time data was also recorded by the Labview program. The test cell was placed in a Faraday cage in order to minimise the noise level.

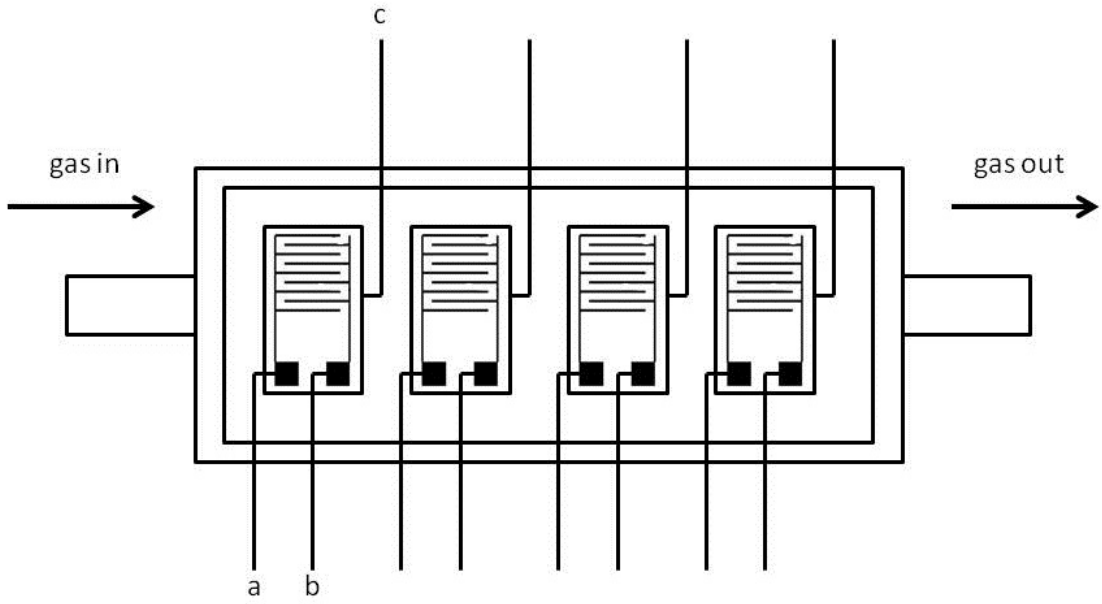

Fig. 35 A Schematic of the custom-made gas tight testing cell

CHAPTER 4

RESULTS and DISCUSSION

4.1 Substrate Structure Characterisation

Substrates (Al/Si/SiO_2/Si_3N_4) with three different types of gold gate electrodes (two-line, 6-30 and 10-10) were fabricated. When coated with carbon Nanotubes, both carbon nanotubes on the substrate and metal electrodes will serve as gate materials. These three different types of the metal gate structures would provide a different ratio of gate function between the carbon nanotubes and the metal electrodes. The electrical properties were investigated to setup a base line for the experiments later.

Capacitance-Voltage (C-V) measurements using a two electrode system of the potentiostat were carried out to characterise the electrical properties of the substrate. Both gate electrodes of the substrates were connected to the working electrode input. The ohmic contact was connected to the counter and reference electrode input. The potential was scanned from -3 to 3 V with an increment of 0.1 V and amplitude of 10 mV at different frequencies (1 Hz, 10 Hz, 100 Hz, 1 kHz, 10 kHz, 100 kHz and 1 MHz).

The C-V curves of the two-line structure are shown in Fig. 36. Three modes (accumulation, depletion and inversion) occurred gradually when the voltage increased from -3 to 3 V on the C-V curves at all frequencies. The accumulation capacitance increased with a decrease in frequency. The increase in accumulation capacitance was due to the change in the measuring area of the gate electrodes. At higher frequencies, the effective gate area was only under the gold electrodes. However at lower frequencies, the effective gate area was enlarged by the lateral diffusion of the charge carriers in silicon. The effective gate area increased from just the size of the gold electrodes area to the whole interdigitated structures. The curves measured at frequencies lower than 100 Hz indicated classic low frequency MIS structure behaviour. The curves at

frequencies higher than 100 Hz showed classic high frequency MIS structure behaviour.

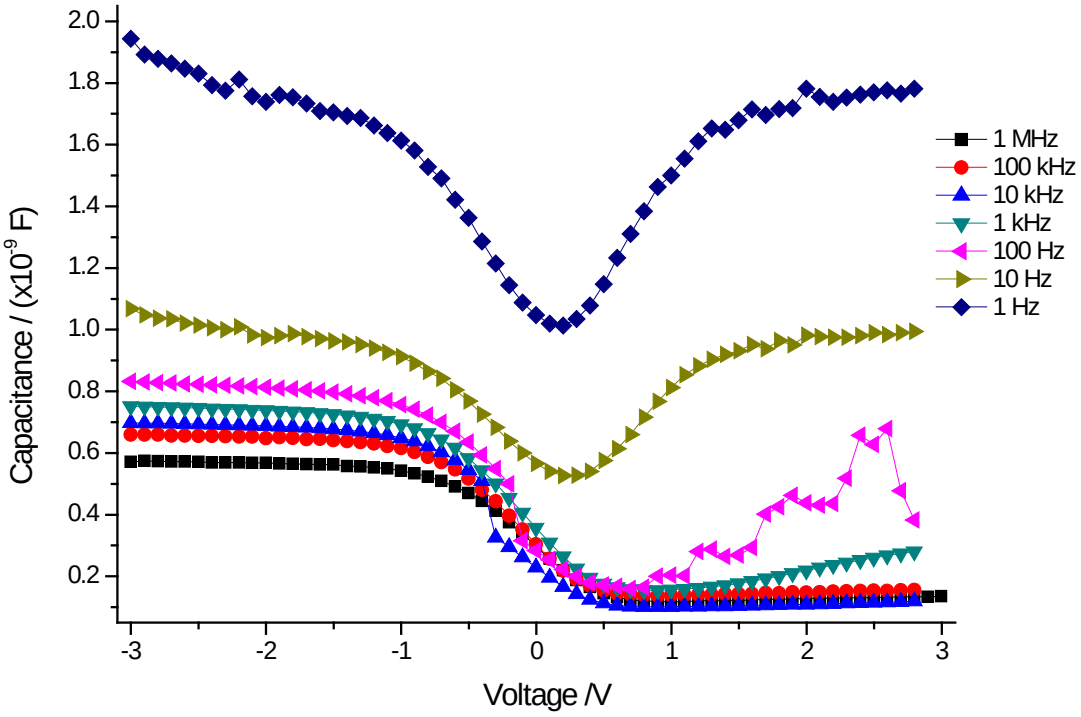

Fig. 36 C-V curves of two-line sample (Al/Si/SiO_2/Si_3N_4 substrate) at different frequencies

The C-V curves of the 6-30 structure and 10-10 structure are given in Fig. 37 and Fig. 38. Three modes (accumulation, depletion and inversion) were also found on the C-V curves at all frequencies when the voltage increased from -3 to 3 V. The three modes occurred at approximate the same voltages. The accumulation capacitance of these two structures also increased with a decrease in frequency. The C-V curves were observed to be noisy at lower frequencies (1 Hz, 10 Hz and 100 Hz) for all three electrodes structures. This is attributed to the limitation of the measurement setup.

The C-V curves measured at 1 kHz were selected for further potentiometic measurements due to the stable C-V curves and the most significant depletion region (Fig. 36-Fig. 38).

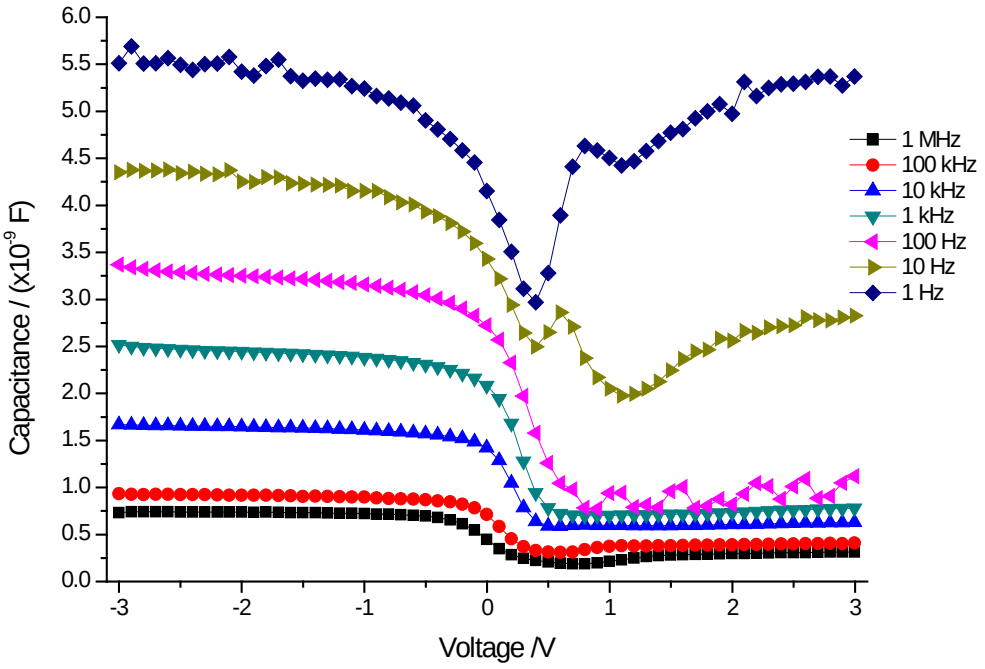

Fig. 37 C-V curves of sample (Al/Si/SiO_2/Si_3N_4 substrate, interdigitated structure, 6-30) at different frequencies

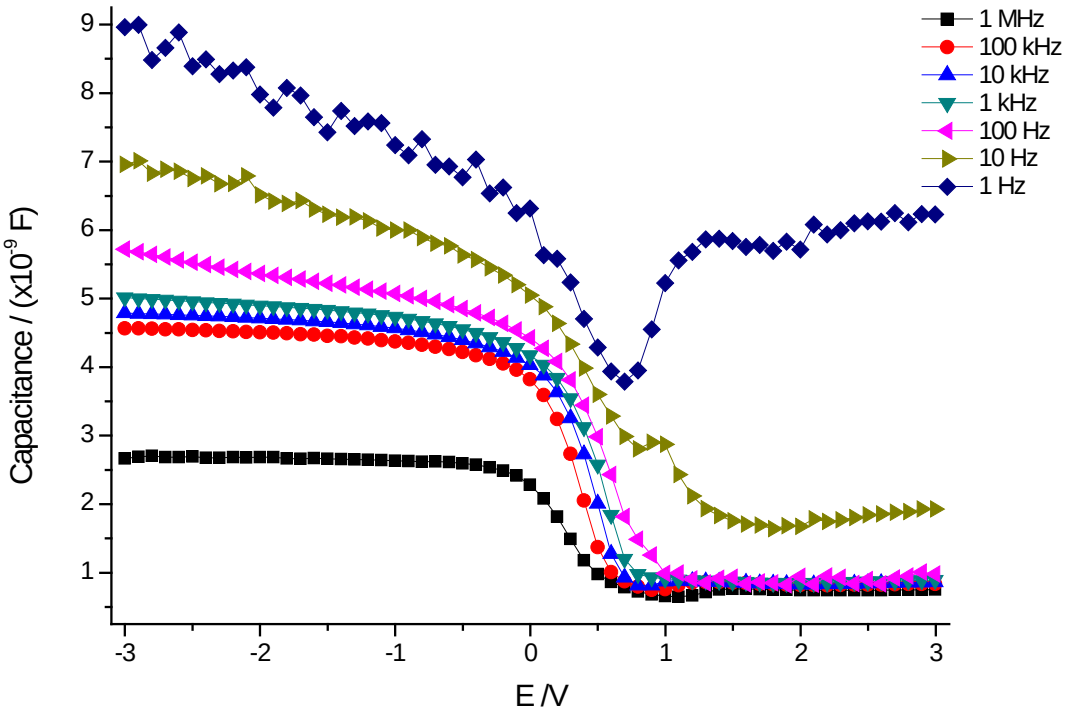

Fig. 38 C-V curves of sample (interdigitated structure, 10-10) at different frequencies

4.2 Drop Coated MWNTs

MWNTs provide better conductivity compared with SWNTs (chapter 2.2.1), they were therefore selected to bridge the two metal gate electrodes. Drop coating was carried out to check the possibility of bridging gate electrodes by MWNTs. Oxygen sensitivity of the coated MWNTs network was measured by the resistive measurement to demonstrate the resistive measurement part of the device.

MWNTs were dispersed in methanol as described in Chapter 3.1.2 and then coated onto the substrates (Al/Si/SiO_2/Si_3N_4) by drop coating. The interdigitated electrode structure (6-30) has a smaller percentage of gold electrodes area on the surface of the substrates. The smaller gold electrodes area was supposed to make MWNTs dominate the gate function in the device for gas detection. It was therefore selected as the substrate. Two substrates were drop coated with different amount of MWNTs (sample 1: 2 drops and sample 2: 5 drops).

Each of the top gate electrodes was connected to the potentiostat by using a two electrodes system. A linear increased voltage from -1 to 1 V with an increment of 0.01 V and an interval per step voltage of 1 second was applied between the two top gate electrodes. The current-voltage curves of sample 1 and 2 are shown in Fig. 39 and Fig. 40. Both samples showed a nonlinear current-voltage curve. The currents of Sample 1 were between -1.37×10^{-6} A and 1.56×10^{-6} A, corresponding to the increasing voltage between -1 to 1 V. With a thicker MWNTs coating, Sample 2 gave a typical 'S-shape' semiconducting current-voltage curve. The currents varied from -6.6×10^{-6} A to 5.78×10^{-6} A when the voltage increased from -1 V to 1 V. The result indicated a higher conductivity when compared with sample 1.

A DC voltage of 10 mV was applied between the two top gate electrodes of sample 1 and sample 2 respectively for resistive measurements. The current of

each sample was recorded every 5 seconds. The test system was cycled between vacuum (1×10^{-5} mbar) and atmospheric pressure oxygen, when the resistance signal became stable. The resistances were calculated. The sensitivity of the senor was defined with changed of resistance minus initial resistance and then divided by initial resistance. The results and plotted against time (Fig. 41). Both samples showed an increase in resistance when switching from vacuum to oxygen, and a decrease in resistance when switching from oxygen back to vacuum. When switching from vacuum to oxygen, sample 1 showed an increase in resistance with a maximum increase of 30 kΩ (12%) approximately, and the maximum resistance increase of sample 2 was 10 kΩ (4%) approximately. The resistance measurements indicated the thinner CNTs film would result a better gas sensitivity. It was also noticed that the resistance was not fully recovered with the cycling gas environment. An increase in sample resistance was observed after each vacuum-oxygen-vacuum cycle.

According to Collins *et al.,* (2000) and Bradley *et al.,* (2000), the absorption of oxygen molecules on the completely desorbed CNT could lead to an increase in the number of hole charge carriers in the CNT networks, therefore, an increase in the density of states at the Fermi level. This could contribute to a decrease in the resistance of the sample. However, Collins *et al.*, (2000) suggested the chemisorbed oxygen could only be removed with a heat treatment (110 - 150ºC for several hours). The samples used in current study were not subjected to such a treatment, the observed increase in resistance for cycling vacuum and oxygen exposure could be caused by the scattering from defects or non-thermal phonons generated by gaseous collisions with the tube walls as suggested by Sumanasekera *et al.* (2000). The oxygen used in this experiment is supplied without humidity, however, the cycling vacuum and gas method could introduce humidity in the system. The water adsorption could increase the resistance of the CNTs (Watts *et al.*, 2007, Na *et al.*, 2005). The electronic properties of CNTs

can be deeply modified by the presence of water. Water molecules were adsorbed in the CNTs and acted as electron donors (Zahab *et al.*, 2000). The conductivity type of the CNTs can be changed from p-type to n-type.

The oxygen gas sensing measurements of sample 1 and 2 demonstrated the function of the resistivity measurement part of the device. Therefore, the main work on this project concentrated on the potentiometric measurements.

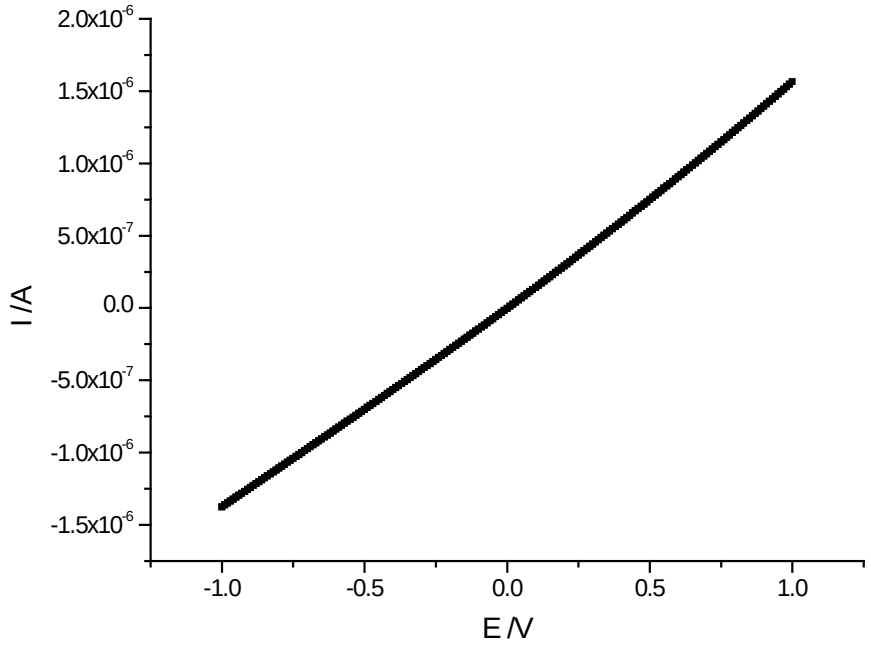

Fig. 39 Current-voltage curve of sample 1 (MWNTs drop coated interdigitated structure, 6-30)

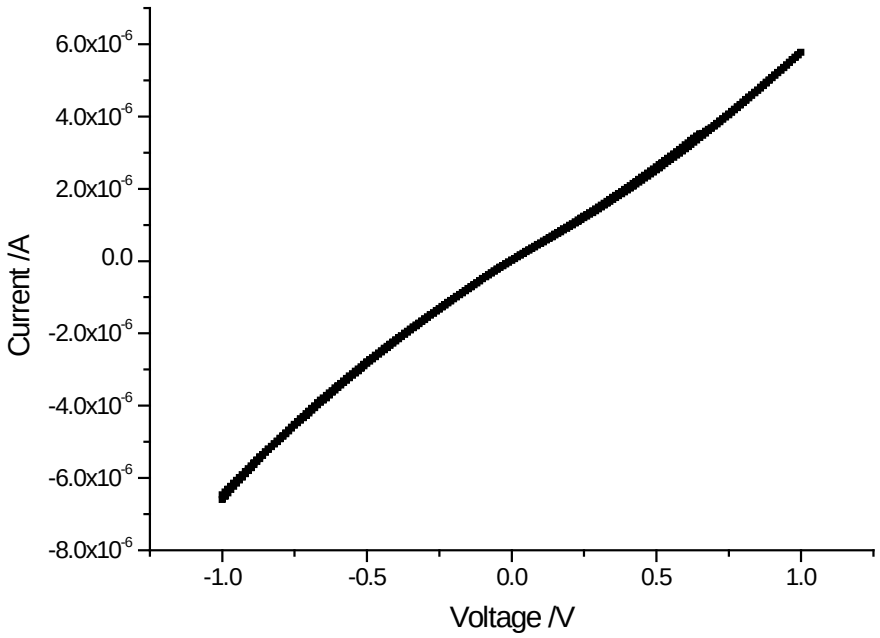

Fig. 40 Current-voltage curve of sample 2 (MWNTs drop coated interdigitated structure, 6-30)

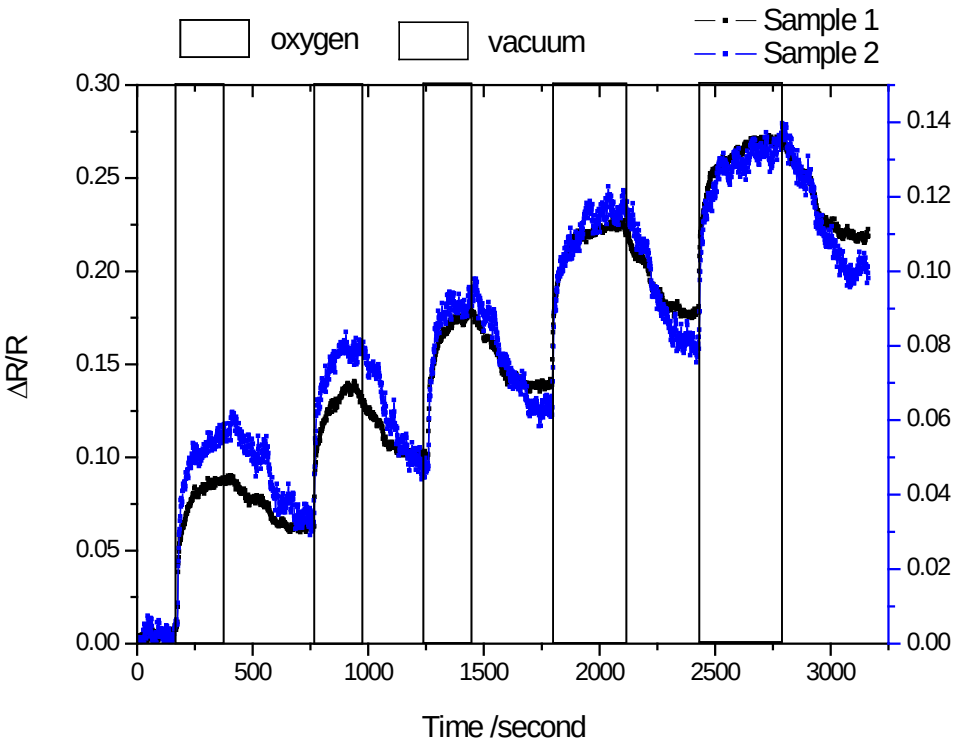

Fig. 41 Oxygen sensing tests with resistive measurements sample1 and 2

The capacitance-voltage (C-V) curves of both samples and a control substrate (no MWNTs coating) were carried out to investigate the gas sensitivity with potentiometric measurements. Leakage current measurements were performed to check the quality of the samples by using the GPES programme with the same connection as C-V measurement. An example of the leakage current-voltage plot is given in Fig. 42, where the small leakage current (-0.5 to 0.37 nA) indicated that the sample was of good quality. The capacitance-voltage (C-V) curves of both samples and a control substrate (no MWNTs coating) were plotted in Fig. 43. The C-V measurements showed a small increase of capacitance in the accumulation and inversion region with the introduction of MWNTs network. As MWNTs have a fairly large diameter, most of the nanotubes were probably not in touch with the Si_3N_4 surface, and not enough carbon nanotubes were distributed on the sample surface. The gas reactions therefore could not be monitored by potentiometric measurements.

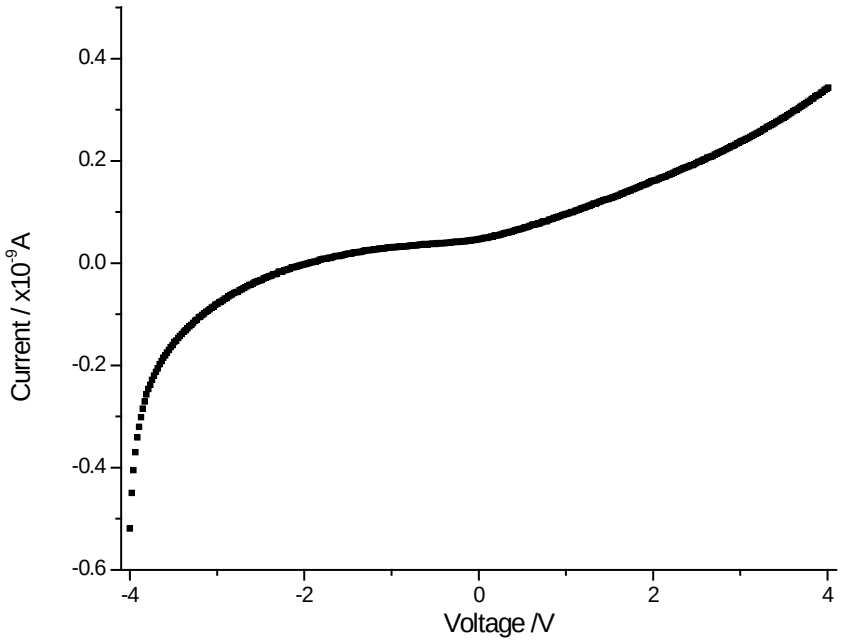

Fig. 42 Leakage current of the drop coated sample (sample 2).

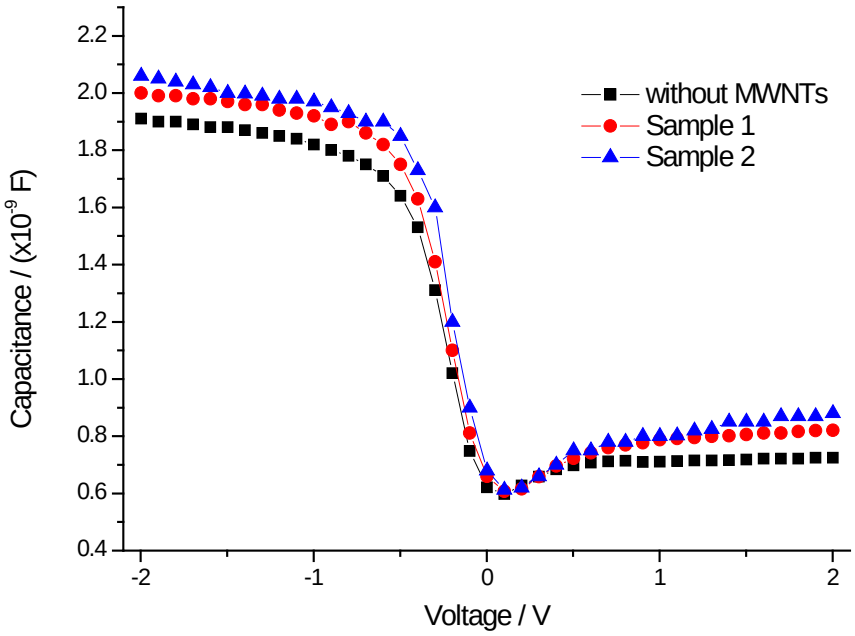

Fig. 43 C-V curves of the sample (interdigitated structure, 6-30) with and without MWNTs coating at a frequency of 1 kHz

There are two ways to improve the CNTs gate function in the sensing device: (i) reduce the gold electrodes area or (ii) increase the contact area between CNTs and the substrate surface. When the metal electrode area was reduced, the gate function would be dominated by the carbon nanotubes network. However, the two top gate electrodes could not be bridged by drop coating MWNTs when the interdigitated electrode structures were simplified to a two metal line structures. The contact area between CNTs and the substrate surface can be increased by replacing MWNTs with SWNTs because of the relative smaller diameter of SWNTs (Fig. 44).

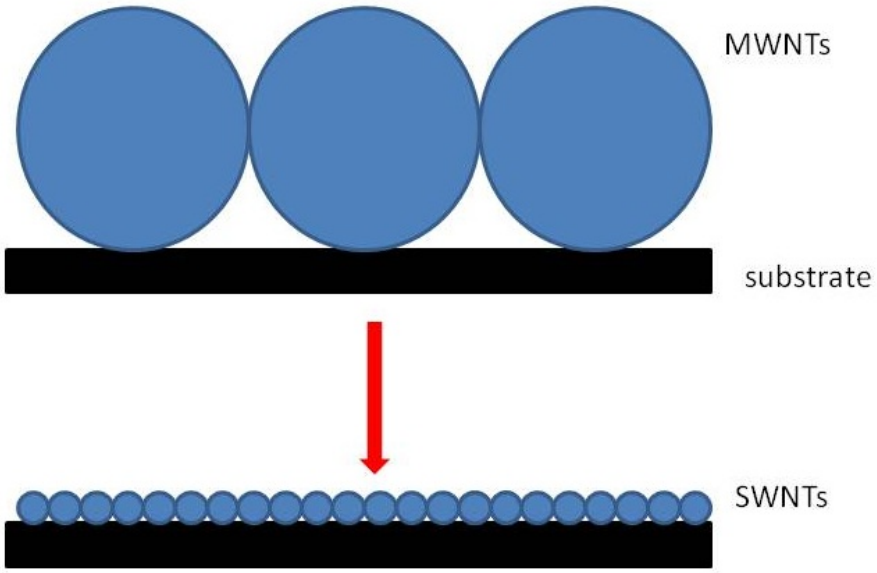

Fig. 44 Schematic of increase in contact area by replacing MWNTs with SWNTs

4.3 Drop Coated SWNTs

In order to increase the contact area between CNTs and the substrate surface, single walled carbon nanotubes (SWNTs) was used to replace the MWNTs. SWNTs were drop coated on the substrates ($Al/Si/SiO_2/Si_3N_4$, 6-30). C-V measurements were carried out to investigate the SWNTs gate function of the device. The leakage current measurements were also employed to check the quality of the sample after each drop of SWNTs. A field emission scanning electron microscope (FEI Inspect F, Oxford Instruments, UK) was used to study the distribution of SWNTs on the sample surface.

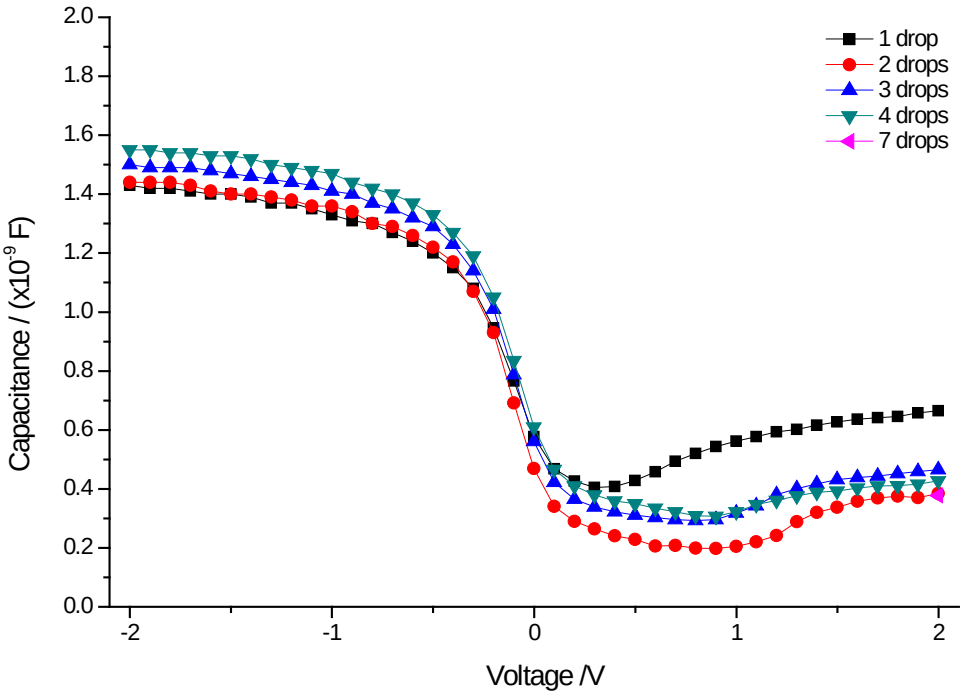

Fig. 45 C-V curves of drop coated sample (SWNTs, interdigitated structure, 6-30) with different amount of SWNTs at a frequency of 1 kHz

Sample with different amount of SWNTs (1-7 drops) were prepared. As shown in Fig. 45, gate function due to carbon nanotubes was not found in the depletion regions of the C-V curves for samples with 1-4 drops of SWNTs. The C-V curve

showed a ‘step’ in the depletion region with 7 drops of SWNTs. This ‘step’ indicated two different gate work functions: gold electrodes and CNTs, among which the carbon nanotubes network gate function could be explored by gas sensing measurements.

The leakage current was measured after each drop of the SWNTs. Samples with up to 4 drops of SWNTS showed a low leakage current (Fig. 46). A high leakage current at a magnitude of 10^{-6} A was detected for the sample coated with 7 drops of SWNTs (Fig. 47), which indicated a short circuit between the top gate electrodes and the back ohmic contact.

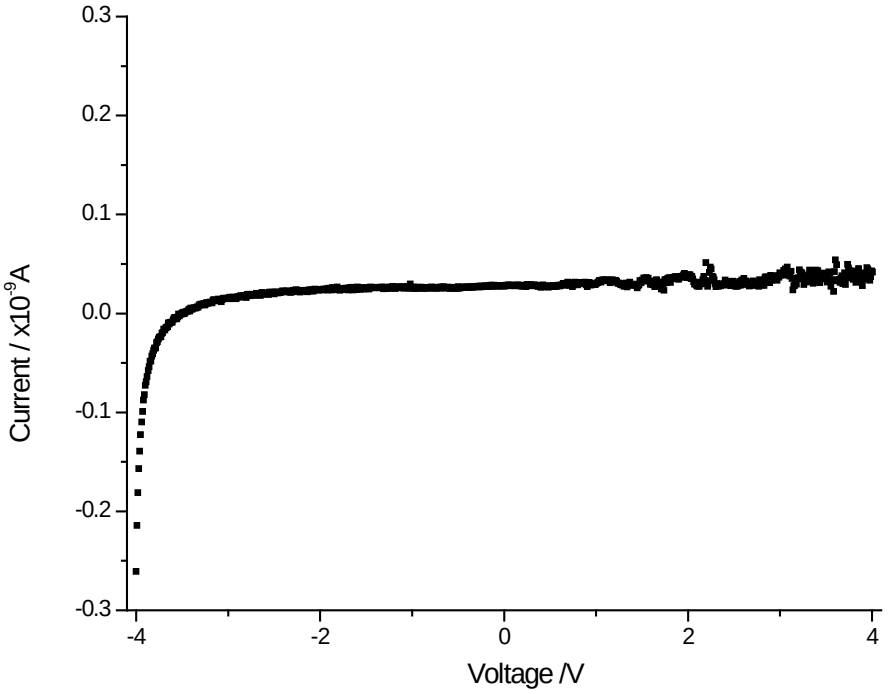

Fig. 46 Current-voltage plot of the drop coated sample (up to 4 drops of SWNTs, interdigitated structure, 6-30) showing a low leakage current

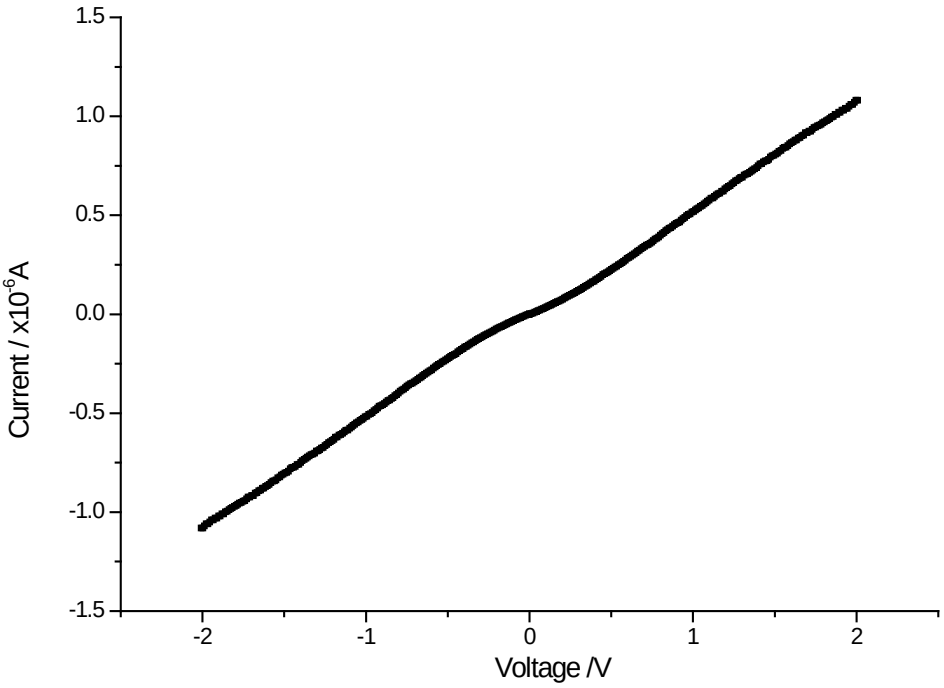

Fig. 47 Current-voltage plot of the drop coated sample (7 drops of SWNTs, interdigitated structure, 6-30) showing a high leakage current

The SWNTs drop coated sample (7 drops, with interdigitated structure, 6-30) was then gold coated and viewed using a field emission scanning electron microscope (FEI Inspect F, Oxford Instruments, UK) at an accelerating voltage of 10 KV and using secondary scanning electron imaging. The SEM images of the sample showed unevenly distributed SWNTs close to the gold electrode (Fig. 48). This is considered as a consequence of the coffee ring effect which suggested that drop coating with SWNTs could not produce an even CNTs films. Therefore, replacing the MWNTs with SWNTs could not achieve the desired properties.

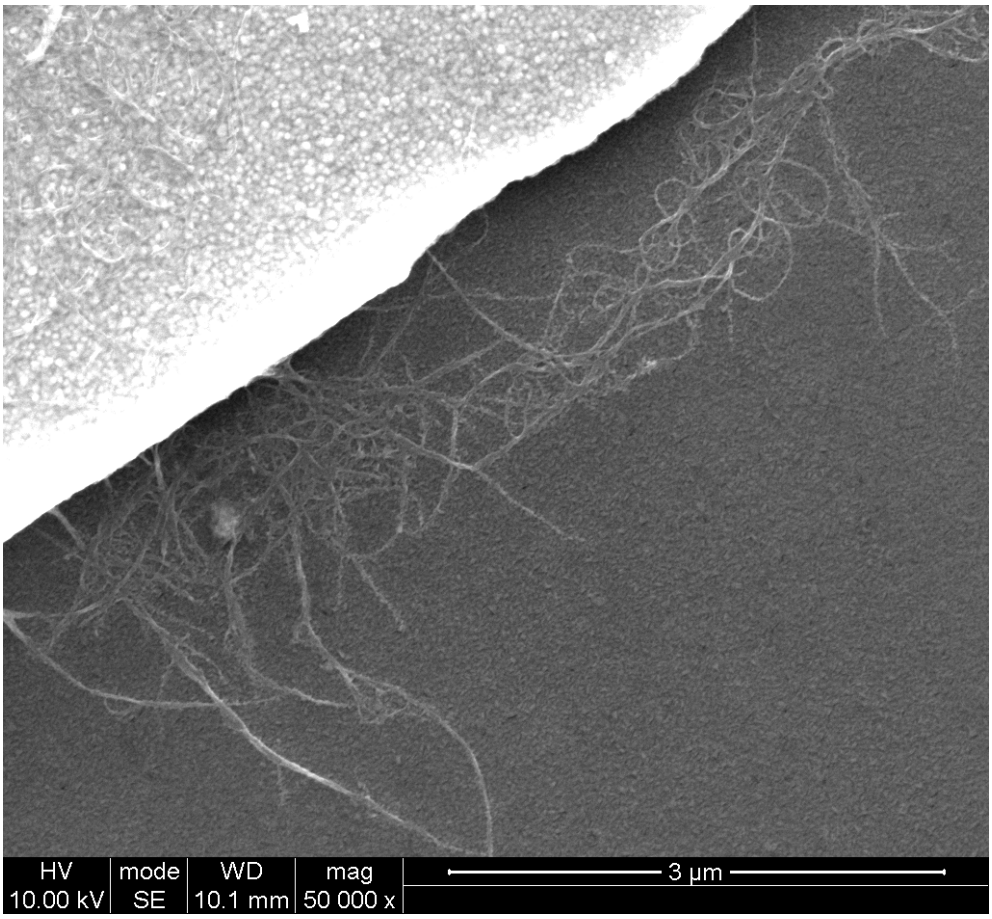

Fig. 48 SEM image of the SWNTs drop coated sample (interdigitated structure, 6-30).

Drop coating of carbon nanotubes (both MWNTs and SWNTs) on the Al/Si/SiO_2/Si_3N_4 substrates in this chapter successfully bridged the interdigitated structure of the two top gold gate electrodes. The CNTs gate function could not be identified in the C-V curves of tested samples until a relatively large amount of SWNTs was applied (Fig. 45). However, the increased number of SWNTs drops also led to a high leakage current which invalidated the sample for the potential sensor application. This suggested CNTs could be useful in detecting gas sensitivity, however, alternative methods which provide better CNTs coverage on the substrate surface without potential short circuit are desired. Spray coating was previously used in achieving CNTs coating (Watson *et al.*, 2005), it will therefore be used in current study.

4.4 Spray Coated SWNTs

Spray coating was employed to achieve an even SWNTs network. The SWNTs networks were using to bridge two different types of metal gate electrodes (6-30 and two-line).

4.4.1 Spray Coated Interdigitated Structure (6-30) with SWNTs

Sample with sprayed coat SWNTs on 6-30 metal gate structure were fabricated. SEM was employed to investigate the distribution of SWNTs on the sample surface. Sample quality was also checked by using leakage current measurements. The electronic property of the sample was tested by using C-V measurements. Oxygen and hydrogen sensitivity were also investigated using nitrogen as the carrier gas. Impedance spectroscopy was used to figure out the electrical properties that SWNTs network contributed on the sample.

The SWNTs were dispersed in DMF solution as described in CHAPTER 3.1.2. The SWNTs suspension was sprayed on Al/Si/SiO_2/Si_3N_4 substrates with interdigitated structure (6-30). The sprayed coated sample was viewed under a secondary electron microscope (FEI Inspect F, Oxford Instruments, UK). The secondary electron microphotograph of the spray coated interdigitated structure (6-30) is presented in Fig. 49. SWNTs were noticed on and between the gold electrode fingers. These carbon nanotubes were bundled and formed a multi-layer network.

The quality of the sample was checked by performing a leakage current measurement. The low leakage current indicated the good quality of the sample (Fig. 50).

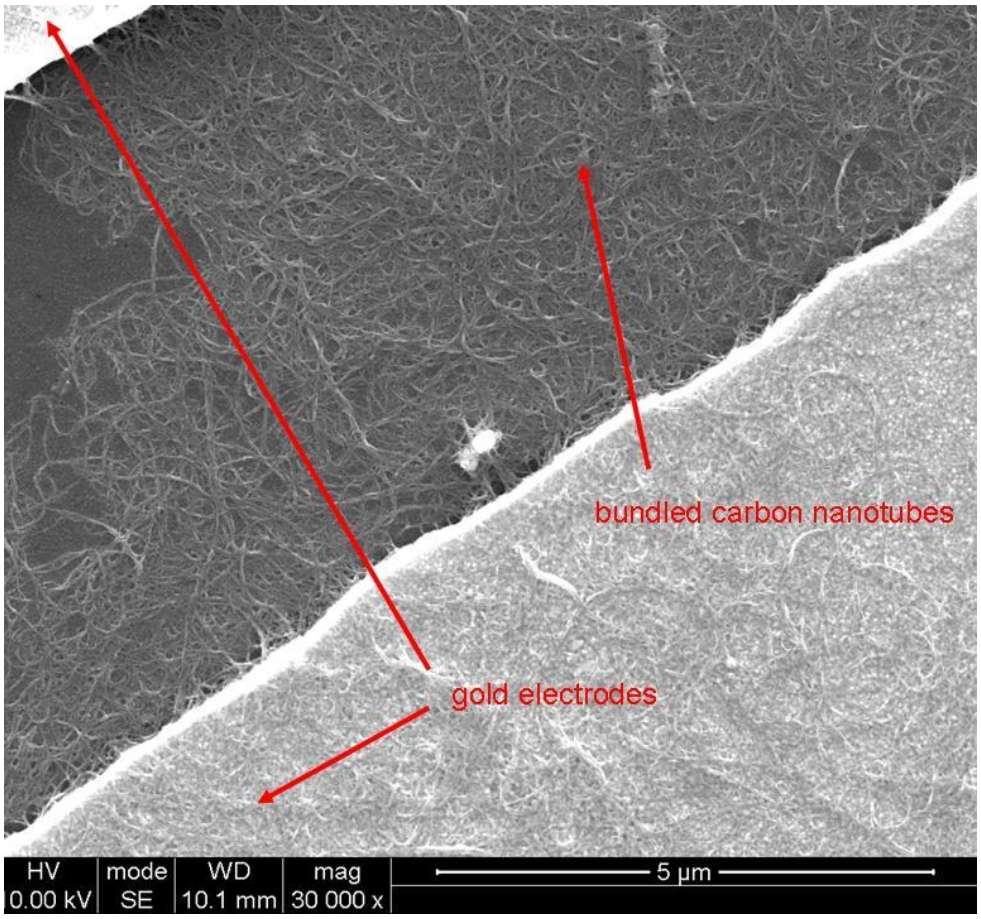

Fig. 49 SEM image of the SWNTs spray coated sample (interdigitated structure, 6-30)

The C-V curves of the interdigitated sample (6-30, spray coated with SWNTs) at different frequencies are presented in Fig. 51. A ‘step’ in the depletion region was found at all different frequencies. The first step next to the accumulation was related to the metal gate electrode and the second step was considered to be associated with the carbon nanotubes gate function. This type of sample could therefore be used to explore the gas sensitivity of carbon nanotubes network for potentiometric measurement.

A voltage ramp from -1 to 1 V with an increment of 0.01 V and an interval of 1 second per step voltage was applied between the two top gate electrodes. A linear current-voltage relationship was shown in Fig. 52. The SWNTs network

showed a metallic behaviour in terms of conductivity. The resistance of the SWNTs network was around 250 ohms.

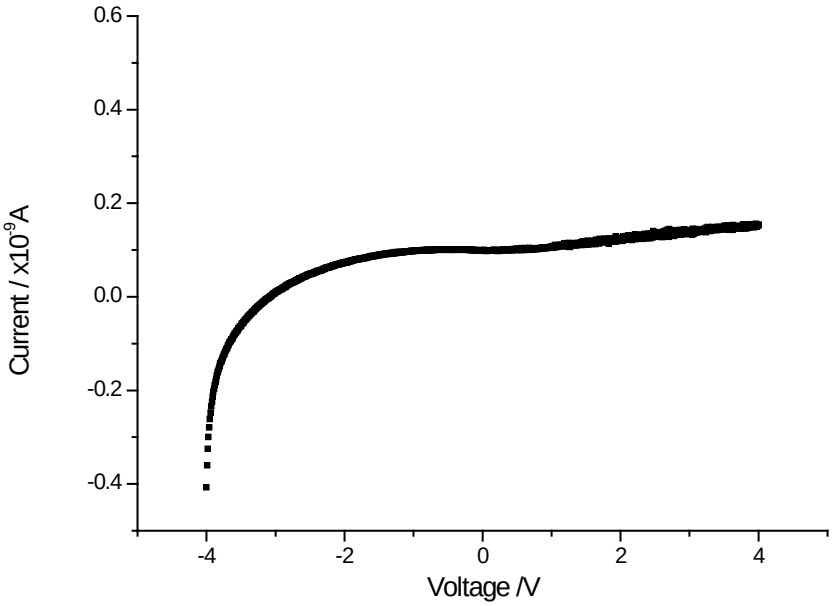

Fig. 50 Current-voltage plot of the SWNTs spray coated sample (interdigitated structure, 6-30) showing a low leakage current

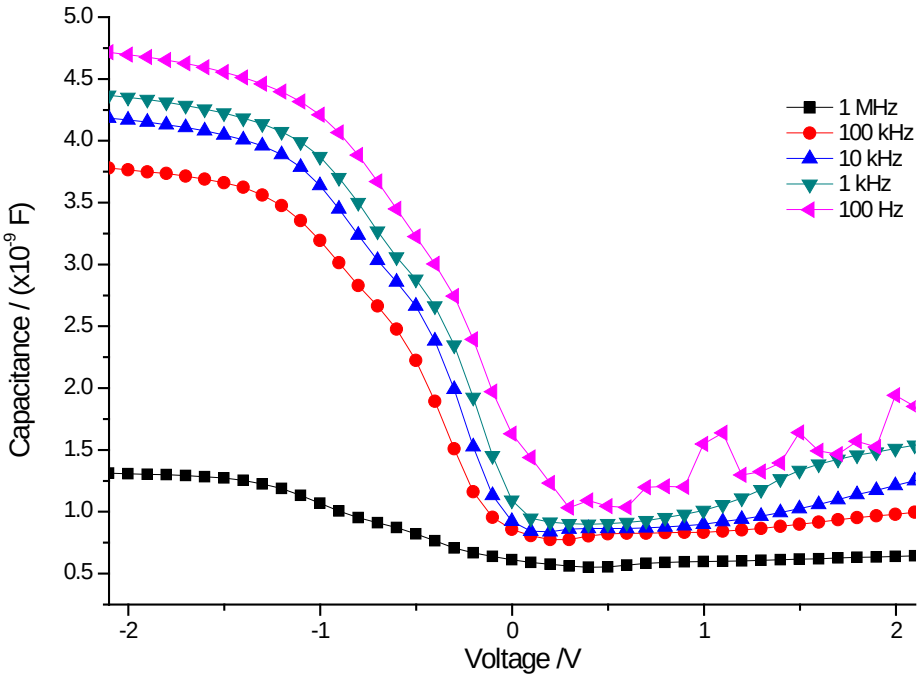

Fig. 51 C-V curves of the SWNTs spray coated sample (interdigitated structure, 6-30) at different frequencies.

Hydrogen and oxygen sensitivities were tested to investigate the reducing and oxidising gas conditions. The sample was placed in the testing box with 20 ppm H_2 mixed with N_2, and changed to 200 ppm H_2 mixed with N_2. The water chiller was set at a temperature of 10°C as described in Chapter 3.2. Therefore, a constant humidity of 9.4 g/L (9410 ppm, 0.94%) was mixed into the gas system. The equilibrium C-V curves of the specimens are shown in Fig. 53. Compared to 20 ppm H_2, an increase in the accumulation capacitance (approximately between -2 to -1.5 V) was observed when a higher H_2 concentration (200 ppm) was present (Fig. 53). This was probably due to the resistance change of the SWNTs network. For the depletion region, the part of the C-V curve associated with the gold electrode was the same, while the part associated with the carbon nanotubes (roughly in the range between -0.5 to 0.1 V) shifted towards lower voltages.

In order to explore the response time of the gas sensitive behaviour, C-V measurements were repeated in a voltage range of -0.5 to 0.1 V. Sample C-V curves at 20 ppm H_2 and different duration with 200 pm H_2 were plotted in Fig. 54. With the increase of H_2 concentration, a clear shift of the C-V curves towards a lower voltage was observed in 2 minutes. Further exposure to 200 ppm H_2 (up to 30 minutes) led to a continuous shift of the C-V curves. However, no clear shift was noticed with longer H_2 exposure. The voltage shifts of three samples were determined by linear interpolation at a capacitance of 2.0 x 10^{-9} F. The voltage-time relationship is presented in Fig. 55. An overall voltage shift of -50 mV was achieved 2 hours after the change of H_2 concentration (from 20 to 200 ppm). Approximately 30% (-15 mV) and 60% (-30 mV) of the change were achieved within the first 2 and 10 minutes respectively.

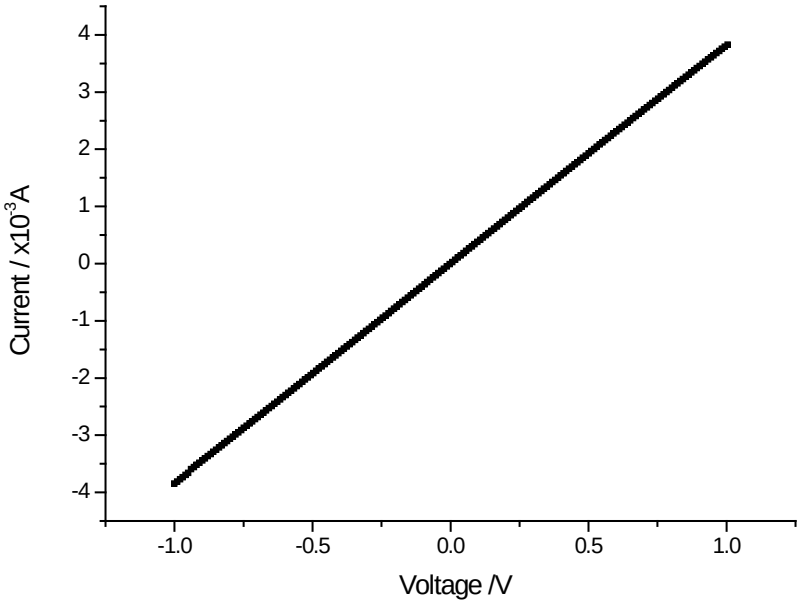

Fig. 52 Current-voltage curve of the SWNTs spray coated sample (interdigitated structure, 6-30)

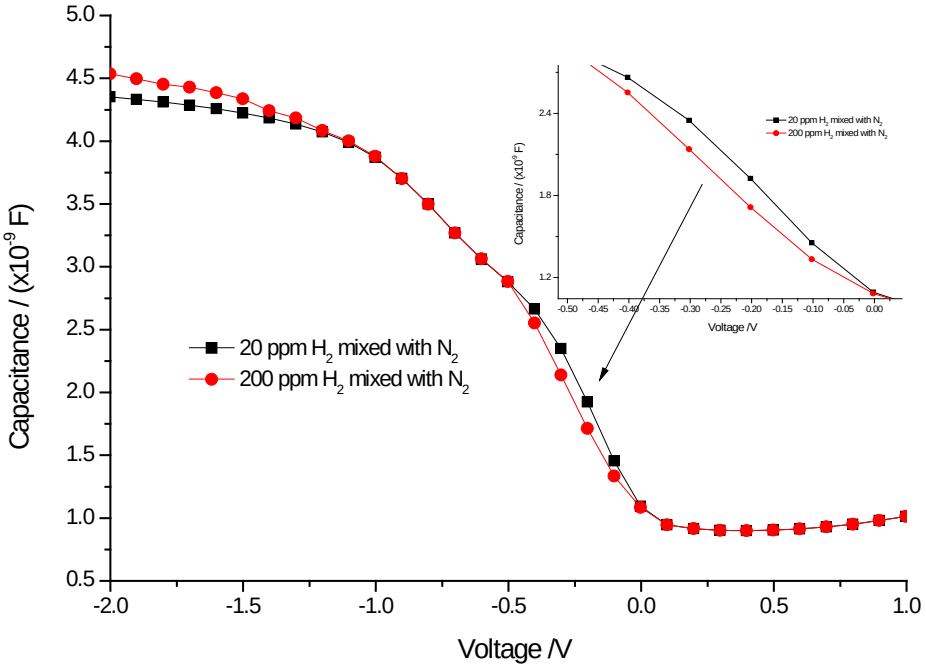

Fig. 53 C-V curves of the hydrogen reaction of the SWNTs spray coated sample (interdigitated structure, 6-30) at a frequency of 1 kHz

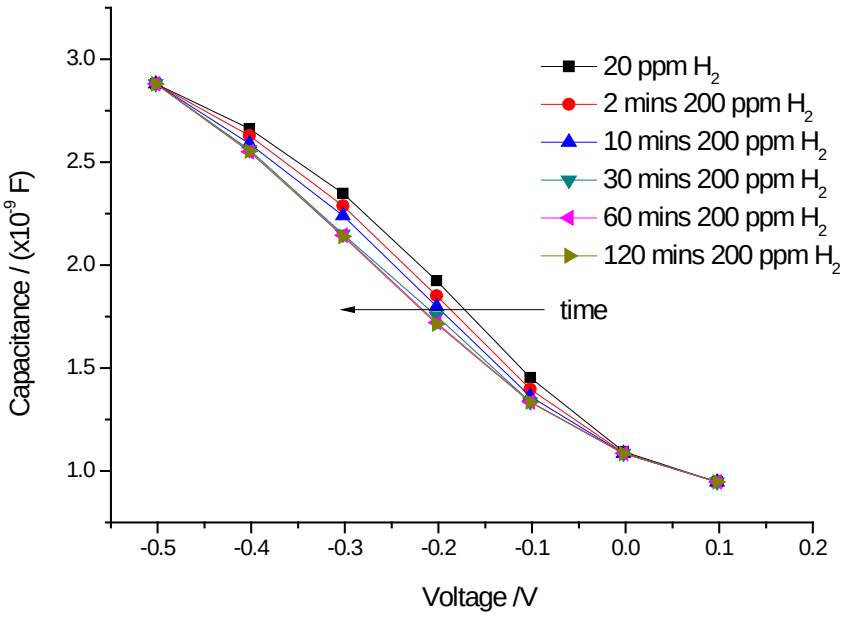

Fig. 54 C-V measurements of the hydrogen reaction of the SWNTs spray coated sample (interdigitated structure, 6-30) at a frequency of 1 kHz

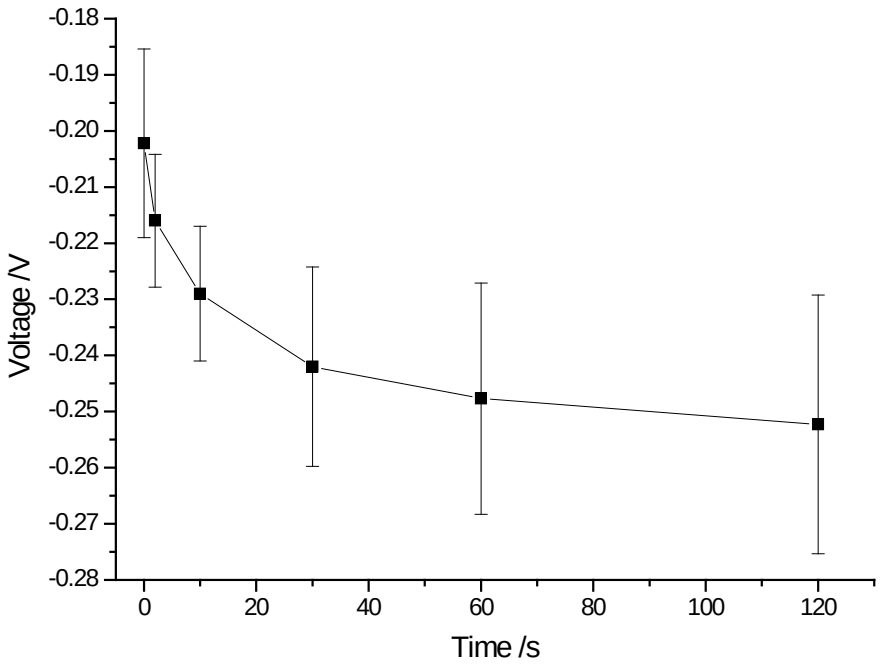

Fig. 55 Voltage-time relationship of the hydrogen reaction of the SWNTs coated sample with interdigitated structure, 6-30)

The test of oxygen sensitivities showed an increase in capacitance when the gas composition switched from a mixture of 1% O_2 with 99% N_2 to 100% O_2. The C-V curves moved to more positive voltages (Fig. 56). The capacitance increase in the accumulation and the depletion regions was nearly the same. The increase in the accumulation capacitance was due to the resistance change associated with the oxygen concentration. The voltage shifts of both parts of the C-V curve associated with the gold electrodes and the CNTs are similar. No oxygen sensitivity was previously documented for the MOS with gold electrodes. The voltage shifts of the gold electrodes part of the C-V curve in the current study was not a result of the oxygen sensitivity, but was attributed to the overall change in capacitance. Therefore, no significant oxygen sensitivity was demonstrated for the spray coated interdigitated structure (6-30) with SWNTs.

Nevertheless, similar to the hydrogen sensitivity study, C-V measurements were repeated in a voltage range of -0.5 to 0.1 V to investigate the response time of the oxygen induced shift of the C-V curve. With the increase of O_2 concentration (1% to 100%), a clear shift of the C-V curves towards a higher voltage was observed after 2 minutes (Fig. 57). Small continuous shifts were noticed with further exposure to 100% O_2 (up to 120 minutes). The shifts of each C-V curves were measured at a capacitance of 2.0 x 10^{-9} F and the voltage-time relationship for three samples was plotted (Fig. 58). An overall voltage shift of 25 mV (approximately) was achieved 2 hours after the O_2 concentration changed from 1% to 100%. Approximately 40% and 70% of the changes were achieved within the first 2 and 10 minutes respectively.

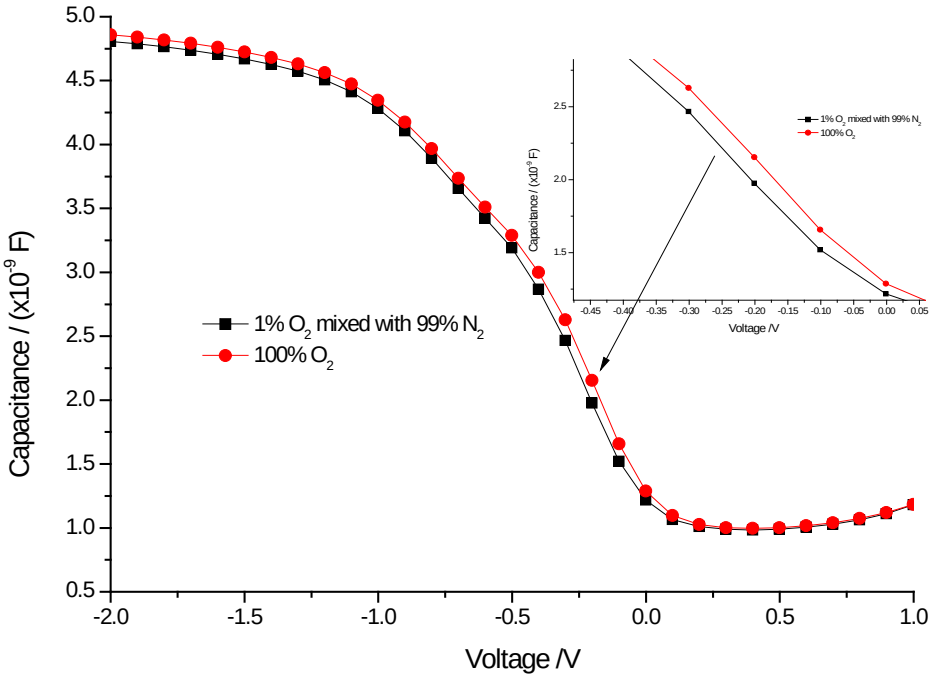

Fig. 56 C-V curves of the oxygen reaction of the SWNTs spray coated sample (interdigitated sample, 6-30) at a frequency of 1 kHz

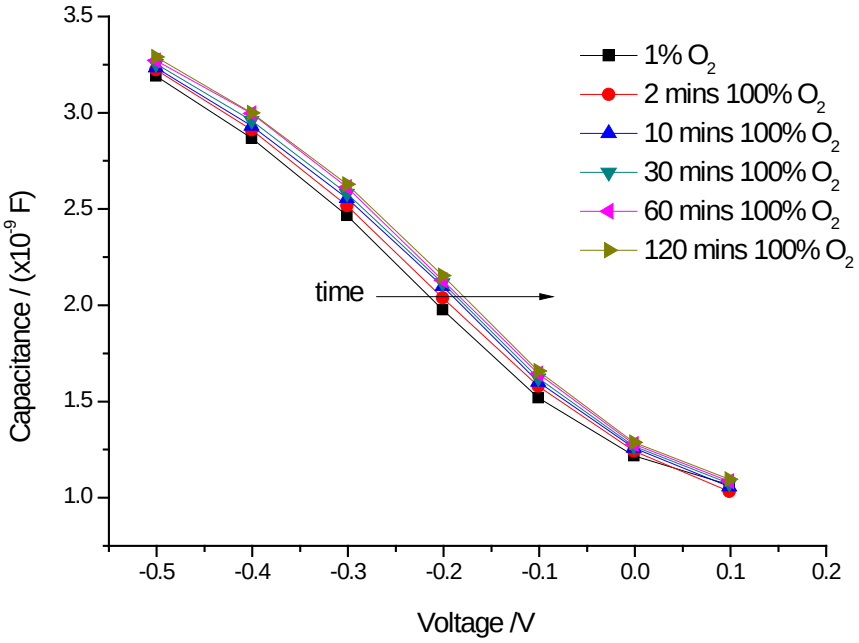

Fig. 57 C-V measurements at different time of the oxygen reaction of the SWNTs spray coated sample (interdigitated sample, 6-30) at a frequency of1 kHz

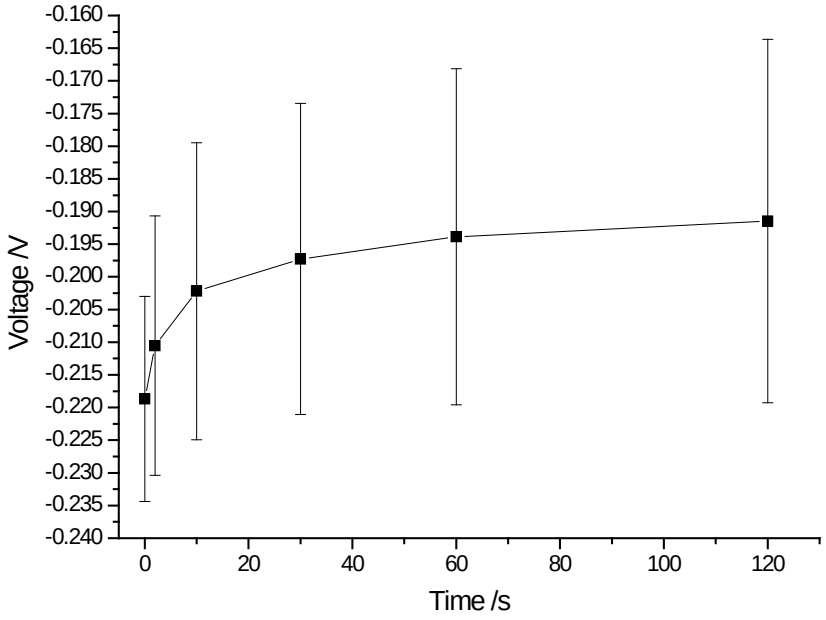

Fig. 58 Voltage-time relationship of the oxygen reaction of the spray coated sample (interdigitated structure 6-30)

Carbon nanotubes were spray coated on the Al/Si/SiO_2/Si_3N_4 substrates with interdigitated structure (6-30) in this chapter. Compared with drop coating, the spray coating introduced a more continuous CNTs layer (Fig. 49), which gave a traceable signal of the CNTs function in the C-V curves. The hydrogen and oxygen sensitivity of the sensor were evaluated at room temperature.

Traditional MIS capacitors with a palladium gate are typically used as hydrogen sensors at room temperature (Lundstrom *et al.*, 1975, Steele *et al.*, 1976). Hydrogen diffused through the Pd metal gate and formed a surface dipole layer at the metal-oxide interface modifying the work function of Pd which shifted the depletion voltage. A voltage shift of 1 V was reported in the C-V curves of Pd capacitive sensor with 50 nm SiO_2 and 10 nm Pd in response to 4% H_2 at 20°C. The response and recovery time were 10 seconds and 1 minute respectively (Steele *et al.*, 1976). In the present study, C-V curves shifted towards lower voltages with an increase in the H_2 concentration (Fig. 53). This is consistent with those found by Lundstrom *et al.,* (1975) and Steele *et al.,* (1976). However, the overall voltage shift (-50 mV) was not significant and the 2 hours response time was too long for a practical application.

The oxygen response of a field-effect capacitor/transistor at room temperature with Si_3N_4 as the insulator has not been reported in the literature. The MIS capacitive oxygen sensor could not operate at room temperature until LaF_3 ion conductor layer was introduced on the top of the Si_3N_4 (Krause *et al.*, 1993). Krause and Moritz prepared a Si/LaF_3/Pt oxygen sensor which gave fast and highly reproducible oxygen sensitivity at room temperature. A voltage shift of 58 mV was reported when the oxygen concentration increase from 7.5% to 52.5% with a response time of 90 seconds. The current study showed an overall voltage shift of 35 mV (approximately) after the O_2 concentration changed from 1% to 100%, however, the sensor response was too slow (2 hours) for practical use.

The absorption process of both hydrogen and oxygen molecules at the interface between the SWNTs and the insulator (Si_3N_4) was considered to be a physical rather than a chemical reaction. The charge transferred involved was generally weaker. Furthermore, the SWNTs were dispersed in DMF and sprayed coated on the substrate which was bundled as found using SEM. It would therefore take longer time for the hydrogen or oxygen molecule to diffuse through those bundled SWNTs. Well dispersed, debundled SWNTs and an ion conductor layer LaF_3 were expected to improve the gas sensitivity and response time.

Impedance Spectroscopy

Impedance spectroscopy was used to characterise the electrical properties of the samples. The sprayed coated sample (Al/Si/SiO_2/Si_3N_4/SWNTS, 6-30) was tested at a voltage of -1.5 V to investigate the sample in accumulation mode. The frequency was set between 1 Hz to 1 MHz with 50 logarithmic increments. Impedance spectra were recorded to display frequency response information.

The impedance and the phase angle of the tested sample at -1.5 V were plotted against frequency respectively (dots and crosses, Fig. 59). The impedance spectrum showed 3 different regions, at high and low frequencies, the sample showed capacitive properties with a phase angle close to 90°. While in a frequency range of 3.16 Hz to 316 Hz, the sample showed resistive properties.

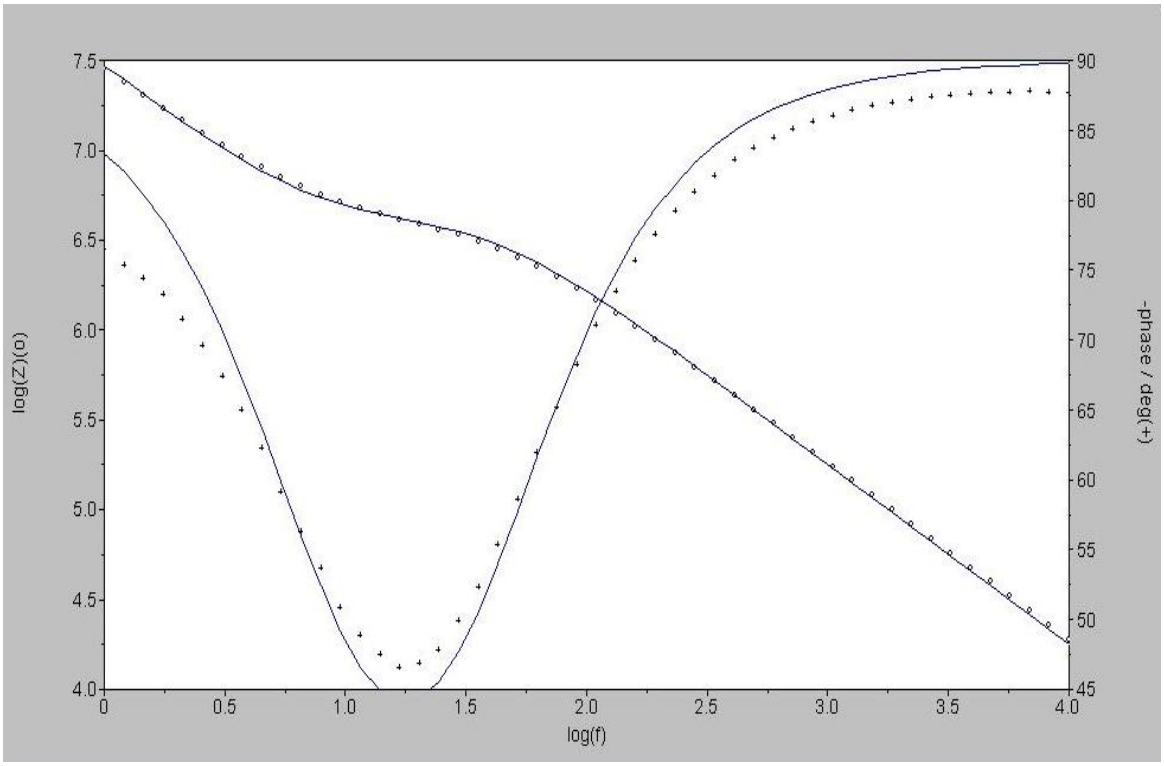

Fig. 59 Impedance spectrum of the sample (SWNTs spray coated, interdigitated structure, 6-30) at a voltage of -1.5 V, where the solid lines are the equivalent circuit fit.

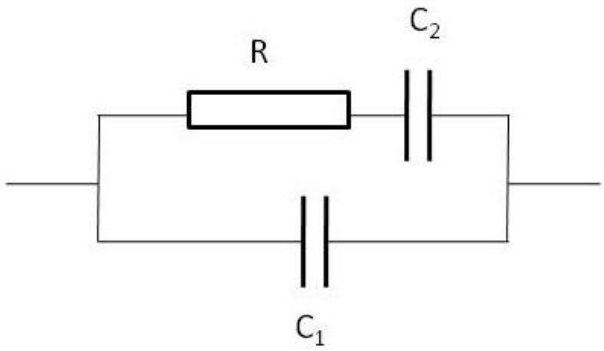

Fig. 60 Equivalent circuit of carbon nanotubes field-effect capacitor

An equivalent circuit was fitted using the FRA programme (Fig. 60). The parameters of the equivalent circuit for the spectrum at -1.5 V are listed in Table 5. C1 is assumed to be the accumulation capacitance under the gold electrodes, while C2 is assumed to be the capacitance of the SWNT network between the electrodes. R corresponds to the resistance of the SWNT network.

Table 5: Parameters of the equivalent circuits.

	C_1 (nF)	R (kohm)	C_2 (nF)
Sample at -1.5 V	12.2	22.73	7.57

The capacitance of the sample can be calculated by assuming the sample was a parallel plate capacitor. The area of gold electrodes and SWNTs network was the area of the parallel plate. The insulator contained two layers (SiO_2 and Si_3N_4). The electric field intensity between the two parallel plates can be calculated by assuming a positive charge on one plate and negative on the other. The electric flux density is independent of permittivity. Therefore, the electric flux density anywhere between the two plates can be calculated by using Gauss's Law. The electric field intensity in the various materials was calculated and then the electric field intensity was integrated to calculate the potential difference between the plates. Division of the assumed charge by the potential difference gave the capacitance.

From Gauss's laws, the electric flux density due to a plate carrying a charge Q is

$$\oint_s D\, ds = \rho_s = Q \tag{4.1}$$

Where ρ_s is the charge density on the upper plate. The latter equals the total charge on the plate, Q, divided by the area of the plate, S_{cap}. The electric flux density outside the capacitor and on the lateral sides of the Gaussian surface is zero. On s_1 the electric field intensity is the negative y direction as is ds, thus

$$\oint_S D\,ds = \int_{S_1} D \cdot ds = D_{S_1} = \frac{Q_{S_1}}{S_{cap}} \rightarrow D = -\hat{y}\frac{Q}{S_{cap}} \tag{4.2}$$

The electric field intensity everywhere is calculated by dividing D by ε. The electric fields in the three materials are;

$$E_{SiO_2} = -\hat{y}\frac{Q}{\varepsilon_{siO_2}\varepsilon_0 S_{cap}} \tag{4.3}$$

$$E_{Si_3N_4} = -\hat{y}\frac{Q}{\varepsilon_{Si_3N_4}\varepsilon_0 S_{cap}} \tag{4.4}$$

where ε_0 is the vacuum permittivity, approximately 8.8542 x 10^{-12} F/m^2,

The potential across the capacitor is (E and dl are in opposite directions):

$$V = -\int_0^{y_2} E \cdot dl = -\int_0^{y_1} (-E_{SiO_2} dy) - \int_{y_1}^{y_2} (-E_{Si_3N_4} dy) \tag{4.5}$$

Substituting the various values gives,

$$V = \frac{Q}{\varepsilon_0 S_{cap}} \int_0^{y_1} \frac{dy}{\varepsilon_{siO_2}} + \int_{y_1}^{y_2} \frac{dy}{\varepsilon_{Si_3N_4}} = \frac{Q}{\varepsilon_0 S_{cap}} \left(\frac{y_1}{\varepsilon_{siO_2}} + \frac{y_2 - y_1}{\varepsilon_{Si_3N_4}}\right) \tag{4.6}$$

The capacitance of the two-layer capacitor is therefore

$$C = \frac{Q}{V} = \frac{\varepsilon_0 s_{cap}}{\frac{y_1}{\varepsilon_{siO_2}} + \frac{y_2 - y_1}{\varepsilon_{Si_3N_4}}} \quad (4.7)$$

The accumulation capacitance of the sample was calculated 3.39 x 10^{-9} F, where s_{cap} is approximately 3.5 x 10^{-6} m^2, y_1 is 20 nm, y_2 is 50 nm, ε_{siO_2} is 3.9 and $\varepsilon_{Si_3N_4}$ is 7.5.

The calculated accumulation capacitance value (3.39 nF) using the real metal gate electrodes area is smaller than the fitted capacitance C1 (12.2 nF). This might be caused by the electric field between the gold finger electrodes and the SWNTs. Assuming the presence of an electric field and SWNTs, we could consider the interdigitated electrodes area as a continuous electrode, the area of the plate s_{cap} was therefore 11 x 10^{-6} m^2. The calculated accumulation capacitance was then 10.7 nF, which was close to the fitted value (12.2 nF). The CNTs coated area was the area that o-ring exposed on the sample surface. Therefore, the area s_{cap} was then 16.13 x 10^{-6} m^2. The calculated accumulation capacitance was then 15.6 nF, which was larger than the fitted value (12.2 nF). This means that C2 cannot be interpreted as the capacitance of the SWNT network between the fingers of the interdigitated structure, but as the capacitance of SWNTs that were spray coated outside the interdigitated structure. This would also explain why the fitted value of R is about 100 times greater than the resistance measured previously (see Fig. 37).

4.4.2 Spray Coated Two-line Structure with SWNTs

Sample with sprayed coat SWNTs on two-line metal gate structure were fabricated. SEM was employed to investigate the distribution of SWNTs on the sample surface. The electronic property of the sample was tested by using C-V measurements. Oxygen and hydrogen sensitivity were also investigated using nitrogen as the carrier gas.

The SWNTs were dispersed in DMF solution as described in CHAPTER 3.1.2. Compared with the interdigitated structure (6-30), the two-line structure required a longer spray coating process to bridge the gold electrodes on the $Al/Si/SiO_2/Si_3N_4$ substrates in order to keep the resistance of the network low. This was expected to yield a thicker CNTs layer.

The secondary electron microphotograph of a spray coated two-line structure sample with SWNTs is given in Fig. 61. A multi-layer carbon nanotubes network was clearly visible where the carbon nanotubes were bundled. However, compared to microstructure of the spray coated interdigitated structure (6-30) (Fig. 49), the difference in the thickness of SWNTs layer could not be quantified.

The capacitance-voltage curves of the two-line structure sample spray coated with SWNTs at different frequencies suggested a decrease in the capacitance of the accumulation region with an increase in frequency (Fig. 62). The depletion regions were clearly separated into two distinct parts at all different frequencies. The part next to the accumulation was related to the metal gate electrode, where the capacitance did not change significantly with frequency change. The second part showed a remarkable capacitance change which was considered to be associated with the carbon nanotubes gate function. The ‘step’ in the depletion region for the spray coated two-line structure sample (with SWNTs) is clearly more significant than that in the spray coated sample with an interdigitated gold

electrode structure (6-30) (Fig. 51). This is considered to be a consequence of the reduced surface area of the gold electrodes and the increased distance between them.

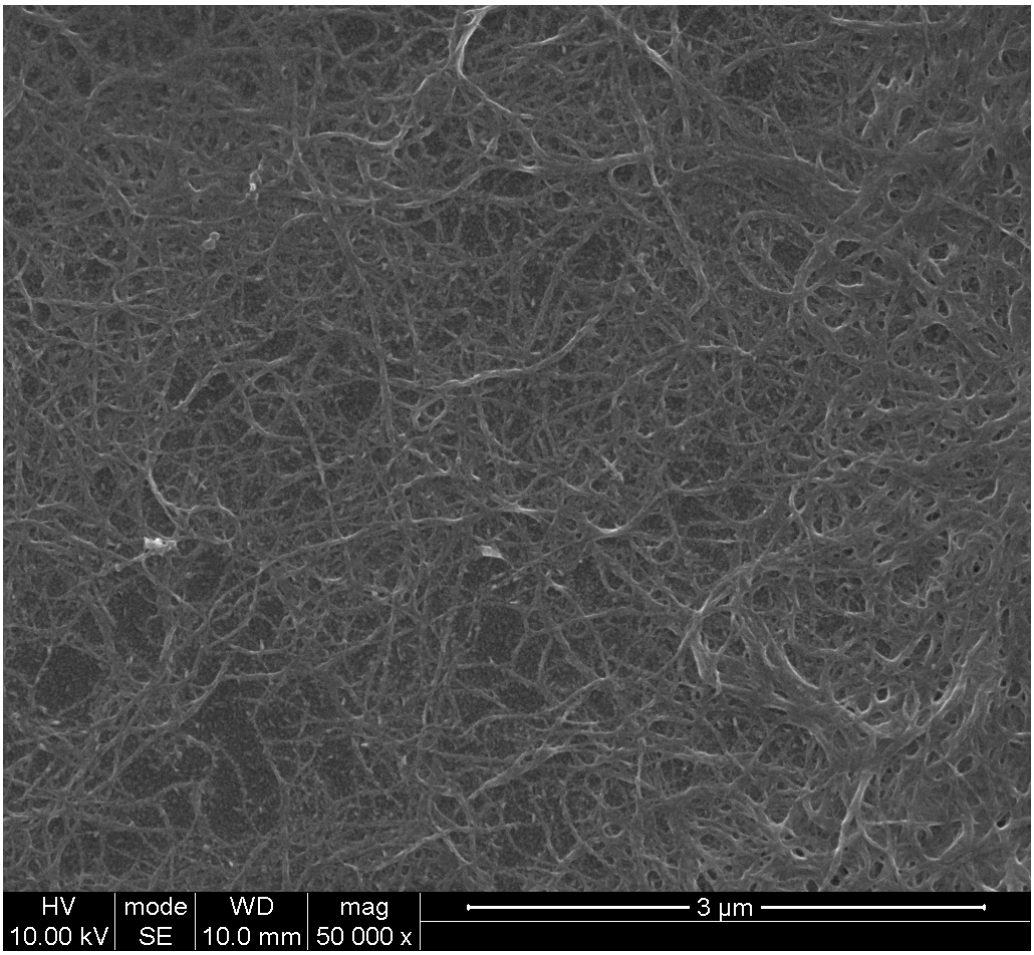

Fig. 61 SEM image of spray coated SWNTs network on two-line structure.

The curve measured at a frequency of 1 kHz demonstrated the highest nanotubes gate function contribution without introducing excess noise. This was in good agreement with the experimental results presented in section 4.1. Hydrogen and oxygen reaction of the spray coated two-line sample with SWNTs were therefore measured at a frequency of 1 kHz. The equilibrium C-V curves of

the specimens in different H_2 gas concentrations are shown in Fig. 63 and Fig. 65.

The accumulation capacitance increased and the carbon nanotubes part of the depletion region shifted towards lower voltages when the H_2 concentration switched from 20 ppm to 200 ppm (Fig. 63). C-V measurements were repeated and the voltage shifts of each curve were quantified at a capacitance of 5.0 x 10^{-9} F. The voltage-time relationship was plotted in Fig. 64. An overall voltage shift of -50 mV was achieved 2 hours after the H_2 concentration change from 20 to 200 ppm. Approximately 20% (-10 mV) and 40% (-20 mV) of the changes were achieved within the first 2 and 10 minutes respectively. The overall voltage shift in 2 hours was similar to the one obtained with spray coated interdigitated structure (6-30); however, the voltage shifts in the same time period (2 and 10 minutes) were smaller (Fig. 55). This could be explained by the amount of spray coated SWNTs on the substrate surface. Longer spray coating for the two-line structure was expected to deposit more SWNTs on the substrate surface when compared to the interdigitated structure. The thicker SWNTs layer resulted in longer equilibration time for the hydrogen molecules to diffuse into the SWNTs network.

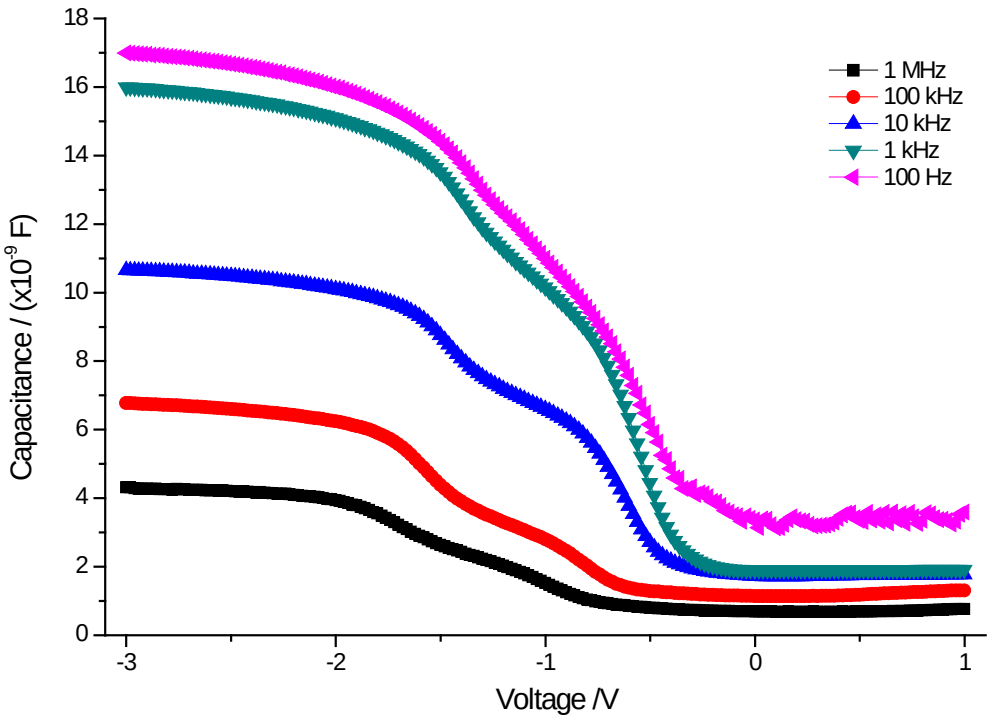

Fig. 62 C-V curves of SWNTs spray coated sample (two-line structure) tested at different frequencies.

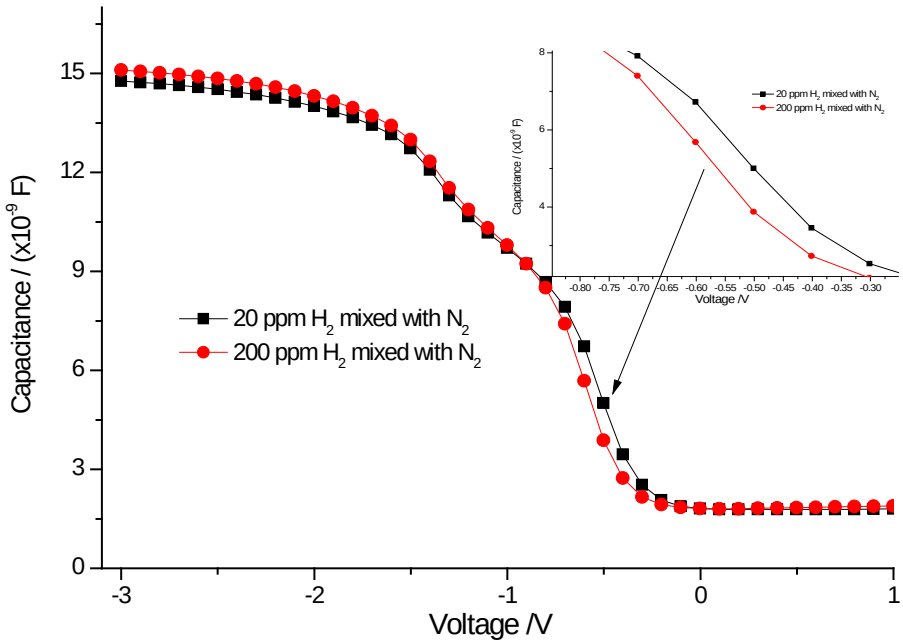

Fig. 63 C-V curves of the hydrogen reaction of the SWNTs spray coated sample (two-line structure) at a frequency of 1 kHz.

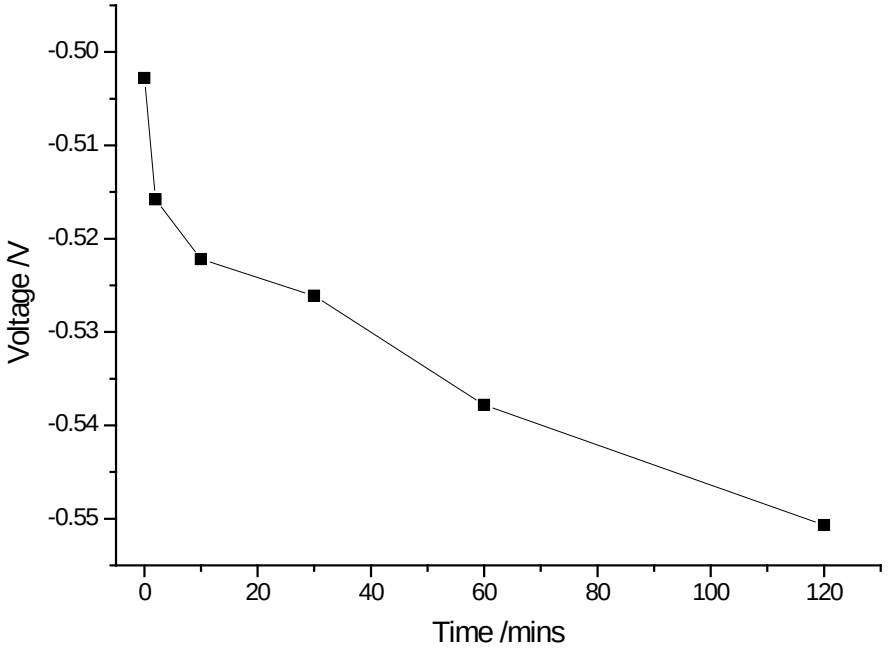

Fig. 64 Voltage-time relationship of the hydrogen reaction of SWNTs spray coated sample (two-line structure)

The C-V curve of the oxygen sensitivity test of the spray coated two-line structure sample is given in Fig. 65. A small increase in the accumulation capacitance and a shift of the C-V curve towards higher voltages were noticed when the O_2 concentration increased from 1% to 100%. C-V measurements were repeated and the voltage shifts of each curve were quantified at a capacitance of 4.8×10^{-9} F. The voltage-time relationship was plotted in Fig. 66. An overall voltage shift of 24 mV was achieved 2 hours after the O_2 concentration changed from 1% to 100%. Approximately 30% (6.7 mV) and 50% (11.5 mV) of the change were achieved within the first 2 and 10 minutes respectively. Compared with the results for the spray coated interdigitated structure (6-30) in Chapter 4.4.1, the overall voltage change for the two-line structure was slightly smaller, and the voltage shifts in the same time period (2

and 10 minutes) were also smaller (Fig. 58). This is consistent with the hydrogen response results and the reason is as explained previously.

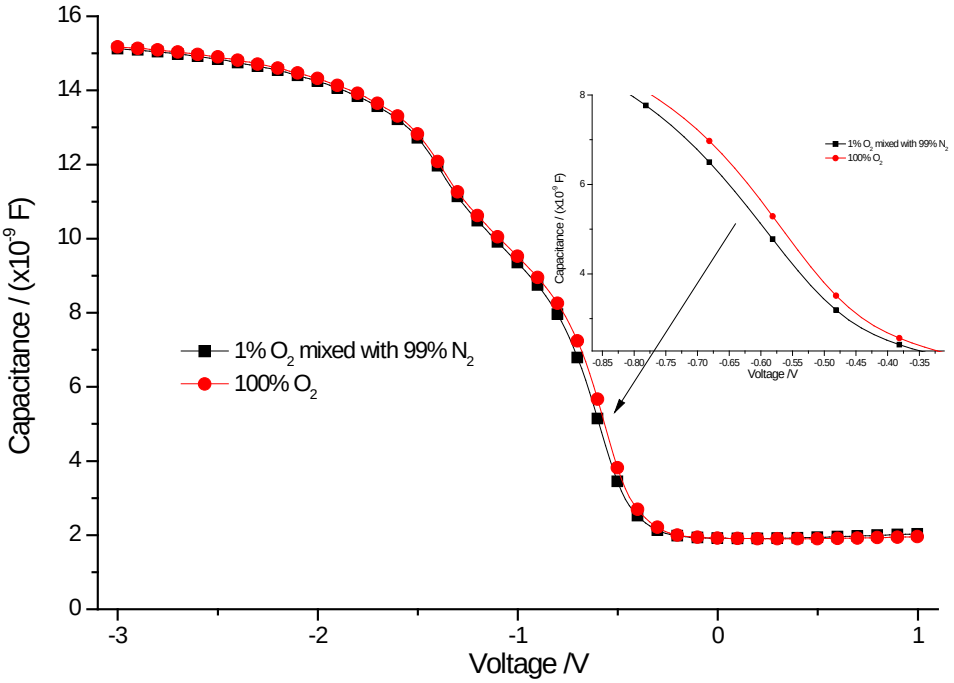

Fig. 65 C-V curves of the oxygen reaction of the SWNTs spray coated sample (two-line structure) at a frequency of 1 kHz.

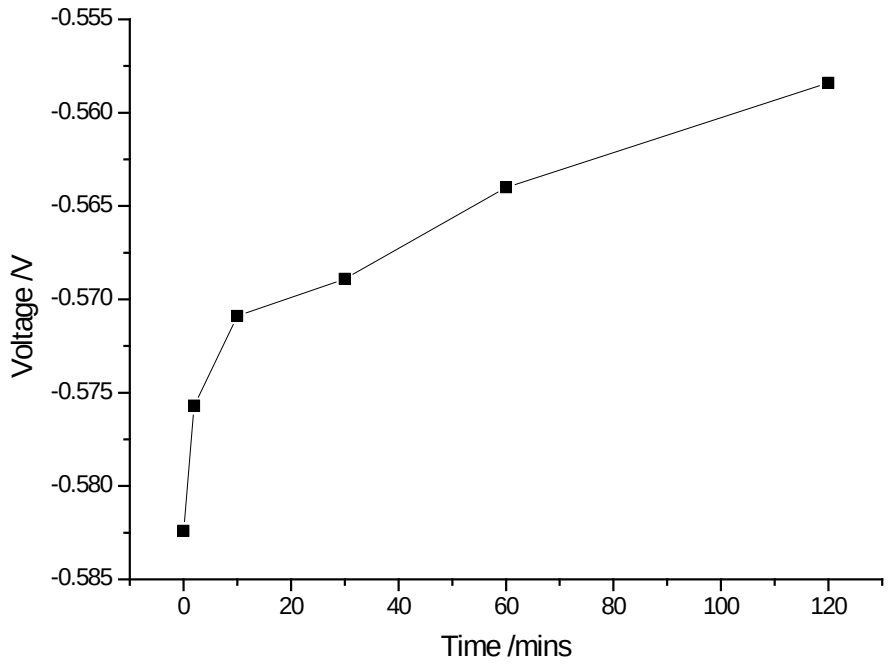

Fig. 66 Voltage shifts-time relationship of the oxygen reaction for the SWNTs spray coated sample (two-line structure)

In conclusion, the shifts of the carbon nanotubes part of the depletion region of the C-V curve were gas dependent. An increase in the oxidising gas (O_2) concentration shifted the depletion region of C-V curves to positive voltages and an increase in the reducing gas (H_2) concentration shifted the depletion region of C-V curves to more negative voltages. The voltage shifts were considered to be influenced by the thickness of the CNTs network where a thinner CNTs network resulted in a shorter response time. The response time was related to the diffusion of the gas molecules.

4.5 Spray Coated SWNTs on a LaF_3-substrate

LaF_3 was introduced to the structure as an ion conductor to improve the gas response of the sensor. A LaF_3 layer on the top of $Al/Si/SiO_2/Si_3N_4$ should increase the possibility of the reaction at the three phase boundary (gas, SWNTs and LaF_3).

4.5.1 AFM Images of the Debundled CNTs with SDS Suspension

SWNTs were dispersed in SDS aqueous solvent. The detergent was used to separate the SWNTs so as to minimise the SWNTs bundling. The debundled SWNTs were expected to increase the reaction speed by avoiding the diffusion effect.

The substrate ($Al/Si/SiO_2/Si_3N_4/LaF_3$) was spray coated with SDS debundled carbon nanotubes. The specimen was viewed using an Atomic Force Microscope. Individual carbon nanotubes were present, which suggested the SDS had a positive effect on defund the SWNTs. A 2D image of an individual carbon nanotube is given in Fig. 67. The individual CNTs demonstrated a nanometre scale dimension (in height), which was not even throughout the carbon nanotube. A more detailed 3D image (Fig. 68) suggested a rough surface of the debundled individual carbon nanotube. The difference in the dimension might be attributed to the attached particles such as SDS and amorphous carbon.

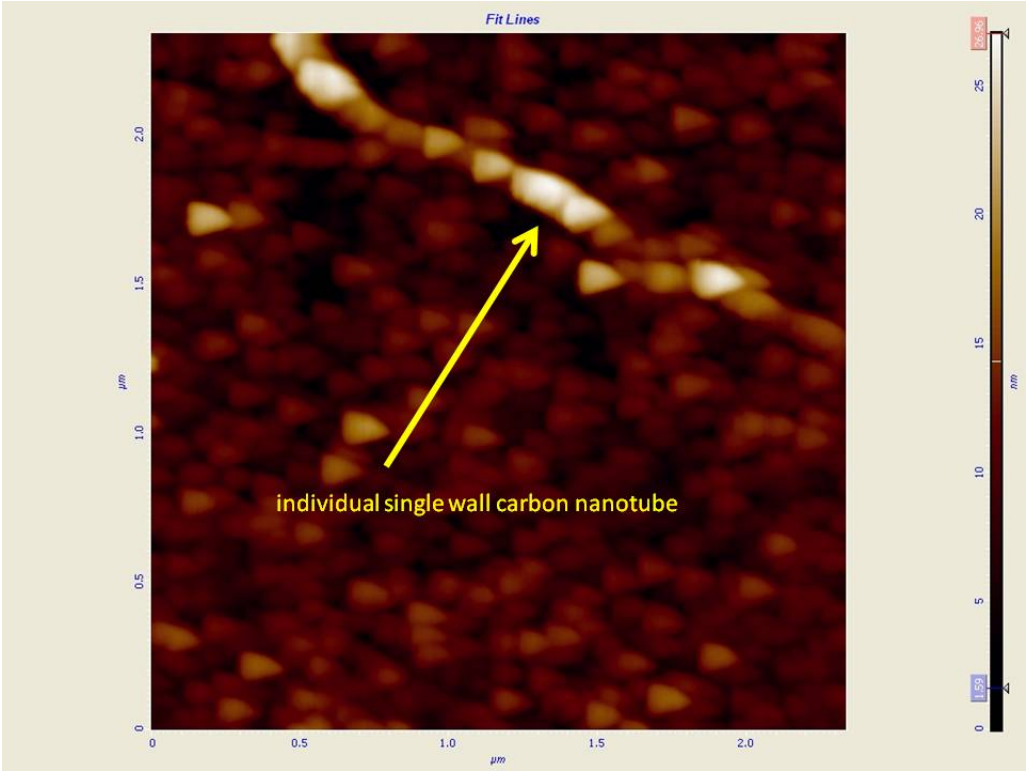

Fig. 67 2-D AFM image of an individual carbon nanotube

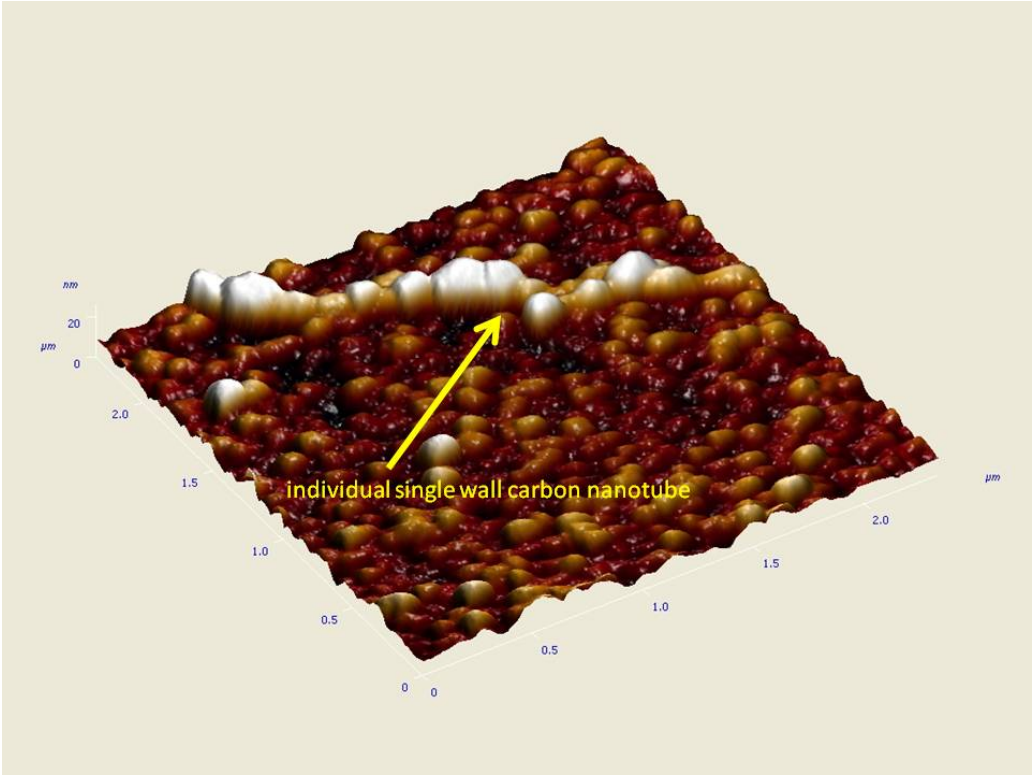

Fig. 68 3D simulation of an individual carbon nanotube

4.5.2 Gas Sensitivity Test of the Spray Coated LaF_3-substrate

4.5.2.1 LaF_3-Substrate with Interdigitated Electrodes

The SWNTs/SDS suspension was sprayed on the substrate with interdigitated electrodes (Al/Si/SiO_2/Si_3N_4/LaF_3, 6-30). The sample was placed in the testing box with 20 ppm H_2 mixed with N_2 for 2 hours before the C-V measurement was carried out. The hydrogen concentration was then increased to 200 ppm and held for 2 hours. The C-V curves under both hydrogen concentrations were plotted (Fig. 69). An increase in the accumulation capacitance was noticed with increased H_2 concentration. For the depletion region, the capacitance of the gold electrode was dominant. The voltage shifts in the depletion region associated with carbon nanotubes was negligible. In contrast, a voltage shift in the carbon nanotube part was observed for the spray coated interdigitated electrodes without LaF_3 (Al/Si/SiO_2/Si_3N_4, 6-30) (Fig. 53). This might be due to the presence of SDS particles. The SDS was introduced to debundle the SWNTs, however, the SDS particles might also lead to an additional layer on top of the SWNTs as suggested in Fig. 68. This SDS layer might block the SWNTs and inhibit the gas reaction at the three phase boundary (gas, SWNTs and LaF_3).

Similar to the hydrogen test, the gas concentration was changed from 1% O_2 (mixed with N_2) to 100% O_2 for oxygen sensitivity measurement. C-V curves were measured after 2 hours in each gas concentration. With an increase in O_2 concentration, a small decrease in the accumulation capacitance was observed (Fig. 70). No voltage shift in the gold electrode part of the depletion region was noticed, while a very small voltage shift in the CNTs part was found which could be negligible. This was similar to the hydrogen sensitivity study.

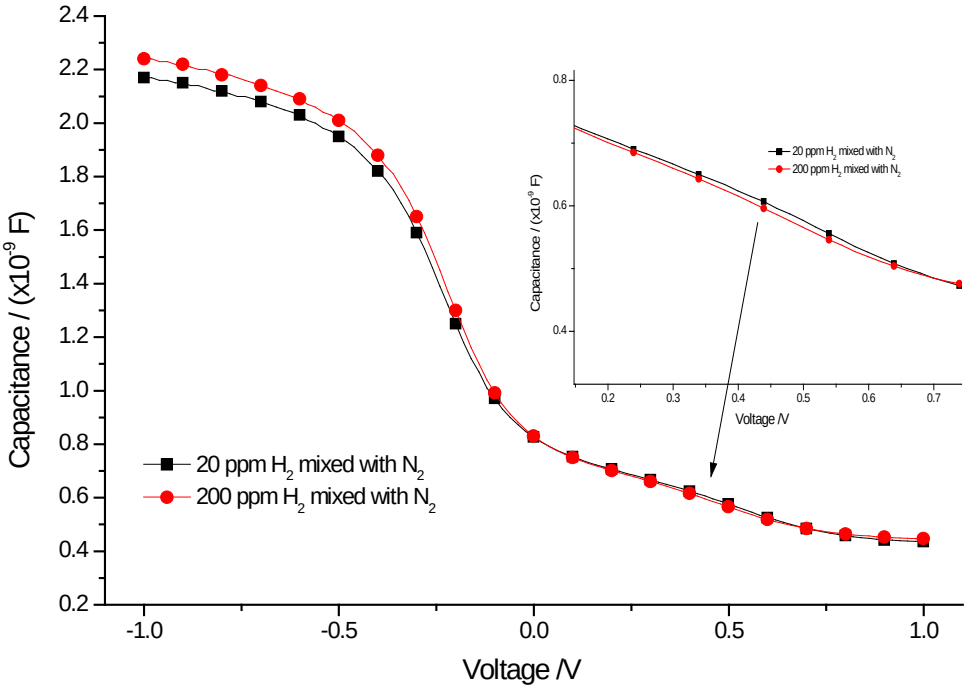

Fig. 69 C-V curves of the hydrogen reaction of the spray coated sample (SWNTs/SDS, LaF_3-substrate, interdigitated structure, 6-30) at a frequency of 1 kHz.

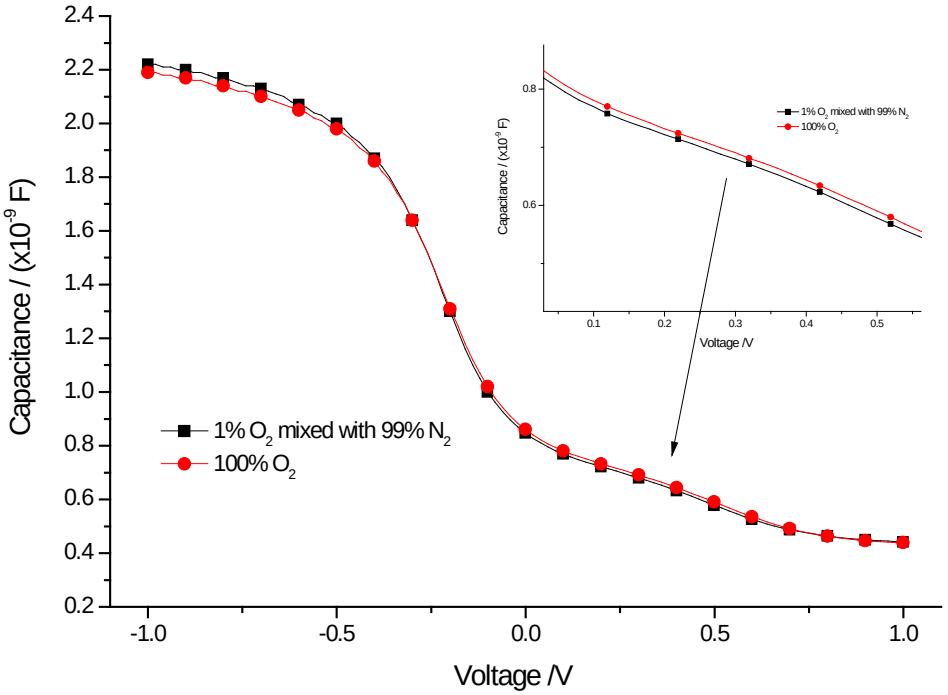

Fig. 70 C-V curves of the oxygen reaction of the spray coated sample (SWNTs/SDS, LaF_3-substrate, interdigitated structure, 6-30) at a frequency of 1 kHz.

Both hydrogen and oxygen sensitivity studies did not give the increase in the sensitivity as expected. This is most likely due to the presence of the SDS molecules which covered the SWNTs surface and inhibited the gas response.

4.5.2.2 LaF_3-Substrate with two-line Structure

The SWNTs/SDS suspension was prepared and sprayed on the two-line substrate (Al/Si/SiO_2/Si_3N_4/LaF_3, two-line). Hydrogen sensitivity tests were performed by increasing the H_2 concentration from 20 to 200 ppm. The C-V curves were measured after 2 hours in each concentration. A decrease in the accumulation capacitance with increased H_2 concentration was observed (Fig. 71). The capacitance change caused an apparent shift of the C-V curves. When we look at individual voltages, the capacitance change in the accumulation and the gold part of the curve is similar. However, the change in the CNT part of the C-V curve is greater than that observed in the accumulation and the gold dominated part of the curve. This indicated that there was a voltage shift towards lower voltages with the increase in H_2 concentration.

The voltage-time relationship was evaluated to investigate the dynamic hydrogen response. The capacitance at different hydrogen concentrations was monitored at a constant voltage of 0.8 V. Considering that the SWNTs part of the depletion region in the C-V curves was linear in the relevant range and did not change shape with different hydrogen concentration (Fig. 71), the voltage shifts therefore had a linear relation with the capacitance change. The voltage-time relationship was calculated from the capacitance-time relationship and given in Fig. 72. The equilibrium voltage shift was around 100 mV, and the equilibration time was around 2000 seconds when the H_2 concentration increased from 20 to 200 ppm. However, it required a longer time (around 3000 seconds) to achieve the equilibrium when the H_2 concentration decreased from 200 to 20 ppm.

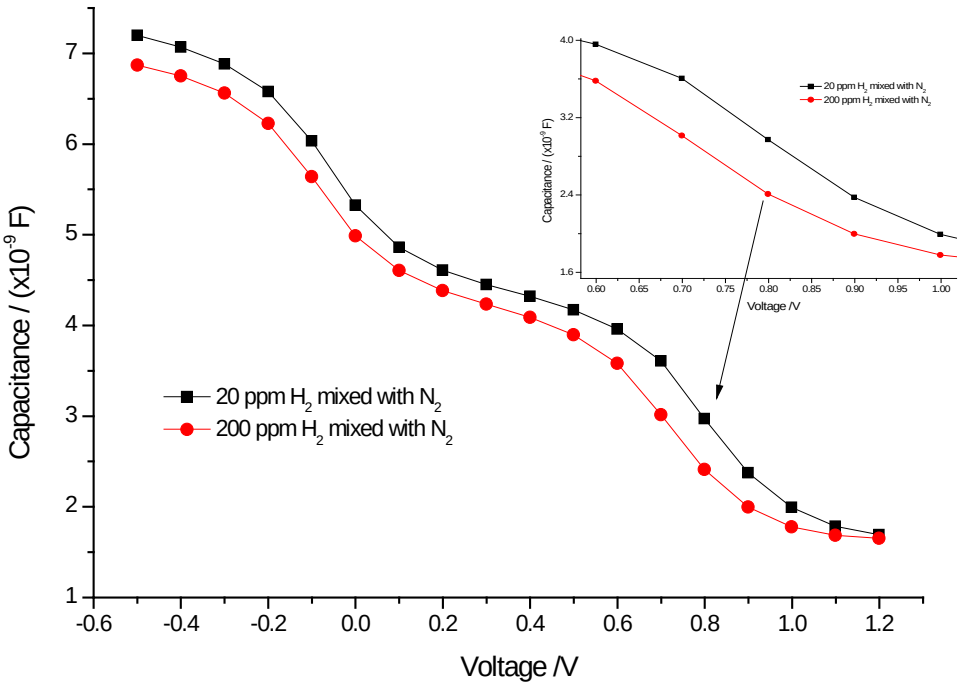

Fig. 71 C-V curves of the hydrogen reaction of the spray coated sample (SWNTs/SDS, LaF_3-substrate, two-line structure) at a frequency of 1 kHz.

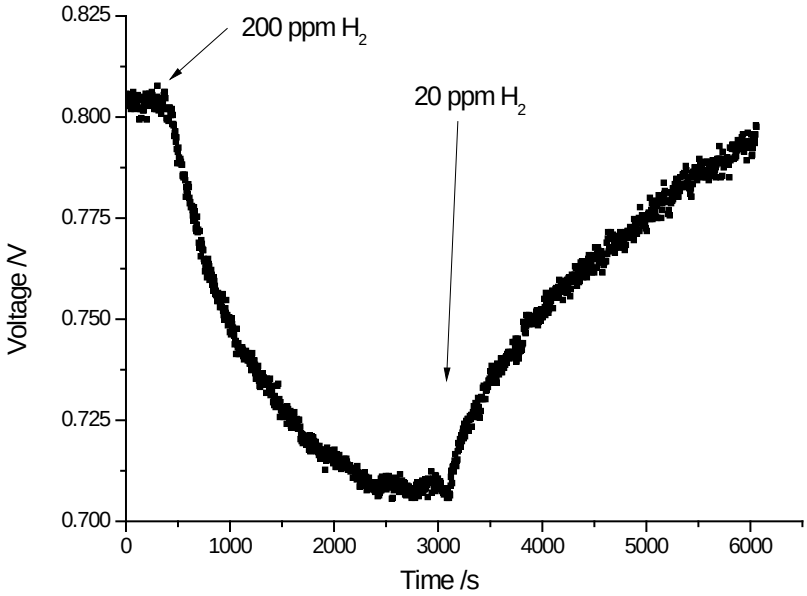

Fig. 72 Voltage shifts-time relationship of the hydrogen reaction for the spray coated sample (SWNTs/SDS, LaF_3-substrate, two-line structure), the capacitance was calculated from the constant voltage measurement at 0.8 V)

A resistive measurement of the sprayed coated (SWNTs/SDS) sample (Al/Si/SiO_2/Si_3N_4/LaF_3, two-line) was carried out to investigate the gas response, which was then used to compare with the potentiometric measurements results. A DC voltage of 1 mV was applied between the two top gate electrodes. The resistances were calculated. The sensitivity of the senor was defined with changed of resistance minus initial resistance and then divided by initial resistance. The result is shown in Fig. 73. The resistance reduced from 0.855 x 10^6 ohm to 0.677 x 10^6 ohm (17%) when the gas concentration was changed from 100% N_2 to 200 ppm H_2 mixed with N_2. The equilibration time was around 600 seconds. A longer time (4000 seconds) was required for recovery when the gas concentration changed back to 100% N_2.

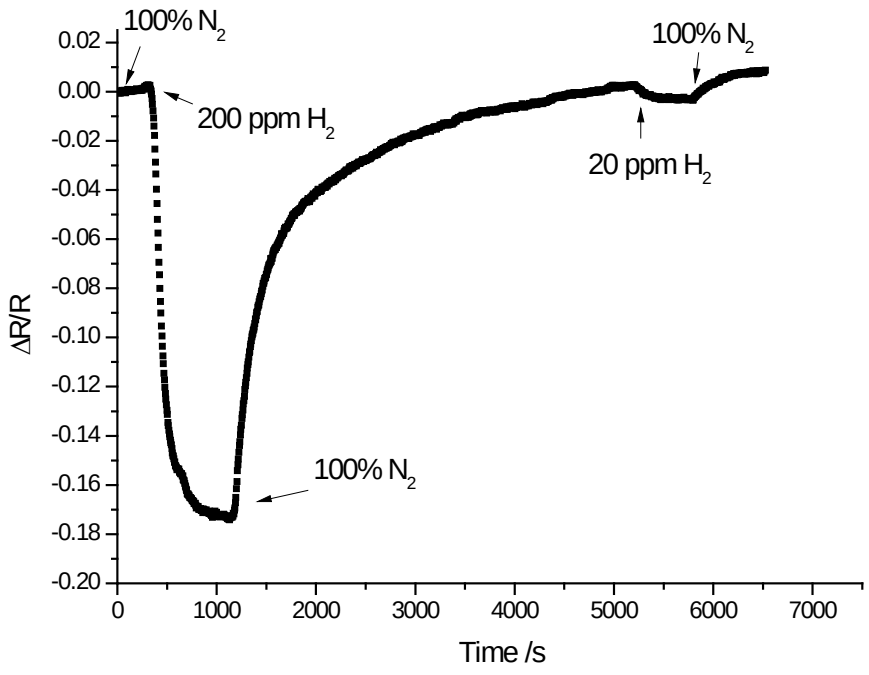

Fig. 73 Resistive measurements of the hydrogen reaction of the spray coated sample (SWNTs/SDS, LaF3-substrate, two-line structure)

The C-V curves of the spray coated (SWNTs) two-line LaF_3-substrate under different O_2 concentrations are illustrated in Fig. 74. With an increase in the O_2 concentration (1% to 100%), a small increase in capacitance was observed. The capacitance changes in all regions including the accumulation, the gold electrode part and the CNTs part were very similar. This is similar to the oxygen response for the spray coated interdigitated structure (6-30) with SWNTs in Chapter 4.4.1 (Fig. 56). The increase in sample capacitance was due to the resistance change associated with the oxygen concentration. The voltage shifts here in the CNTs part might not be a reaction to the oxygen sensitivity as discussed previously. Sample capacitance under different oxygen concentration was measured at a constant voltage of 0.7 V. The voltage-time relationship was obtained as described in the hydrogen sensitivity measurement. An overall voltage shift of approximately 28 mV was given from the voltage-time relationship plot (Fig. 75).

Resistive measurements of the spray coated (SWNTs) two-line LaF_3-substrate was performed at different gas concentrations. The system was circulated with 100% N_2 before replacing with 100% O_2. The resistance of the sample increased with the introduction of O_2. This is a consequence of the decrease in sample conductivity. However, no clear equilibrium was achieved after 30 minutes. The gas concentration was then changed back to 100% N_2 for recovery. After the stabilisation of the sample resistance, 1% O_2 was introduced and a clear increase in the resistance was noticed which was then recovered with 100% N_2.

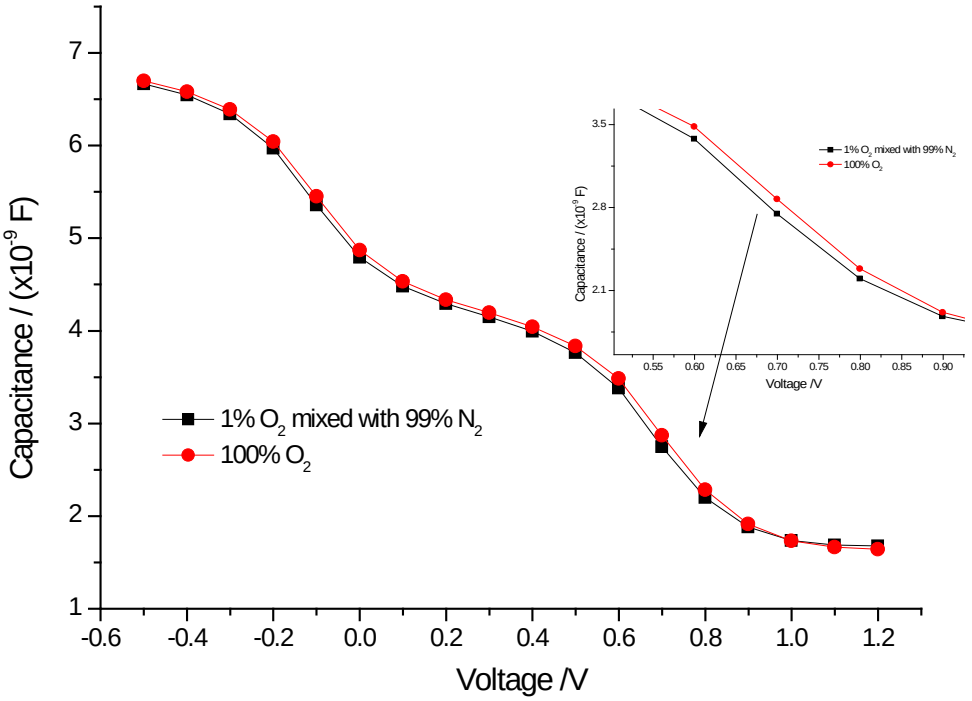

Fig. 74 C-V curves of the oxygen reaction of the of the spray coated sample (SWNTs/SDS, LaF_3-substrate, two-line structure) at a frequency of 1 kHz.

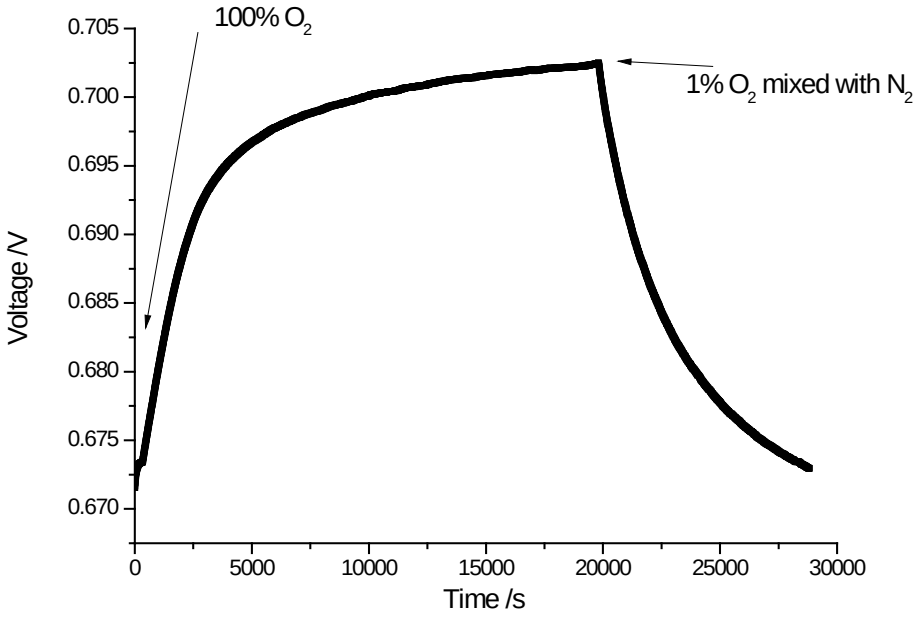

Fig. 75 Voltage-time relationship of the oxygen reaction of the spray coated sample (SWNTs/SDS, LaF_3-substrate, interdigitated structure, 6-30)

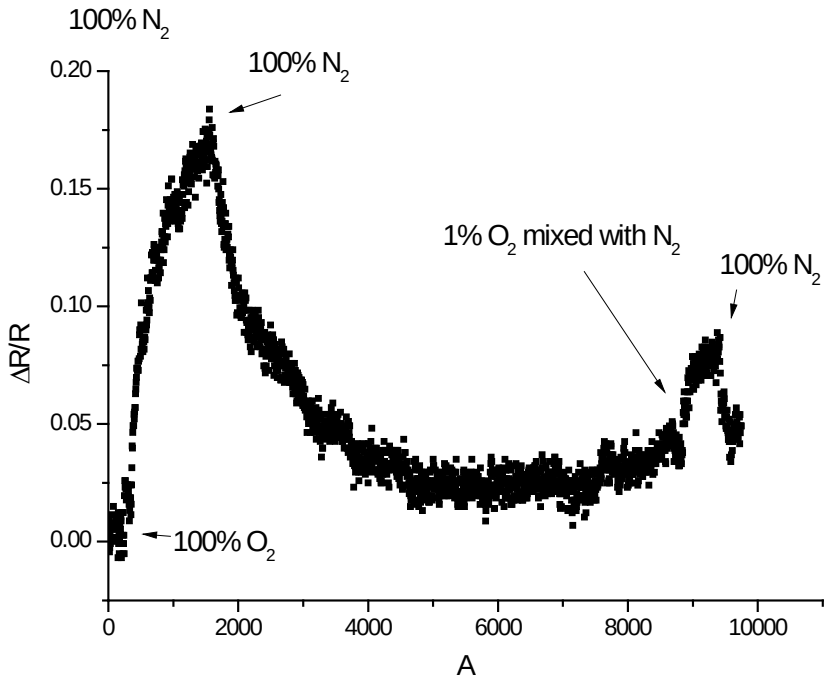

Fig. 76 Resistive measurements of the oxygen reaction of the spray coated sample (SWNTs/SDS, LaF3-substrate, two-line structure)

The hydrogen and oxygen sensitivities using both resistivity and potentiometric measurements were successfully completed for the spray coated (SWNTs/SDS aqueous solution) LaF_3-substrate with a two-line structure. The resistive measurements showed a faster H_2 sensing than potentiometric measurements (Fig. 72). The difference in equilibration time between the capacitive and resistive measurements indicated two different mechanisms of the gas sensing behaviour. Therefore, it is proved that the two sensing mechanisms were combined in the same gas sensor.

The resistance of the carbon nanotube network decreased with an increase in the H_2 concentration and a decrease in the O_2 concentration. This contradicts with some results reported in the literature (Star *et al.*, 2006b, Wong *et al.*, 2003b). The electronic properties of CNTs can be deeply modified by the presence of water (Zahab *et al.*, 2000). Zahab and co-workers proposed that

water molecules were absorbed by the CNTs and acted as electron donors. The conductivity type of the CNTs can therefore be changed from p-type to n-type. In current study, the testing gas was mixed with a constant humidity of 9.8 g/L. The present of the water molecules might have changed the conductivity behaviour of the CNTs network.

The SDS effectively debundled the SWNTs. When sprayed coated on an interdigitated electrode structure, those individual SWNTs gave a negligible voltage shift in the CNTs part. This could possibly be explained with residual SDS creating a coating layer on SWNTs, which inhibited the formation of a LaF_3-SWNTs-gas three phase boundaries for the gas reaction. On a two-line structure, small but genuine voltage shifts were noticed for the H_2 and O_2 sensitivity measurement. This could be due to the fact that a larger amount of CNTs were required to bridge the two-line structure than the interdigitated structure. Although, the presence of residual SDS insulated the contact between some SWNTs and the LaF_3 surface, there were still some SWNTs which were in contact with the LaF_3 surface. This allowed the formation of LaF_3-SWNTs-gas three phase boundaries and led to detectable gas sensing response.

4.5.3 Spray Coated LaF_3-Substrate with DMF Suspension

CNTs surface modification for a minimum affinity on the surface was considered beneficial for the sensing response. From the experimental results in chapter 4.5.2, SDS was effective in terms of defunding the SWNTs, however, the residual SDS molecules showed a negative impact on the sample sensing properties. Lab experiments aimed the removal of the SDS molecules and surface analysis suggested that the SDS molecules were difficult to remove once introduced. DMF has been used to separate SWNTs and was successfully removed by heat treatment (Lee *et al.*, 2008b).

Therefore, DMF was employed to suspend the SWNTs. The SWNTs/DMF suspension was spray coated on the LaF_3-substrate (two-line structure) and then heated on a hotplate at 300ºC for 30 minutes to remove DMF. The sample was viewed under a secondary electron microscope. The SEM image showed an even distribution of debundled carbon nanotubes (Fig. 77).

C-V measurements were carried out on a spray coated sample both before and after heat treatment. The C-V curves of the sample (Fig. 78) showed an increase in the accumulation capacitance after heat treatment. An apparent ‘step’ in the depletion region associated with the gold electrodes and the carbon nanotubes was visible for the sample before heating. However, no clear step was noticed for the sample after heat treatment. This phenomenon was not described in the literature and might be attributed to an improvement of the electrical contact between the carbon nanotube network and the gold electrodes on the one hand and a worsening of the physical contact between carbon nanotubes and LaF_3 due to the evaporation of DMF on the other.

A linear increase of the voltage from -1 to 1 V with an increment of 0.01 V and an interval of 1 second per step was applied between the two top gate electrodes.

The current-voltage curves of the spray coated sample (SWNTs/DMF, two-line, LaF_3) before and after heating were given in Fig. 79. Before heating, the sample current increased from -8.96×10^{-8} to 7.03×10^{-8} A when voltage varied from -1 to 1 V. After heating, an increase in current by approximately two orders of magnitude was noticed when the same voltage was applied. The current increased from -2.07×10^{-6} to 1.37×10^{-6} A when voltage varied from -1 to 1 V. This suggested that heating could contribute to an improvement in the conductivity of SWNTs network and improve the contact between the network and the gold electrodes. The improved conductivity can also have contributed to the increase in accumulation capacitance as illustrated in Fig. 78.

Hydrogen sensitivity of the spray coated sample (SWNTs/DMF, two-line, LaF_3-substrate) was investigated by controlling the H_2 concentration (20 ppm to 200 ppm mixed with N_2). Two hours were allowed before taking the C-V measurements for samples under each gas concentration. An increase in the accumulation capacitance was noticed with increased H_2 concentration (Fig. 80). However, the voltage shift of the C-V curves was not observed.

The accumulation capacitance was measured at a constant voltage (-1.5 V). A gas mixture of 20 ppm H_2 with N_2 was first applied to the testing box, and changed to a gas mixture with a higher hydrogen concentration (200 ppm H_2 mixed with N_2) after an equilibrium of the capacitance signal was achieved. An increase in the capacitance was noticed with the increase of H_2 concentration (Fig. 81). The gas concentration was then changed back to 20 ppm H_2 (mixed with N_2). A decrease in the capacitance was observed.

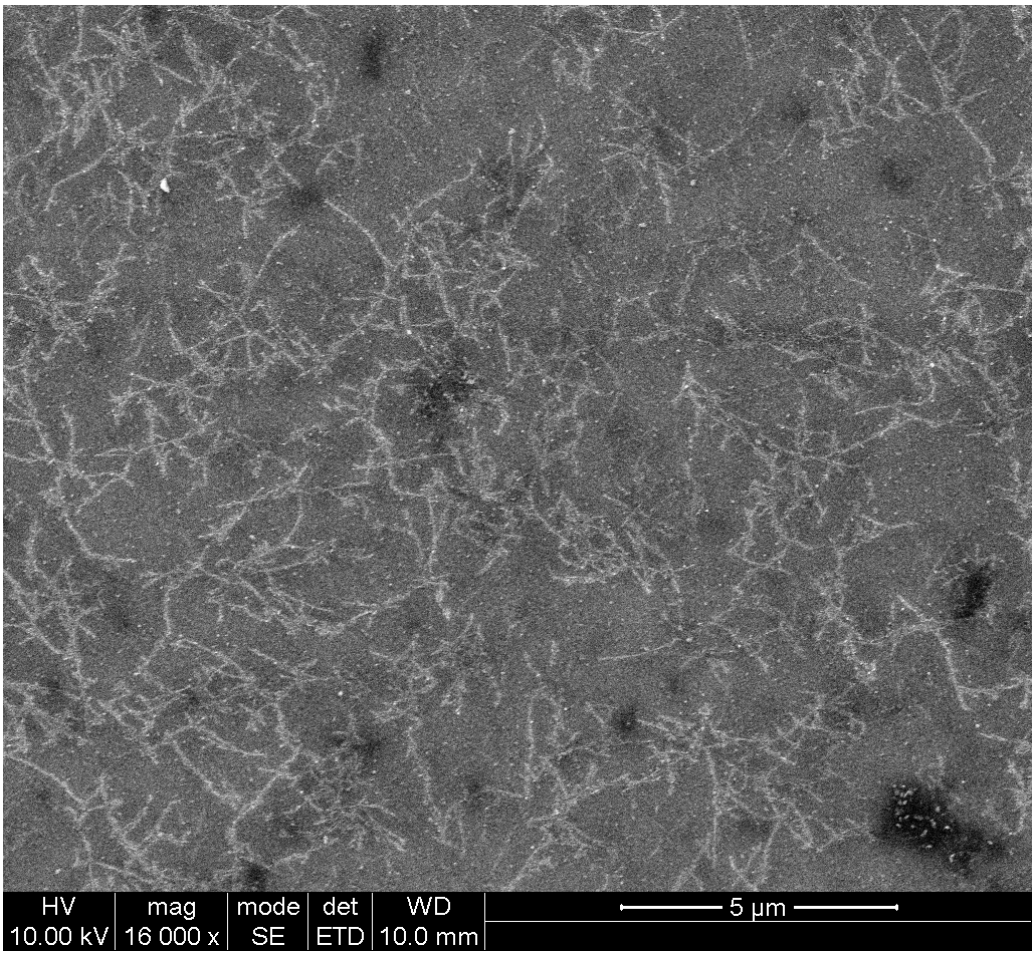

Fig. 77 SEM microphotograph of the spray coated sample (SWNTs/DMF, LaF_3-substrate two-line structure) showing an even distribution of carbon nanotubes

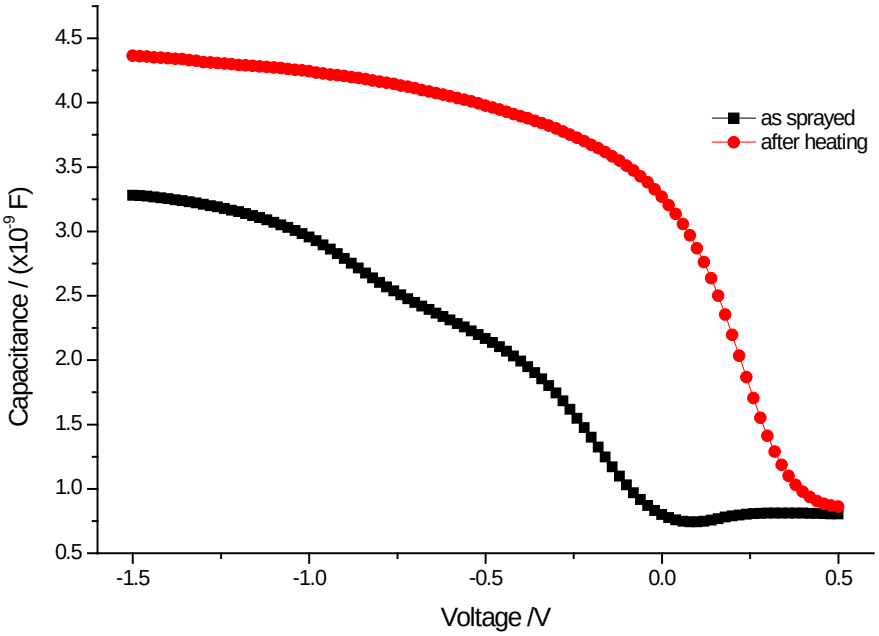

Fig. 78 C-V curves of spray coated sample (SWNTs/DMF, LaF_3-substrate, two-line structure) at a frequency of 1 kHz, showing the effect of heat treatment

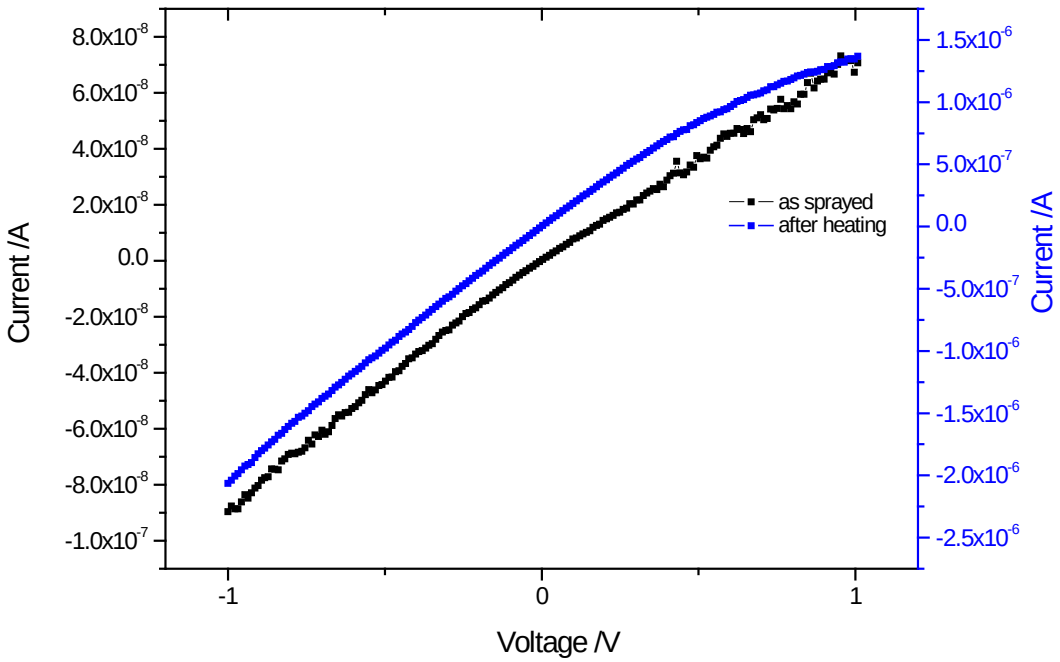

Fig. 79 Current-Voltage curves of the spray coated sample (SWNTs/DMF, LaF_3-substrate, two-line structure) before and after heating

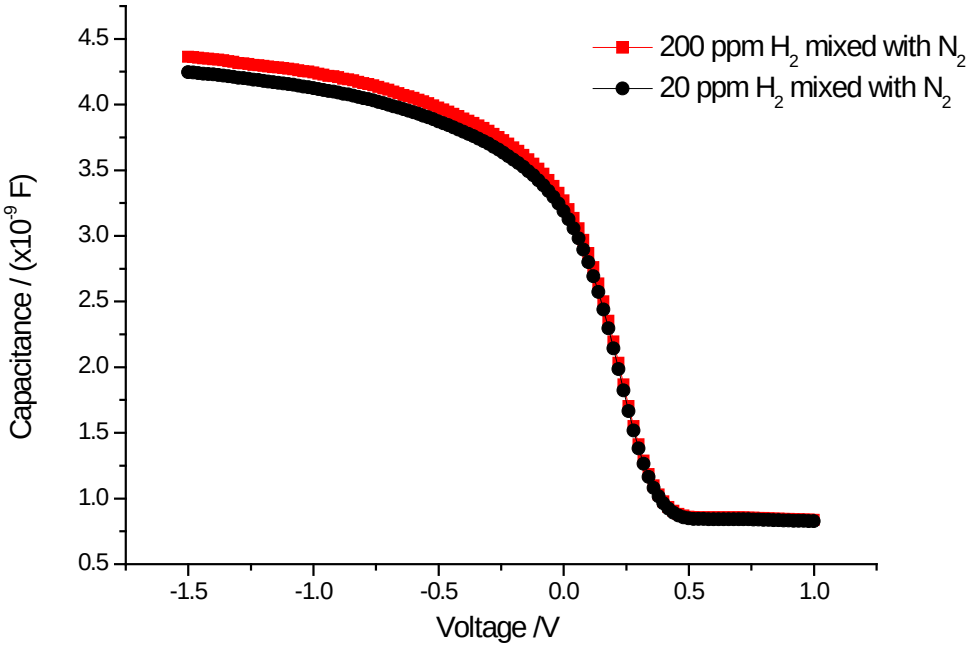

Fig. 80 C-V curves of the hydrogen reaction of the spray coated sample (SWNTs/DMF, LaF_3-substrate, two-line structure) at a frequency of 1 kHz.

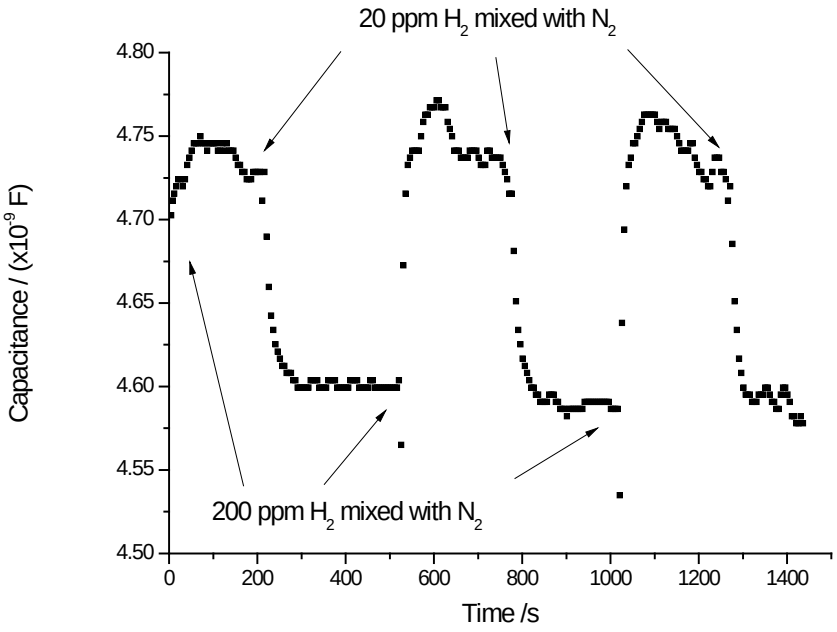

Fig. 81 Capacitance-time relationship of the hydrogen reaction of the spray coated sample (SWNTs/DMF, LaF_3-substrate, two-line structure)

Resistive measurements of the SWNTs network were carried out. A voltage of 1 mV was applied between the two top gate electrodes and the same gas concentrations were employed. A decrease in resistance (approximately 15%) was found when the H_2 concentration increased from 20 to 200 ppm (Fig. 82). The resistance change was approximately 20% smaller than the one found for the spray coated sample (SWNTs/SDS, two-line structure, Fig. 73), The response time for the SWNTs/DMF coated sample was shorter than that for the SWNTs/SDS coated sample (Fig. 82 and Fig. 73).

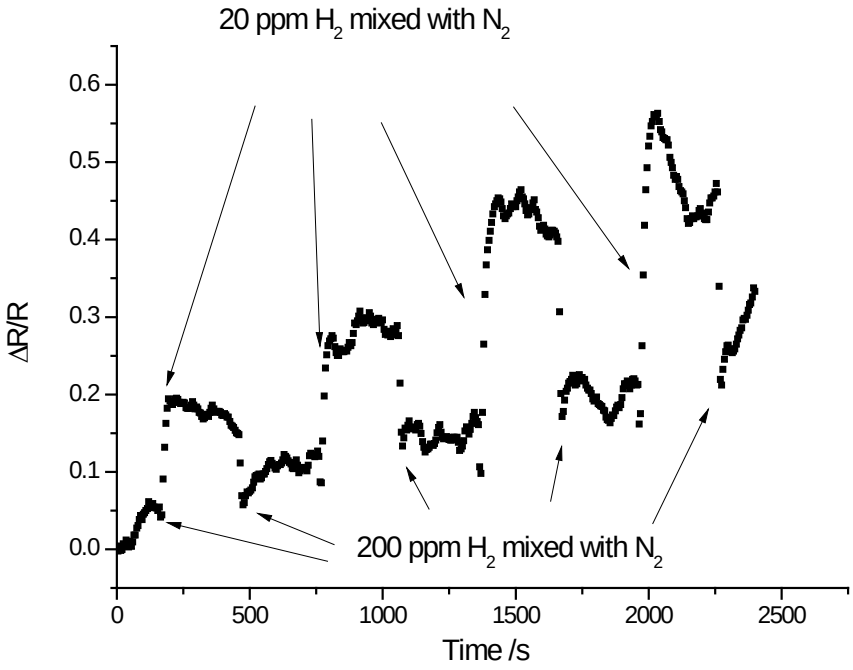

Fig. 82 Resistive measurements of the hydrogen reaction (spray coated SWNTs/DMF, LaF_3-substrate, two-line structure)

The oxygen sensitivity was tested by using 1% O_2 (mixed with 99% N_2) and 100 % O_2. Oxygen (1%) was first applied to the testing box, and then changed to 100%. A decrease in the accumulation capacitance was noticed with increased O_2 concentration (Fig. 83). However, no voltage shift of the C-V curves was observed when the O_2 concentration increased. The capacitance-time

relationship was plotted in Fig. 84. A decrease in the capacitance was noticed with the increase of O_2 concentration which suggested an increase in O_2 concentration could result in an increase in the capacitance. The resistive measurement was carried out, and the results are shown in Fig. 85. The resistance of the carbon nanotubes network increased when the O_2 concentration increased from 1% to 100%. However, the percentage change of the resistance change was quite small, around 3%. This is in the same range as the resistance changes measured for the SWNTs/SDS coated sample (approximately 8.5%, Fig. 76).

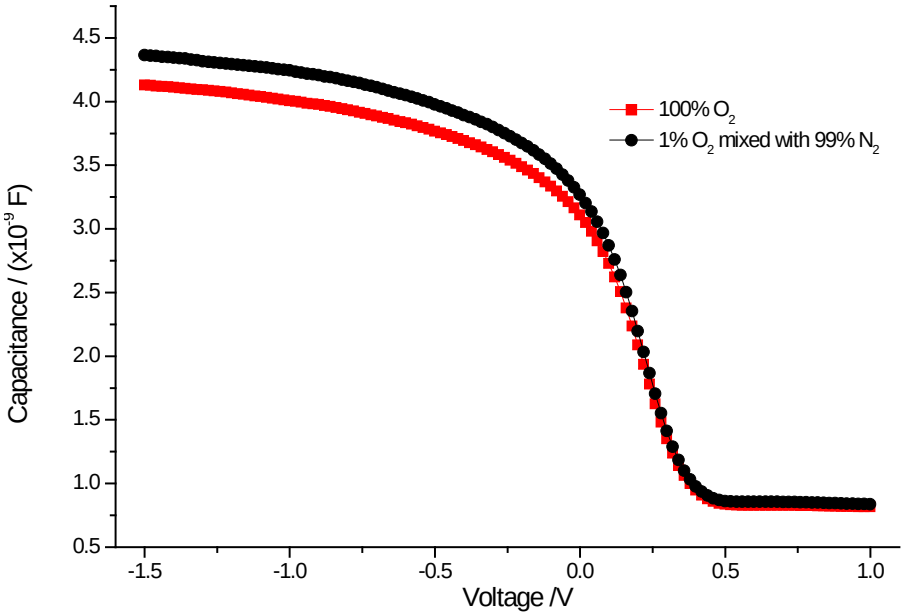

Fig. 83 C-V curves of the oxygen reaction of the spray coated sample (SWNTs/DMF, LaF_3-substrate, two-line structure) at a frequency of 1 kHz

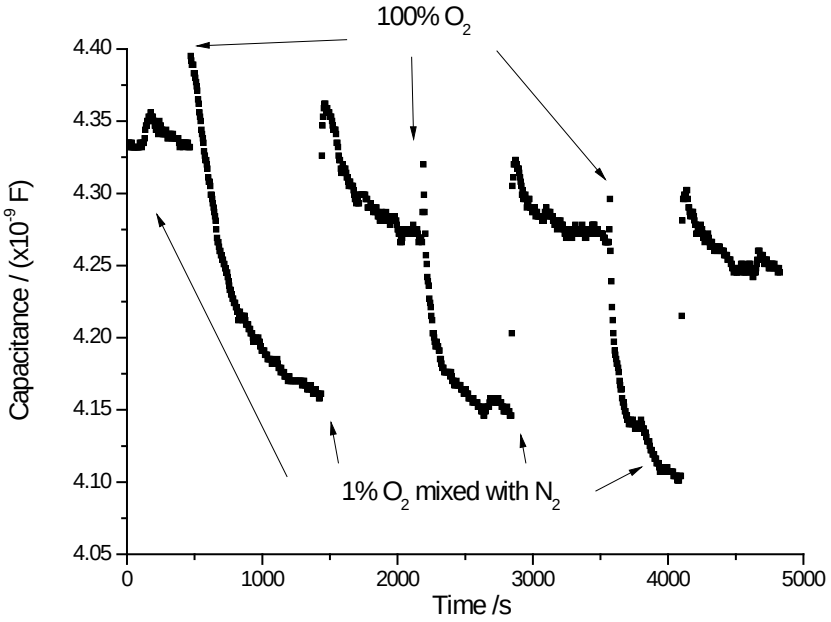

Fig. 84 Capacitance-time relationship of the oxygen reaction of the spray coated sample (SWNTs/DMF, LaF_3-substrate, two-line structure)

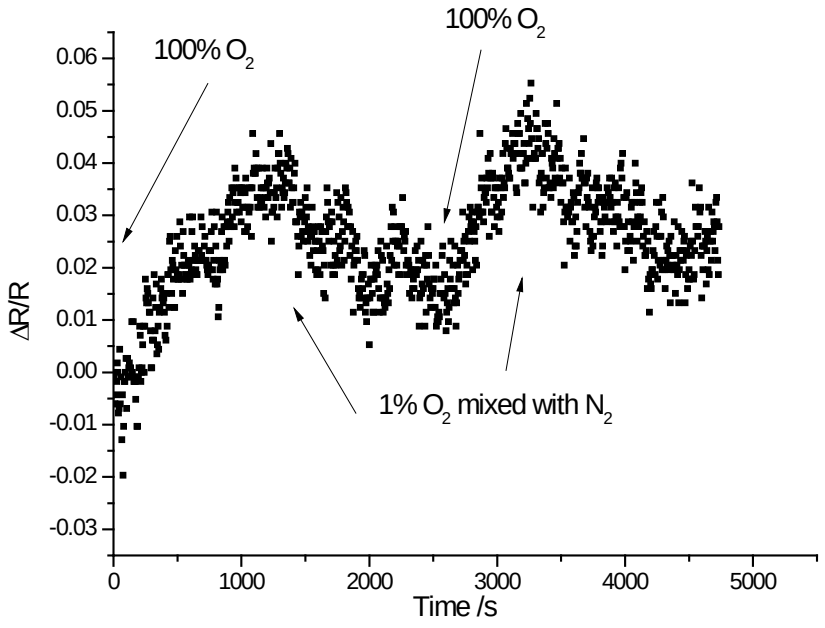

Fig. 85 Resistive measurements of the oxygen reaction (spray coated SWNTs/DMF, LaF_3-substrate, two-line structure)

In this section, DMF was used to disperse the SWNTs. Samples were heated to remove the DMF after spray coating. The conductivity of the CNTs network was improved after heating, which suggested a better contact between CNTs and the gold contact. However, the step in the depletion region of the C-V curve for the spray coated (SWNTs/DMF) two-line structure disappeared after heating. This could be a consequence of a physical detachment of CNTs from the LaF_3 surface during heating. No clear gas (O_2 and H_2) sensing response was found for the heated sample in the potentiometric measurement. The poor physical contact of the CNTs with the surface after heating was considered to have a detrimental impact on the gas sensor.

With an increase in H_2 concentration, the resistance of the SWNTs network decreased (Fig. 82). The reduced resistance could result in an increase in the effective gate area during the C-V measurement, which further contribute to an increase in the accumulation capacitance increase. This is consistent with the results given in Fig. 81. When O_2 was applied, the resistance of the SWNTs network increased with an increased O_2 concentration (Fig. 85). The increased resistance could lead to a decrease in the effective gate area during the C-V measurement. This is consistent with the results given in Fig. 84. Therefore, accumulation capacitance change is resistance dependent.

4.6 Spray Coated LaF_3-Substrate with Pt Deposition

4.6.1 Microstructure of the Pt Deposited Samples

Platinum has been used previously as a catalytically active material in field-effect gas sensors (Arbab *et al.*, 1993, Lee *et al.*, 1997). The Pt decoration of CNTs was introduced in current study for an expected improvement in the H_2 and O_2 sensitivity. SWNTs network showed a large resistance at a level of 10^6 ohm; therefore Pt particles could only be deposited on those CNTs which were along the gold electrodes using the chosen method of electrodeposition. Substrates with an increase in the gold electrode area and a decrease in the distance between the electrodes could therefore maximise the amount of Pt deposition, which in turn increased the effect of Pt on the gas sensing behaviour. LaF_3-substrates with interdigitated structure (10-10) have a smaller gap (10 µm) between the gold electrodes than the previously used interdigitated (6-30) and two-line structures and were therefore selected for the Pt deposition study.

The SWNTs were well dispersed in DMF solvent and then spray coated on the substrate with interdigitated structure ($Al/Si/SiO_2/Si_3N_4/LaF_3$, 10-10). The SWNTs coated substrate was then heated on a hotplate at 300ºC for 30 minutes for the removal of DMF solvent. Platinum was electro-deposited on the spray coated substrate (as described in chapter 3.1.3). Two samples were fabricated with 5 seconds and 30 seconds platinum deposition. Thirty second Pt deposition on a substrate without SWNTs was used as control sample. Samples were then viewed under a secondary electron microscope and the SEM images are given in Fig. 86 - Fig. 89. Pt particles were found attached to the SWNTs on and between the gold electrodes for the 5 seconds deposited specimen (Fig. 86). The Pt particles were around 10 to 20 nm diameter. With a longer deposition time (30 seconds), Pt particles were larger in size (10 to 500 nm) and were also

found on and between the gold electrodes (Fig. 87). On the gold electrode edges, the Pt particles tended to accumulate and grow along the edges and formed a line. The SEM image of the 30 seconds Pt deposited specimen at a higher magnification (100 K x) showed the coexistence of larger Pt clusters on the gold electrode edge (the left hand size of the image) and fine Pt particles on SWNTs (middle of the images, Fig. 88). In contrast, a Pt layer was observed on the gold electrodes for the sample without SWNTs (Fig. 89). The Pt particles tended to grow as uniformly sized particles without CNTs on the gold electrodes.

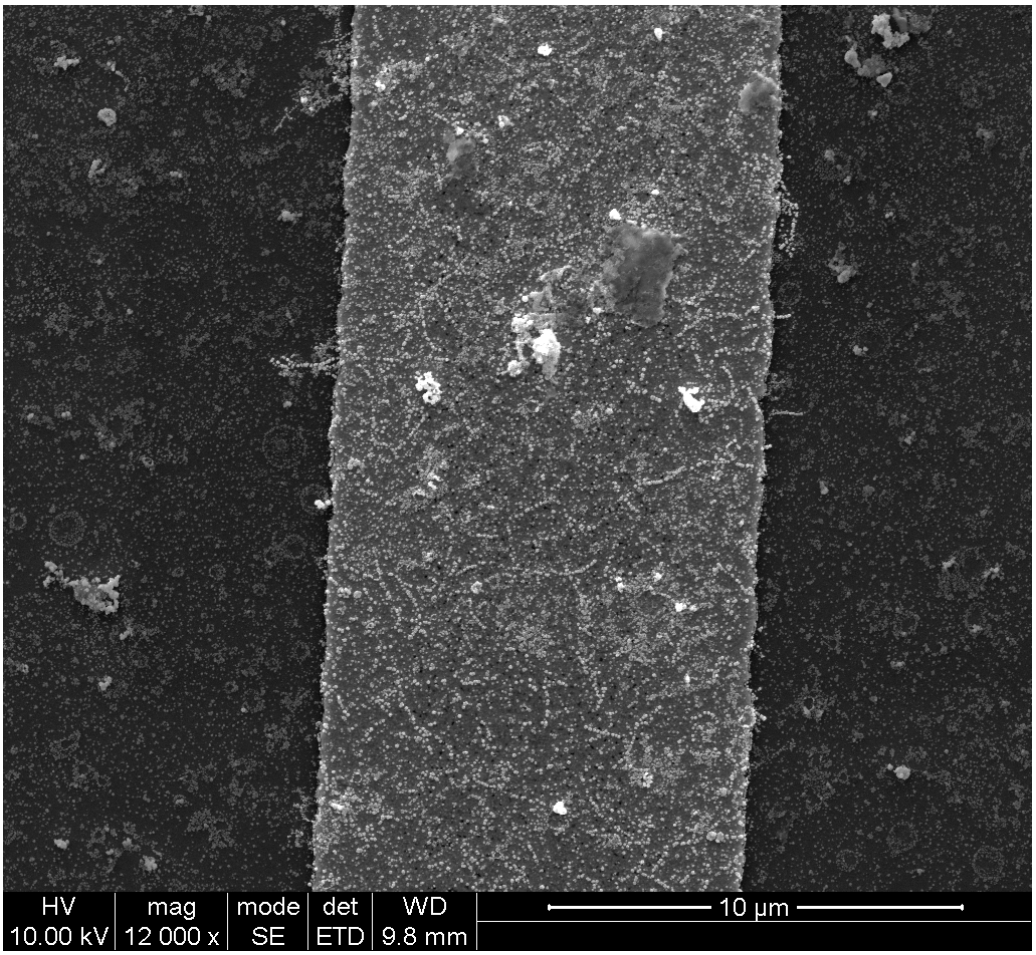

Fig. 86 SEM micrograph of the 5 seconds Pt deposited sample (SWNTs/DMF spray coated, LaF_3-substrate, 10-10), showing Pt particles on the gold electrode and the SWNTs network.

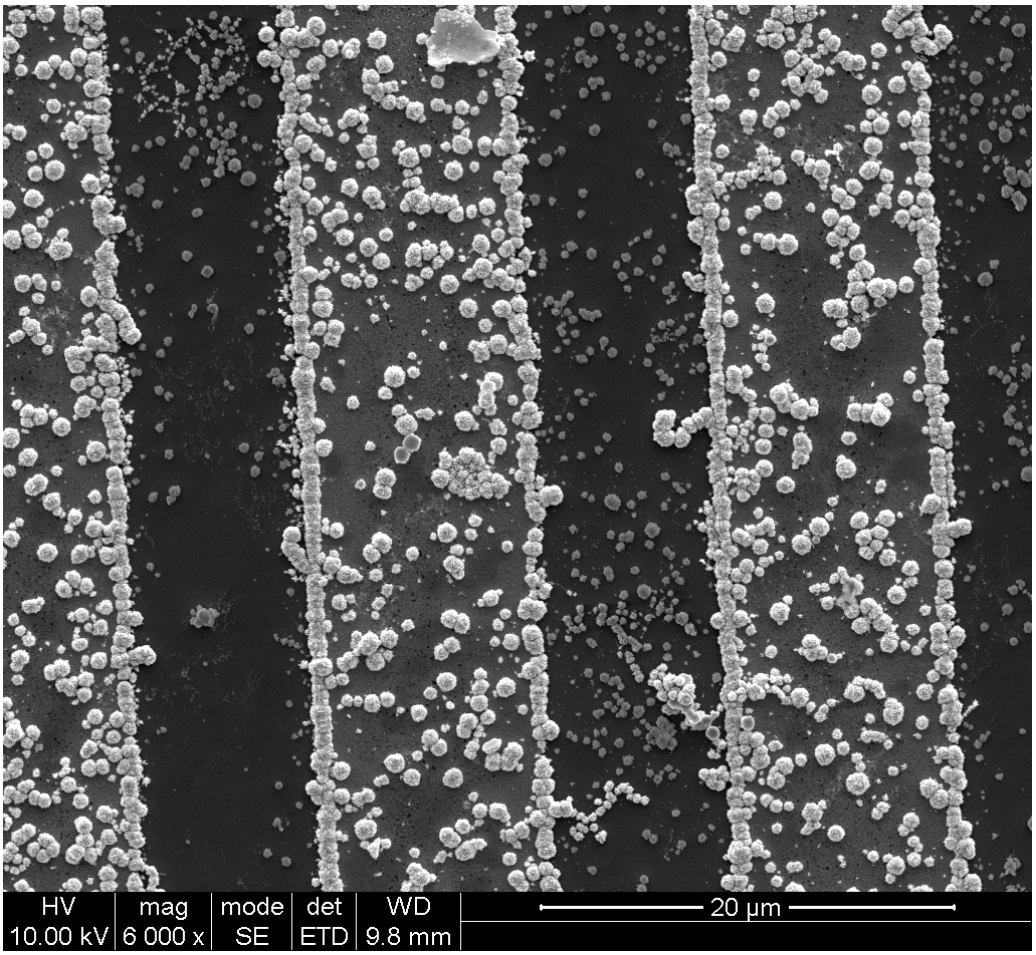

Fig. 87 SEM microphotograph of the 30 seconds Pt deposited sample (SWNTs/DMF spray coated, LaF_3-substrate, 10-10), showing Pt particles and clusters on the sample surface.

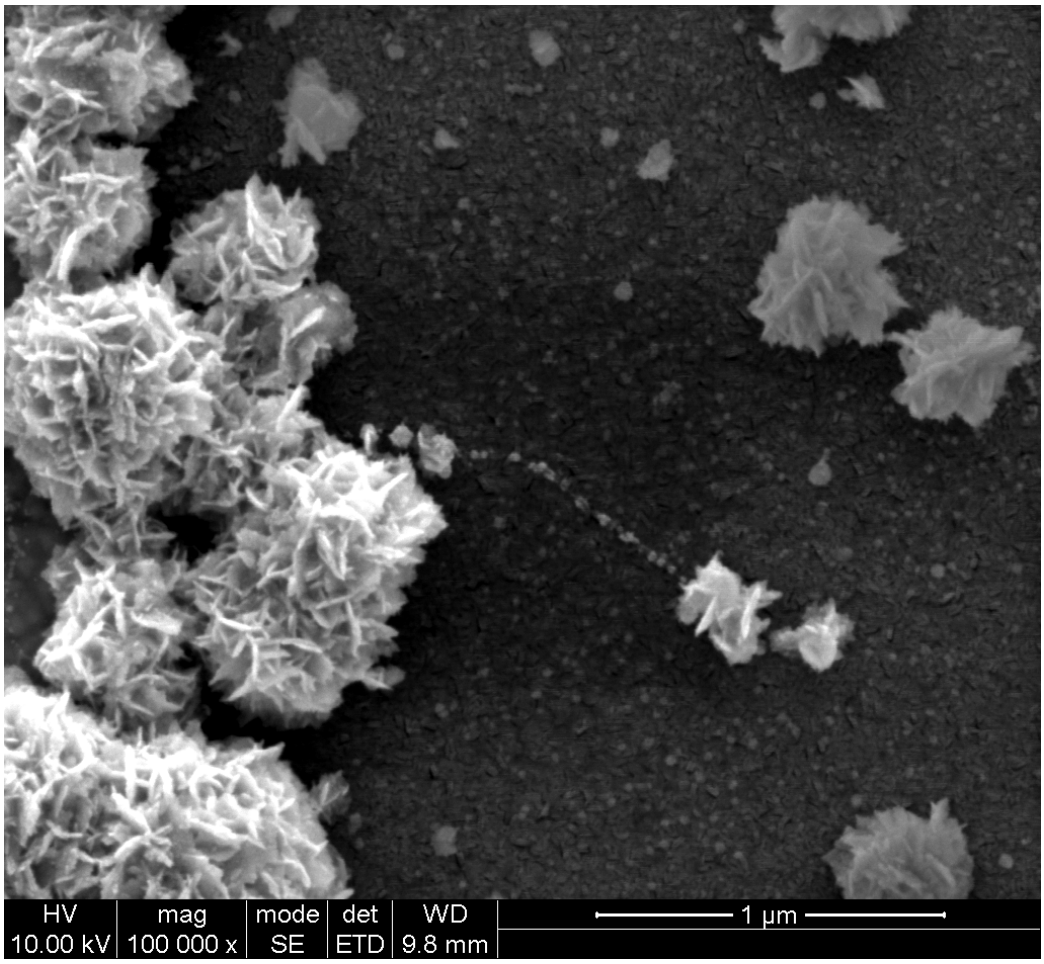

Fig. 88 SEM microphotograph of the 30 seconds Pt deposited sample (SWNTs/DMF spray coated, LaF_3-substrate, 10-10); showing Pt clusters and carbon nanotubes with fine Pt particles on the SWNTs.

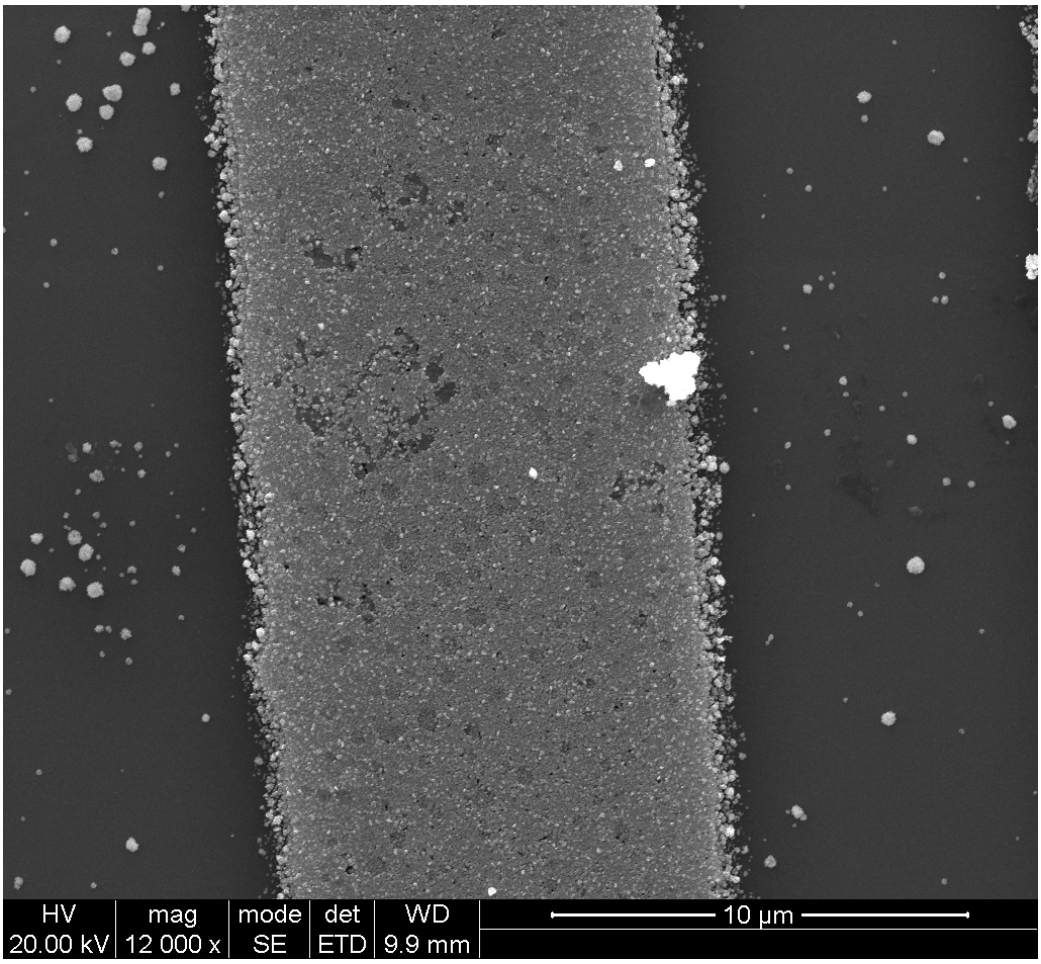

Fig. 89 SEM microphotograph of the 30 seconds Pt deposited sample (LaF_3-substrate, 10-10, without SWNTs) showing Pt on gold electrodes.

4.6.2 Gas Sensitivity of the 5 Second Pt Deposited Sample

The C-V measurements were carried out for the samples with 5 and 30 seconds Pt deposition. The C-V curves of the 5 second platinum deposited sample (before and after Pt deposition) are given in Fig. 90. An increase in the accumulation capacitances was observed after Pt deposition. This indicated that Pt deposition increased the gate area.

The sensor sensitivity towards H_2 and O_2 was evaluated. The 5 second Pt deposited sample was placed in the testing box. Gas with different H_2 concentration (0, 1, 10 and 100%, mixed with N_2) was supplied for the system in sequence. The C-V measurements were performed correspondingly and the equilibrium C-V curves at different hydrogen concentrations are presented in Fig. 91. With increased H_2 concentration, no significant changes in the accumulation capacitance and the inversion capacitance were observed. However, the part in depletion region next to accumulation shifted towards a more negative value (Fig. 91), and the overall shape of the C-V curves changed with hydrogen concentration. This is attributed to the hydrogen sensitivity of the deposited Pt particles. The hydrogen sensitivity was quantified at a capacitance of 3.20×10^{-9} F in terms of the voltage shift. The voltages shifts were -37, -128 and -398 mV with the increase of H_2 concentration (1%, 10% and 100%).

Due to the shape change in the C-V curves, it was not ideal to calculate the voltage shifts by using capacitance change. The capacitance change at a constant voltage (-0.3 V) under different H_2 concentration was used to indicate the response rate. The sample was exposed to 1% H_2 to allow equilibrium of the sample capacitance. The H_2 concentration was increased to 100%, a dramatic decrease in capacitance was noticed within the first 10 seconds (Fig. 92). The capacitance was then slowly decreased until equilibrium was achieved (around

200 seconds, Fig. 92). A gradual increase in capacitance with time (approximately 500 seconds) was noticed before full recovery when the H_2 supply was changed back to 1%.

The gas response of different O_2 concentrations (1% to 100%) was also studied. A small increase in the accumulation capacitance was noticed when the O_2 concentration changed from 1% to 100% (Fig. 93). However, no clear voltage shift was observed with the change in the O_2 concentration.

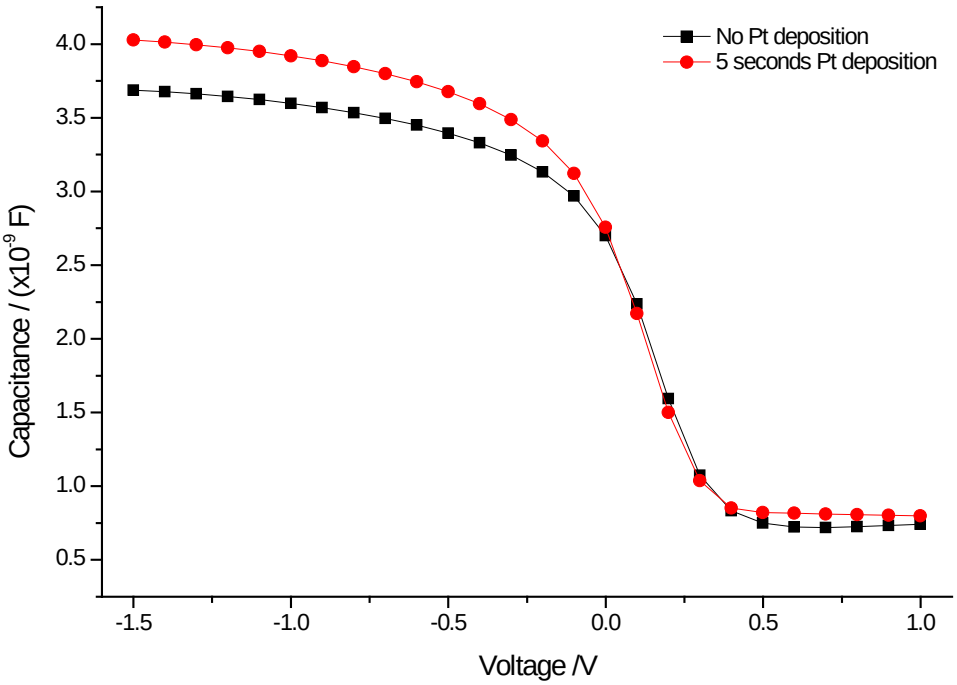

Fig. 90 C-V curves of the 5 seconds Pt deposited sample (SWNTs/DMF spray coated LaF_3-substrate, 10-10)

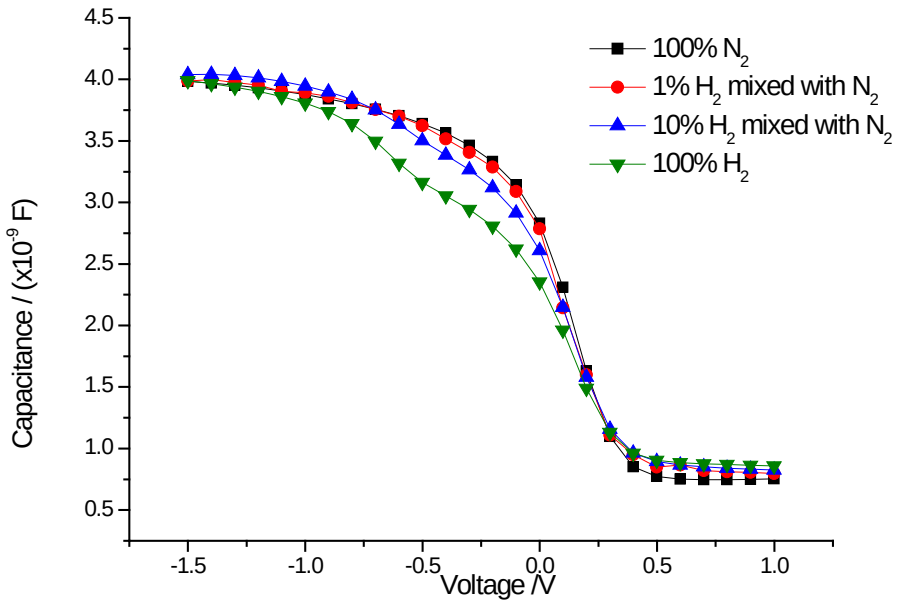

Fig. 91 C-V curves of the hydrogen reaction of the 5 seconds Pt deposited sample (SWNTs/DMF spray coated LaF_3-substrate, 10-10).

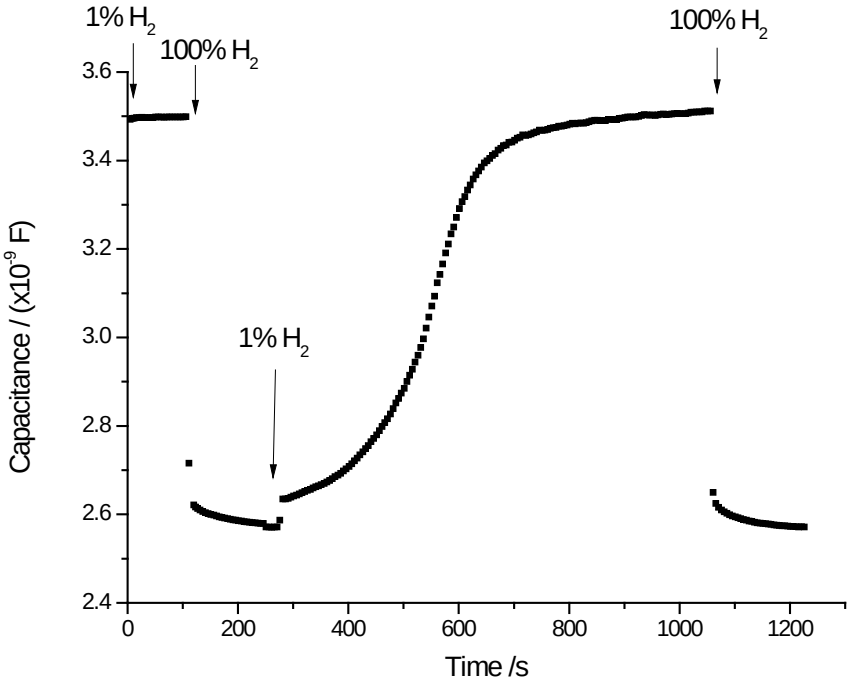

Fig. 92 Capacitance-time relationship of H_2 reaction of the 5 seconds Pt deposited sample (SWNTs/DMF spray coated LaF_3-substrate, 10-10).

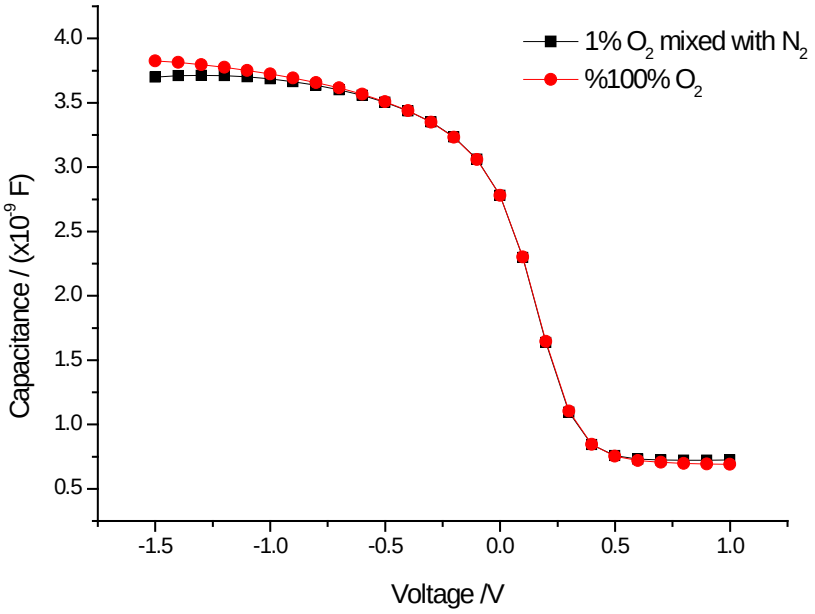

Fig. 93 C-V curves of the oxygen reaction of the 5 seconds Pt deposited sample (SWNTs/DMF spray coated LaF_3-substrate, 10-10).

4.6.3 Gas Sensitivity of the 30 Second Pt Deposited Sample

Similar C-V measurements and the sensor sensitivity evaluation towards H_2 and O_2 were also carried out for the 30 seconds Pt deposited sample. A significant increase in the accumulation capacitance was noticed after 30 seconds Pt deposition (Fig. 94). This could be explained as the Pt deposition resulted in an increase in the gate area. The C-V curves at different hydrogen concentrations of the 30 second Pt deposited sample are illustrated in Fig. 95. Similar to the 5 second Pt deposited sample, the voltage of the depletion region shifted towards negative values with an increase in the H_2 concentration. It was noticed that there was a decrease in the accumulation capacitance when the H_2 concentration increased from 1 to 100%. An apparent change in the shape of C-V curves was noticed when the H_2 concentration increased to 100% (Fig. 95). This phenomenon was not reported in the literature, and a complicated time dependent behaviour was observed.

After the equilibration of the C-V curve at 1% H_2, 100% H_2 was introduced, a series of C-V measurements were carried out at 2, 4, 6, 8 and 10 minutes. The C-V curves were plotted and presented in Fig. 96. A voltage shift (-0.36 V) was completed in the first 2 minutes with a change in the shape of C-V curve. With increased time, the accumulation capacitance decreased continuously which led to a change in the slope of the part of C-V curve in depletion next to the accumulation (Fig. 96). The accumulation capacitance of the sample at a voltage of -1.5 V was plotted against time at 100% H_2. The changes of the accumulation capacitance were clearly visible, which first increased with the increase in H_2 concentration and then decreased with time (Fig. 97). This phenomenon might be due to the contribution of both water molecules and Pt particles. As described in chapter 4.2, the water molecules present in the system were absorbed by the CNTs and acted as electron donors (Zahab *et al.*, 2000). This could result in a

decrease in the resistance of the SWNTs network, which lead to an increase in the accumulation capacitance with increased H_2 concentration. The Pt particles could react with H_2 molecules without the interference of the water molecules and have an opposing effect. The reaction contributed to an increase in the resistance and decrease in the accumulation capacitance. Alternatively, it is possible that the accumulation of hydrogen atoms at the Pt/LaF_3 interface reduced the accumulation capacitance.

Due to the change in the slope of the depletion region next to accumulation, capacitance change at a constant voltage (-0.4 V) was used to indicate the response rate instead of the voltage change at a constant capacitance. The H_2 response rate was given by the capacitance-time relationship in Fig. 98. A fast drop in capacitance was noticed when the gas environment changed from 1% H_2 to 100% H_2. A further steady decrease in capacitance with time was observed. The fast drop is considered correspond to the voltage shift, and the further decrease is attributed to the decrease in the accumulation capacitance.

The voltage-time relationship can be given by calculating Fig. 96 and Fig. 98. The major voltage shift (-361 mV) was completed within the first two minutes as shown the ‘steep’ part in Fig. 98. The residual decrease of capacitance in Fig. 98 was due to the decrease of accumulation capacitance, which caused a further -92 mV voltage shifts. Therefore, the voltage-time relationship was given in Fig. 99. Instead of a rapid capacitance increase, the capacitance increased gradually when the gas environment changed back to 1% H_2. The sensor response was completely reversible as illustrated by the repeat measurement (Fig. 83).

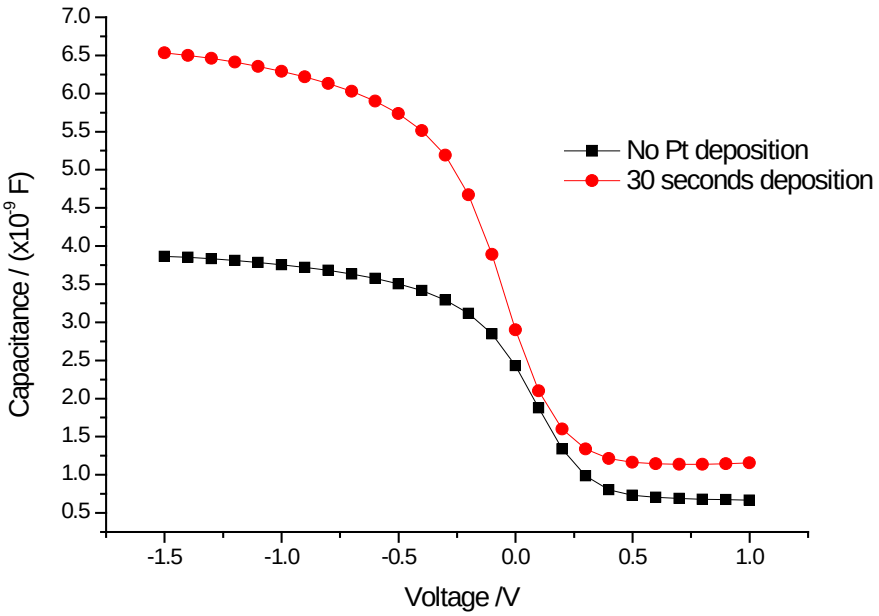

Fig. 94 C-V curves of the oxygen reaction of the 30 seconds Pt deposited sample (SWNTs/DMF spray coated LaF_3-substrate, 10-10).

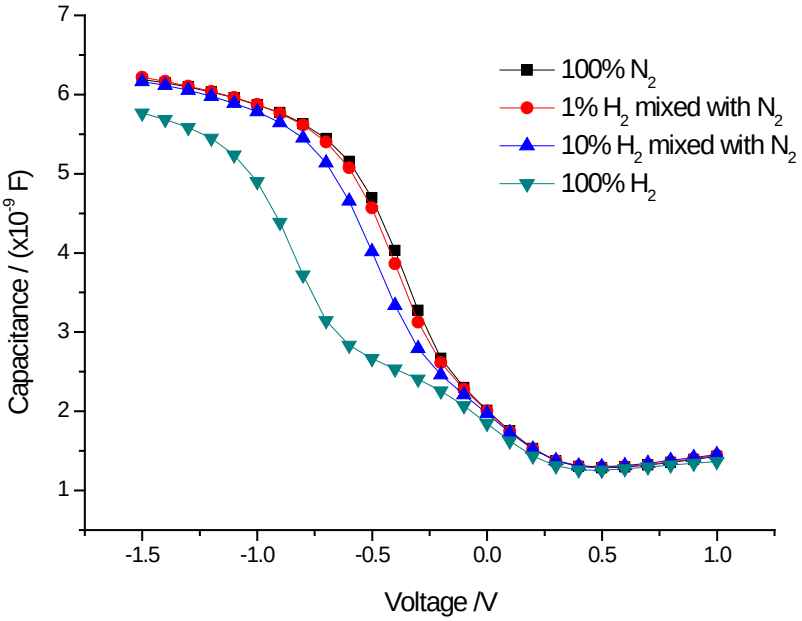

Fig. 95 C-V curves of the 30 seconds Pt deposited sample (SWNTs/DMF spray coated LaF_3-substrate, 10-10).

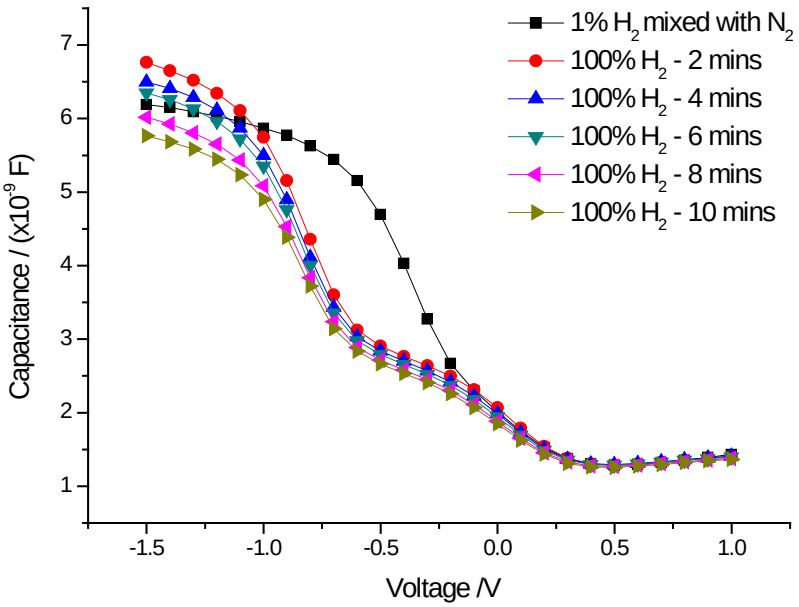

Fig. 96 C-V curves of the hydrogen reaction with time of the 30 seconds Pt deposited sample (SWNTs/DMF spray coated LaF_3-substrate, 10-10).

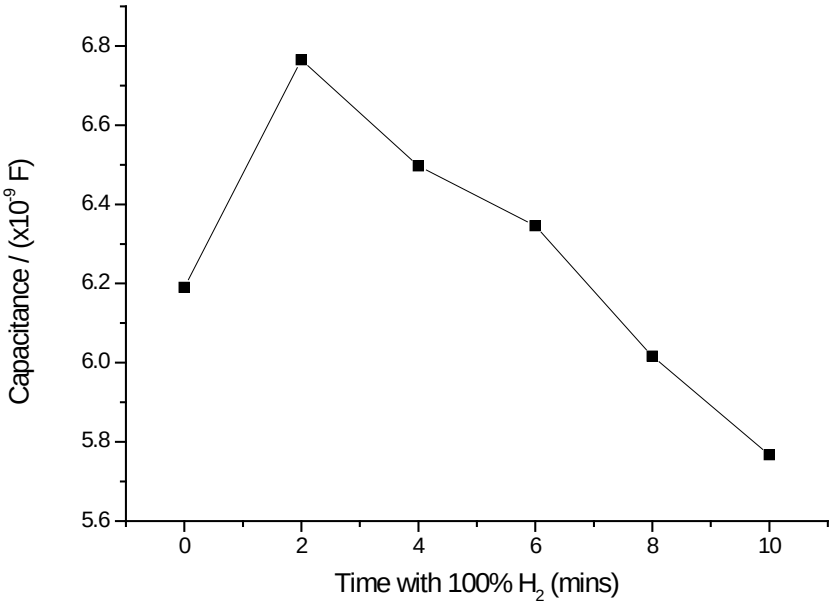

Fig. 97 Capacitance-time curve of the 30 seconds Pt deposited sample (SWNTs/DMF spray coated LaF_3-substrate, 10-10) under 100% H_2 at a voltage of -1.5 V.

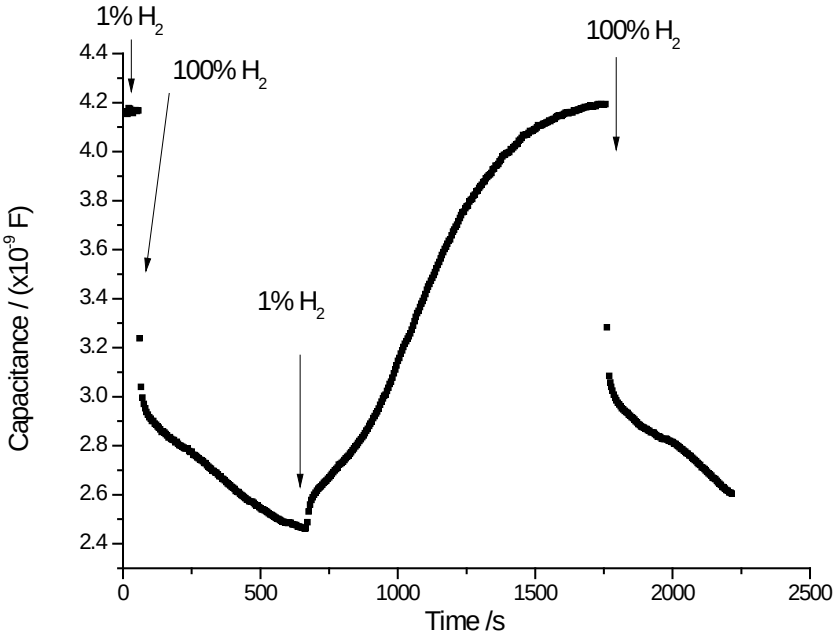

Fig. 98 Capacitance-time relationship of H_2 reaction of the 30 seconds Pt deposited sample (SWNTs/DMF spray coated LaF_3-substrate, 10-10) at a voltage of -0.4 V.

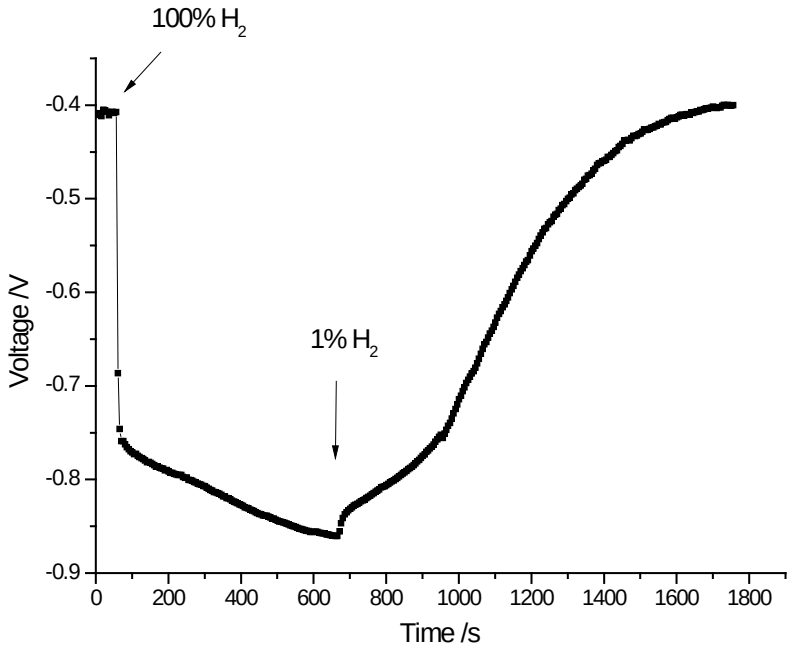

Fig. 99. Voltage-time relationship of H_2 reaction of the 30 seconds Pt deposited sample (SWNTs/DMF spray coated LaF_3-substrate, 10-10) at a capacitance of 4 nF.

The O_2 sensitivity was also investigated. The C-V measurement of the 30 second Pt deposited sample under different O_2 concentration (0, 1% and 100%) was carried out. A small voltage shift (25 mV) was noticed when the O_2 concentration changed from 0 to 1% (Fig. 100). When the O_2 concentration increased from 1 to 100%, a clear increase in the accumulation capacitance and a significant voltage shift in depletion towards positive values were clearly identified from the C-V curves. Compared with the H_2 response, the gold electrodes also showed oxygen sensitivity. This may due to the Pt coating on the gold electrodes. The significant change in the accumulation capacitance changed the shape of C-V curves and invalidated the direct voltage shift calculation from the C-V curve. In order to quantify the voltage shift, the first derivative of the C-V curves (Fig. 100) was plotted and given in Fig. 101. The separation of the two peaks (1% O_2 and 100% O_2) gave a voltage shift of 0.5 V, which was higher than reported in the literature. Moritz *et al.* (2001) demonstrated an oxygen sensitivity with a voltage shift of 0.12 V using a $Si/SiO_2/Si_3N_4/LaF_3/Pt$ structure when the oxygen concentration was changed from 1 to 100%.

The capacitance-time relationship of the sample was investigated at a constant voltage of -0.3 V to explore the O_2 response time. A continuous increase in capacitance was observed when the O_2 concentration changed from 1 to 100% where a continuous decrease in capacitance was found when O_2 concentration changed back to 1% (Fig. 102). The response time was much longer (2000 seconds) when compared with the H_2 response (500 seconds, Fig. 98). The oxygen reaction was reversible. The voltage-time relationship was calculated and is shown in Fig. 103.

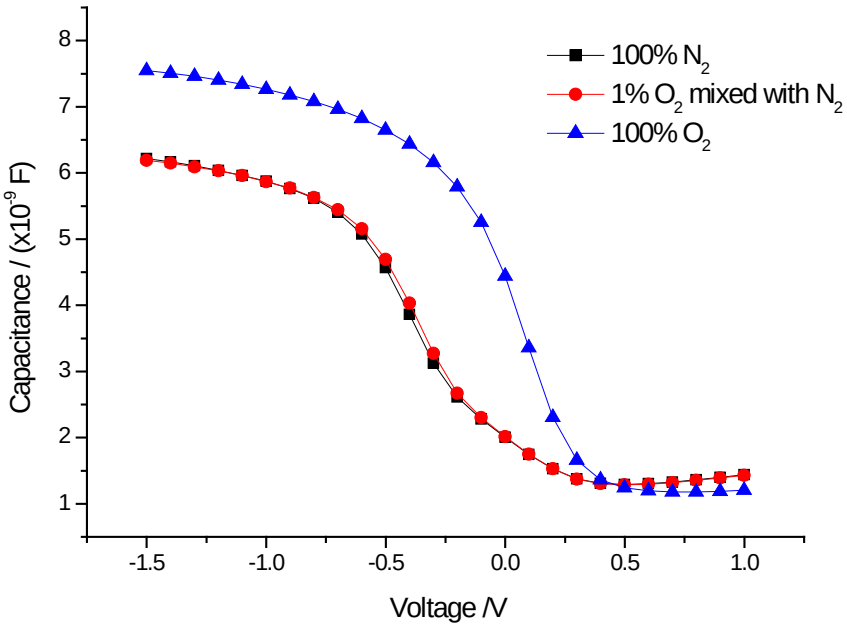

Fig. 100 C-V curves of the oxygen reaction of the 30 seconds Pt deposited sample (SWNTs/DMF spray coated LaF_3-substrate, 10-10)

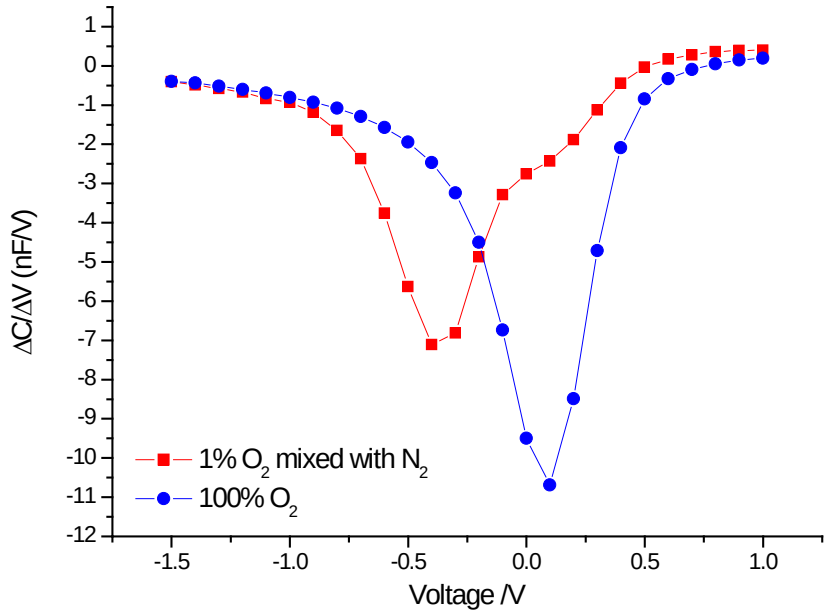

Fig. 101 First deviation plot of the C-V curves (oxygen reaction of the 30 seconds Pt deposited sample (SWNTs/DMF spray coated LaF_3-substrate, 10-10))

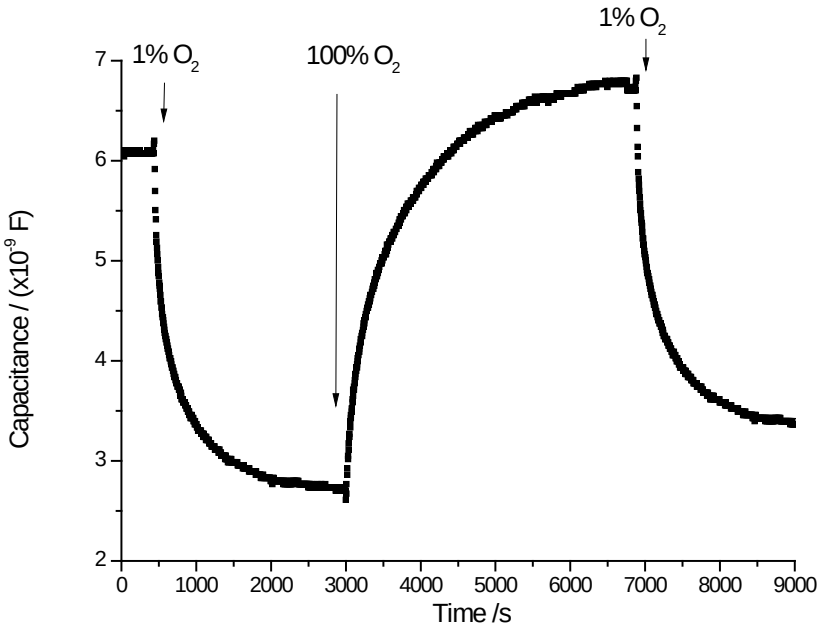

Fig. 102 Capacitance-time relationship of oxygen reaction of the 30 seconds Pt deposited sample (SWNTs/DMF spray coated LaF_3-substrate, 10-10) at a constant voltage of -0.3 V

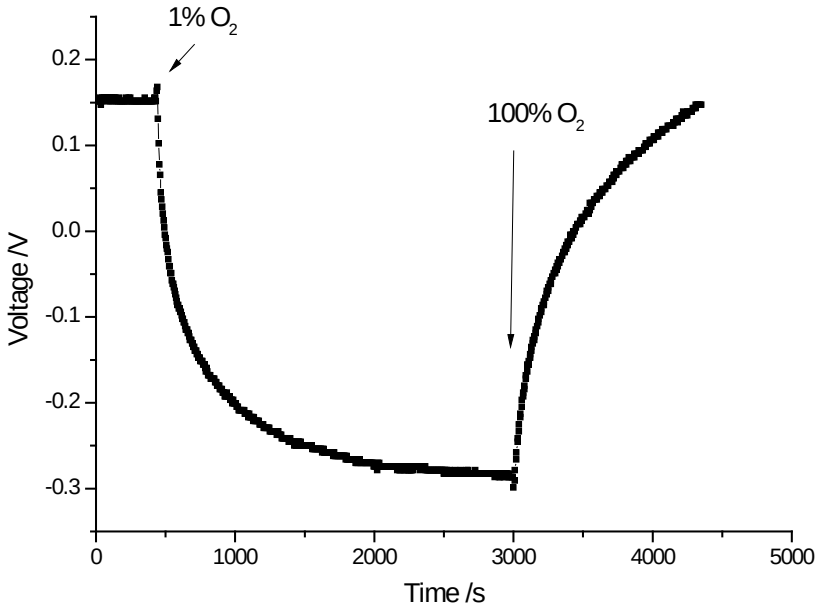

Fig. 103 Voltage-time relationship of oxygen reaction of the 30 seconds Pt deposited sample (SWNTs/DMF spray coated LaF_3-substrate, 10-10) at a constant capacitance of 2.5 nF

4.6.4 Gas Sensitivity of the 30 Second Pt Deposited Sample without SWNTs coating

The hydrogen response of a 30 second Pt deposited sample without SWNTs was also tested. The C-V curves of the sample suggested that there were no changes in the accumulation capacitance with the increase in the H_2 concentration (1% to 100%, Fig. 104). The voltage of the depletion region shifted towards negative values.

A series of C-V measurements were carried out at different times up to 30 minutes with 100% H_2 to study the hydrogen reaction of the 30 second Pt deposited interdigitated LaF_3-substrate without SWNTs. The C-V curves shifted toward the negative side when the H_2 concentration increased from 1% to 100% (Fig. 105). With continuous H_2 supplied, continuous voltage shift was observed. The voltage shift and time relationship was plotted at a capacitance of 1.4×10^{-9} F. An overall voltage shift of -350 mV was achieved in 30 minutes (Fig. 106). When the sample was coated with SWNTs, the predominant voltage shift was achieved within 2 minutes (approximately -361 mV, Fig. 96 and Fig. 98). This indicated that sample with SWNTs demonstrated a significantly better sensor response time. The SWNTs network worked as a template for the Pt deposition and Pt particle growth (Fig. 87). Compared with the direct Pt deposition on gold electrodes (without SWNTs, Fig. 89), the SWNTs coated sample gave large Pt cluster and fine Pt particles. This created more three-phase boundary for the gas detection.

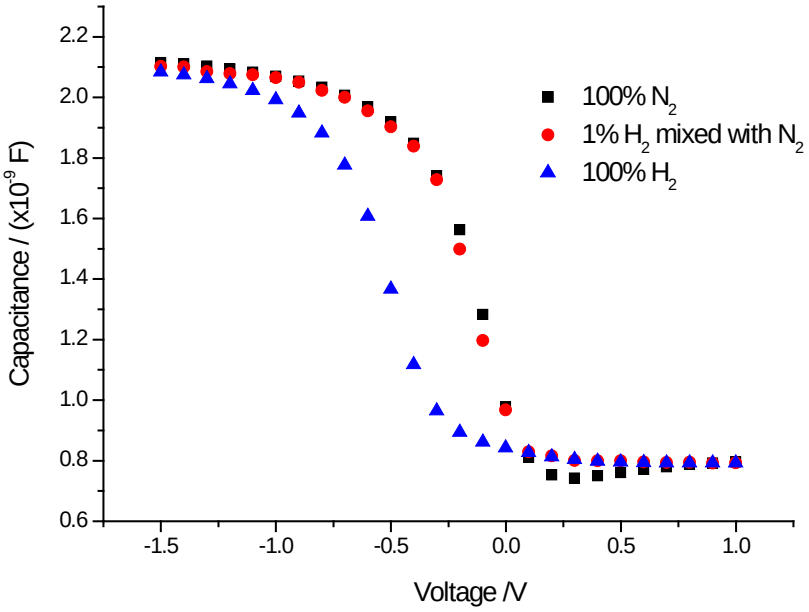

Fig. 104 C-V curves of the hydrogen reaction of the 30 seconds Pt deposited sample (LaF_3-substrate, interdigitated structure, 10-10, without SWNTs coating)

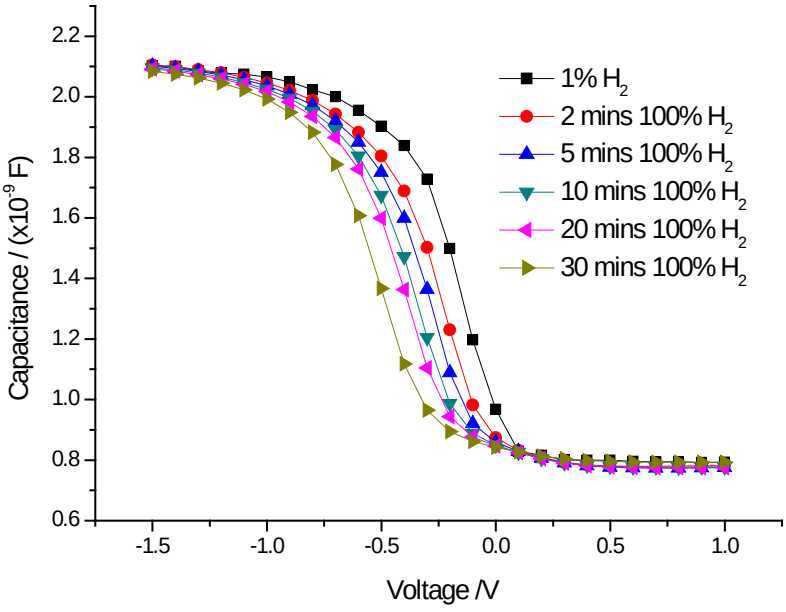

Fig. 105 C-V curves of the hydrogen reaction of the 30 seconds Pt deposited sample (LaF_3-substrate, interdigitated structure, 10-10, without SWNTs coating).

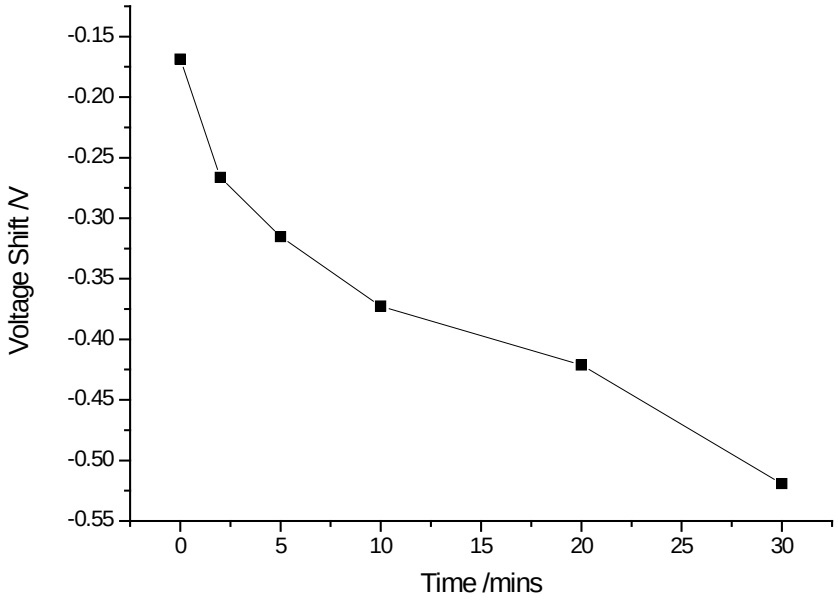

Fig. 106 Voltage shift-time curve of the 30 seconds Pt deposited sample (LaF_3-substrate, interdigitated structure, 10-10, without SWNTs coating) at a capacitance of 1.4 x 10^{-9} F

4.6.5 Hydrogen Sensitivity of the 30 Second Pt Deposited Sample

Based on the proven gas sensing sensitivity against both O_2 and H_2, 30 seconds Pt deposited samples (spray coated with SWNTs, LaF_3-substrate) were selected for further study. To mimic real live gas environment and study the relationship between the sensor signal and the H_2 concentration, the gas response of the sample was tested in a series of gas mixtures (different concentration of H_2 in air). The C-V curves of the 30 seconds Pt deposited samples showed that the C-V curves shifted towards lower voltages with an increase in H_2 concentration (Fig. 107). The dynamic H_2 response was given by the capacitance-time relationship measured at a voltage of -0.5 V (Fig. 108). The H_2 reaction was reversible when the gas concentration changed between 100% and 0% H_2 in air. The voltage shifts at a constant capacitance of 3.3 nF with different H_2 concentration were calculated. A calibration curve where voltage shifts versus log of the hydrogen concentration was normally used as a guideline to evaluate the sensor. A linear relationship with an R^2 of 0.993 was found for the calibration curve of the 30 seconds Pt deposited sample (Fig. 109). The hydrogen sensitivity was determined around 270 mV/logpH_2. This suggested a reliable sensing behaviour.

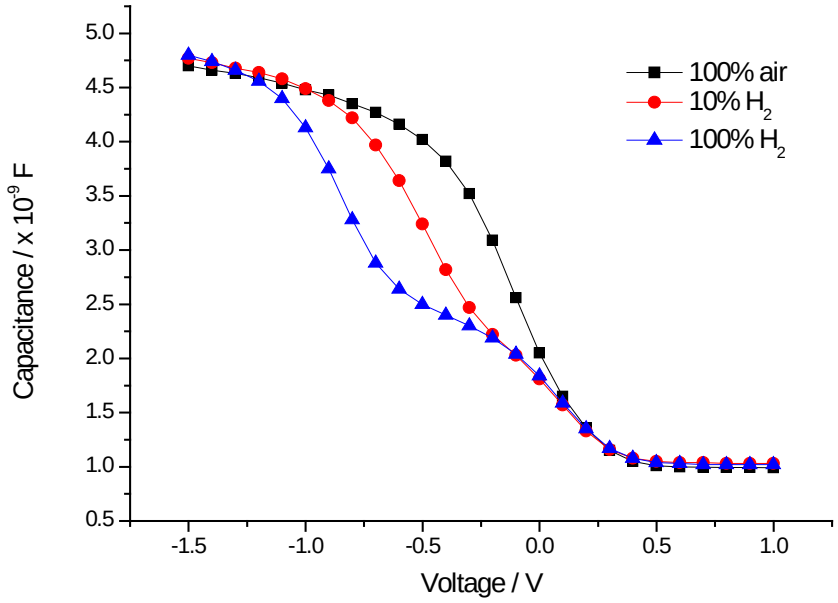

Fig. 107 Capacitance-voltage curves of the 30 seconds Pt deposited sample (SWNTs/DMF, spray coated LaF_3-substrate, 10-10) with different H_2 concentration

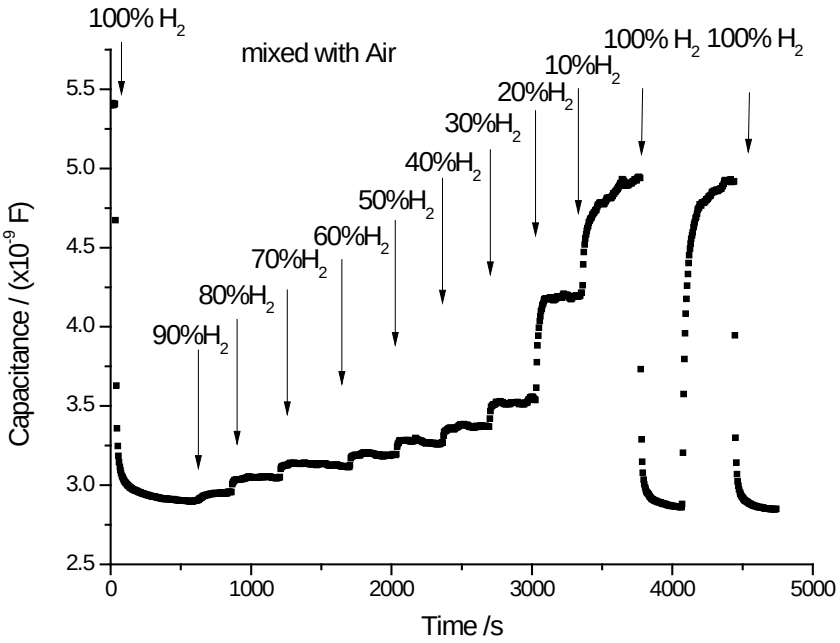

Fig. 108 Capacitance-time relationship of hydrogen reaction of the 30 seconds Pt deposited sample (SWNTs/DMF spray coated LaF_3-substrate, 10-10)

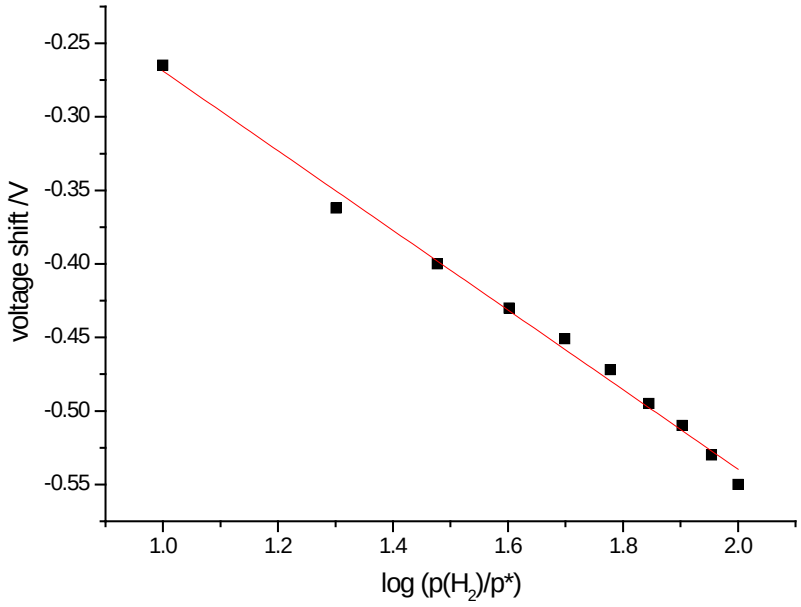

Fig. 109 Calibration curve of the 30 seconds Pt deposited sample (SWNTs/DMF spray coated LaF_3-substrate, 10-10)

The aging effect of the sample was studied by comparing the capacitance-time relationship of the fresh sample and one week old sample with different H_2 concentration. The capacitance-time relationship was obtained at a voltage of -0.5 V. When the gas concentration changed from air to 100% H_2, a rapid drop followed by a steady decrease in the capacitance was observed for the freshly made sample (Fig. 110). A rapid increase followed by a steady increase in capacitance was given when the air was introduced back to the environment. An equilibrium capacitance can be achieved within 200 seconds. By comparison, a continuous capacitance change was found for the sample which was used 1 week after preparation. The time required to achieve the equilibrium capacitance was longer than for the freshly prepared sample. Filippov *et al.* (2006) studied the room-temperature hydrogen sensitivity of a MIS-structure based on the Pt/LaF_3 interface. They found that the sensor gave hydrogen sensitivity at ppm level and has rather fast response time and recovery time. However, the sensor

demonstrated an aging effect, which made the sensor lifetime too short for practical application. In current study, the one week sample showed a slower initial gas response when compared to the freshly prepared sample. The capacitance change within the same period of time (4 minutes) was similar. This suggested the sample was subjected to an aging effect. This problem could be solved by applying a heat treatment for the sample. Field effect gas sensors with a Pt gate have been reactivated by heating at 300°C for 10 seconds (Moritz *et al.*, 2001). This re-activation procedure can be repeated without limitations and could also be applicable to the sensor described in this thesis.

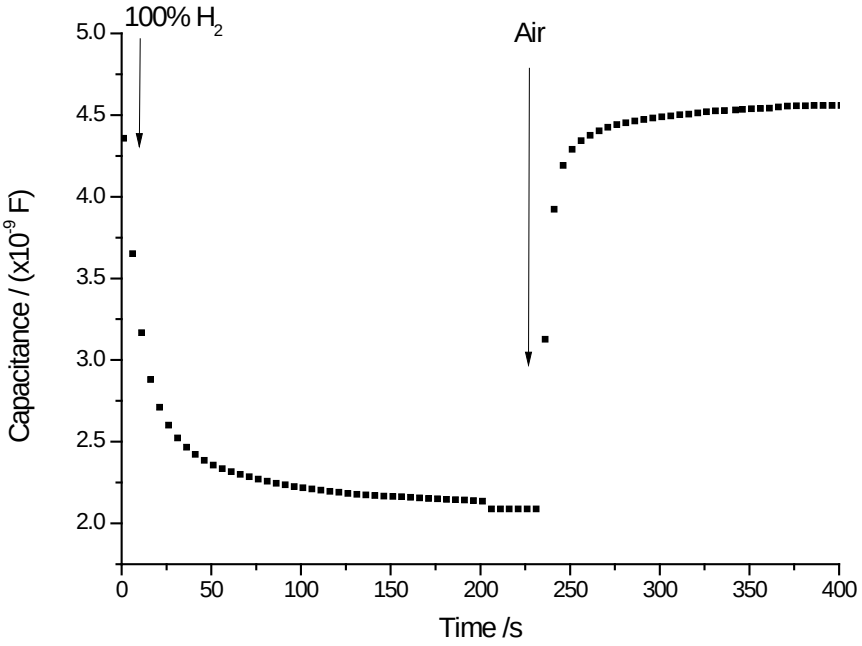

Fig. 110 Capacitance-time relationship of hydrogen reaction of the 30 seconds Pt deposited sample (SWNTs/DMF spray coated LaF_3-substrate, 10-10), fresh sample

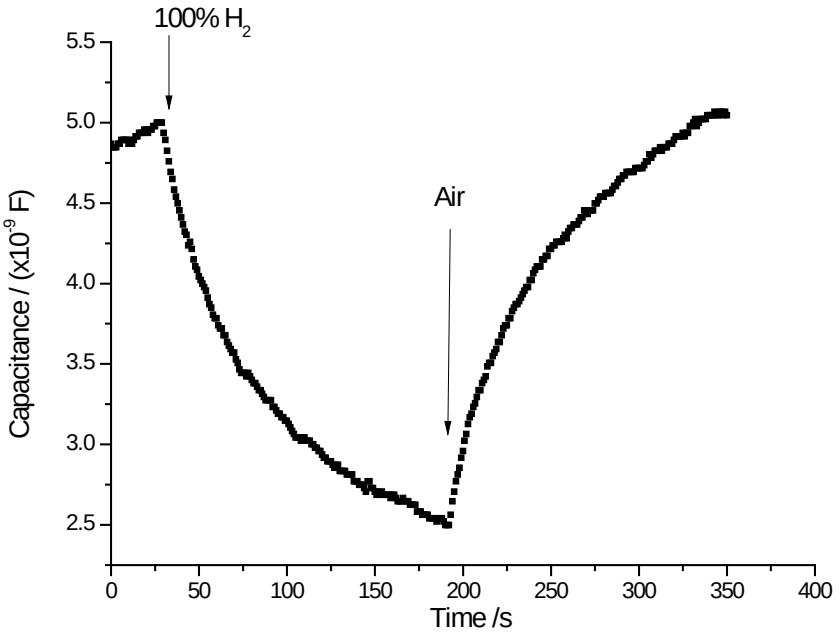

Fig. 111 Capacitance-time relationship of hydrogen reaction of the 30 seconds Pt deposited sample (SWNTs/DMF spray coated LaF_3-substrate, 10-10) one week old

CHAPTER 5

CONCLUSIONS

The study focused on the development of carbon nanotube field-effect gas sensor using carbon nanotubes as gate material. For the very first time, resistance and potentiometric measurements were successfully completed in the same structure.

Two gold electrodes were fabricated on the top of the insulator (Si_3N_4). A multi-walled carbon nanotubes network was used to bridge the two electrodes. The resistance of the CNTs network was monitored to test the gas sensitivity. Compared with vacuum, increased resistance was reported when oxygen was present. Thinner carbon nanotube networks resulted in a greater increase in resistance. However, the resistance increase could not be fully recovered within a short periods without providing additional energy.

Drop coating of the multi-walled carbon nanotubes network on interdigitated gate electrode structures showed negligible CNTs gate function on the C-V curve. With smaller tube diameter and longer tube length, a single-walled carbon nanotube network was then used in order to increase the nanotubes effect on the C-V curves and the sensor response. However, uneven bridging and leakage current were reported when larger amount of SWNTs were applied. This suggested the limitation of drop coating.

An even SWNTs film was produced by spray coating, which bridged the gaps between the two metal electrodes structures. The depletion region in the C-V curve was clearly separated into two distinct parts which were related to the metal gate function contribution and the carbon nanotubes network function contribution. C-V curves shifted by -50 mV with an increase in the H_2 concentration by a factor of 10 (20 - 200 ppm) with a response time of 2 hours. An overall voltage shift of 35 mV (approximately) and a response time of around 2 hours were observed for the same sensor structure when the O_2 concentration changed from 1% to 100%.The sensing response time was too long for practical

applications. The resistance changes of the CNTs network were also measured simultaneously. These two measurements based on different principles were successfully achieved within the same sample structure, which gave the possibility of improvement in the selectivity of sensors.

SDS was used to debundle CNTs. The SDS molecules successfully debundled the SWNTs and created an even SWNTs film. However, it also led to an additional layer on the SWNTs that inhibited the gas reaction at the three phase boundary. DMF was used to separate SWNTs and successfully removed by heat treatment. However, the heat treatment may cause physical detachment of the CNTs from the sample surface. This was considered having a detrimental impact on the gas sensor.

LaF_3 were also introduced to improve the gas sensitivity. However, no improvement of gas sensitivity was observed when the ion conductor level (LaF_3) was added to the system.

Platinum deposited samples (Pt/CNTs/LaF_3/Si_3N_4/SiO_2/Si) demonstrated good hydrogen and oxygen sensitivity. When the gas concentration changed from 1 to 100% H_2, the platinum deposited sample gave a voltage shift of -450 mV. The hydrogen response (an equilibration time of 2 minutes) was faster than that of a sample without the CNTs layer (equilibration time of 30 minutes). A voltage shift of 500 mV was achieved when the oxygen concentration increased from 1% to 100%. The voltage shift achieved was much greater than what was reported in the literature (120 mV, Pt/ LaF_3/Si_3N_4/SiO_2/Si). Both hydrogen and oxygen gas sensitivities suggested that CNTs could significantly improve the sensitivity when using as a template for Pt deposition. However, an aging effect was still noticed in the platinum deposited sample. Moritz *et al.* (2001) successfully reactivated aging samples by applying heat treatment (300°C for 10 seconds). Similar heat treatment could be used to resolve the aging effect of the Pt deposited samples.

The work presented in this thesis clearly suggested the possibility of developing a new carbon nanotube based gas sensor which combines the resistivity measurements with potentiometric measurements for improved sensitivity and selectivity. This is of great interest for prospective applications. It created the possibility to find a fingerprint for different gases based on these two measurements. The combination of these two measurement principles was expected to achieve a higher level of gas selectivity, which would otherwise not be achieved by a single sensor.

CHAPTER 6

FUTURE WORK

The thesis mainly focused on the development of a new type of field-effect capacitive gas sensor with carbon nanotubes as the gate material. The gas (hydrogen and oxygen) response was successfully achieved. However, response time was not promising for application unless further modification was employed. Several attempts have been made to improve the sensitivity of the CNTs gate field-effect capacitive gas sensor. Platinum deposition was introduced and achieved a better hydrogen and oxygen sensitivity. More work is required to explore the possibility to improve the sensitivity of the sensor.

It was reported that polyaniline (PANI) could be formed on the surface of CNTs electrochemically. The PANI/CNTs composite showed some very promising gas sensitive behaviour at room temperature.

UV light induced molecular desorption from SWNTs had been reported previously. The use of UV light was expected to optimise the absorption ability of the CNTs, which should therefore increase sensitivity of the sensor. It will be interesting to explore the effect of the UV light on current sensor structure.

Scanning light pulse technique (SLPT) can also be introduced to this gas sensor (Lofdahl *et al.*, 2001). The local gas response at different points of the gate area can be measured by SLPT. The CNTs could be loaded with different metal particles (Pd, Pt etc) and coated in different area of the surface. The SLPT can be used for identical gases and concentrations.

Further studies should be carried out to explore the effect on the CNTs field-effect gas sensor by other gases. All of the results should be analysed and be used to identify the finger-print of the gases.

CHAPTER 7

REFERENCES

A. Salomonsson, SR, C. Aulin, L. Ojamäe, P.-O. Käll, M. Strand, M. Sanati, A. Lloyd Spetz 2005. RuO2 and Ru Nanoparticles for MISiC-FET Gas Sensors. *Nanotechnology,* 2**,** 269 - 272.

Ajayan, PM, Lambert, JM, Bernier, P, Barbedette, L, Colliex, C and Planeix, JM 1993. Growth Morphologies during Cobalt-Catalyzed Single-Shell Carbon Nanotube Synthesis. *Chemical Physics Letters,* 215**,** 509-517.

Arbab, A, Spetz, A and Lundstrom, I 1993. Gas Sensors for High-Temperature Operation Based on Metal-Oxide-Silicon Carbide (Mosic) Devices. *Sensors and Actuators B-Chemical,* 15**,** 19-23.

Baird, T, Fryer, JR and Grant, B 1974. Carbon Formation on Iron and Nickel Foils by Hydrocarbon Pyrolysis - Reactions at 700degreesc. *Carbon,* 12**,** 591-602.

Baker, RTK and Chludzinski, JJ 1980. Filamentous Carbon Growth on Nickel-Iron Surfaces - the Effect of Various Oxide Additives. *Journal of Catalysis,* 64**,** 464-478.

Baker, RTK, Harris, PS, Thomas, RB and Waite, RJ 1973. Formation of Filamentous Carbon from Iron, Cobalt and Chromium Catalyzed Decomposition of Acetylene. *Journal of Catalysis,* 30**,** 86-95.

Baughman, RH, Zakhidov, AA and de Heer, WA 2002. Carbon nanotubes - the route toward applications. *Science,* 297**,** 787-792.

Bittencourt, C, Felten, A, Espinosa, EH, Ionescu, R, Llobet, E, Corteig, X and Pireaux, JJ 2006. WO_3 films modified with functionalised multi-wall carbon nanotubes: Morphological, compositional and gas response studies. *Sensors and Actuators B-Chemical,* 115**,** 33-41.

Bradley, K, Jhi, S-H, Collins, PG, Hone, J, Cohen, ML, Louie, SG and Zettl, A 2000. Is the Intrinsic Thermoelectric Power of Carbon Nanotubes Positive? *Physical Review Letters,* 85**,** 4361-4364.

Cantalini, C, Valentini, L, Lozzi, L, Armentano, I, Kenny, JM and Santucci, S 2003. NO2 gas sensitivity of carbon nanotubes obtained by plasma enhanced chemical vapor deposition. *Sensors and Actuators B-Chemical,* 93**,** 333-337.

Chang, H, Lee, JD, Lee, SM and Lee, YH 2001. Adsorption of NH3 and NO2 molecules on carbon nanotubes. *Applied Physics Letters,* 79**,** 3863-3865.

Chen, D-J, Lei, S, Wang, R-H, Pan, M and Chen, Y-Q 2012. Dielectrophoresis Carbon Nanotube and Conductive Polyaniline Nanofiber NH3 Gas Sensor. *Chinese Journal of Analytical Chemistry,* 40**,** 145-149.

Chen, RJ, Zhang, Y, Wang, D and Dai, H 2001. Noncovalent Sidewall Functionalization of Single-Walled Carbon Nanotubes for Protein Immobilization. *J. Am. Chem. Soc.,* 123**,** 3838-3839.

Chopra, N, Kichambare, PD, Andrews, R and Hinds, BJ 2002. Control of multiwalled carbon nanotube diameter by selective growth on the exposed edge of a thin film multilayer structure. *Nano Letters,* 2**,** 1177-1181.

Chopra, S, McGuire, K, Gothard, N, Rao, AM and Pham, A 2003. Selective gas detection using a carbon nanotube sensor. *Applied Physics Letters,* 83**,** 2280-2282.

Collins, PG, Bradley, K, Ishigami, M and Zettl, A 2000. Extreme oxygen sensitivity of electronic properties of carbon nanotubes. *Science,* 287**,** 1801-1804.

Dai, LM, He, PG and Li, SN 2003. Functionalized surfaces based on polymers and carbon nanotubes for some biomedical and optoelectronic applications. *Nanotechnology,* 14**,** 1081-1097.

Danielsson, B, Lundstrom, I, Mosbach, K and Stiblert, L 1979. New Enzyme Transducer Combination - Enzyme Transistor. *Analytical Letters Part B-Clinical and Biochemical Analysis,* 12**,** 1189-1199.

Davis, WR, Slawson, RJ and Rigby, GR 1953. An Unusual Form of Carbon. *Nature,* 171**,** 756-756.

Day, TM, Unwin, PR, Wilson, NR and Macpherson, JV 2005. Electrochemical Templating of Metal Nanoparticles and Nanowires on Single-Walled Carbon Nanotube Networks. *Journal of the American Chemical Society,* 127**,** 10639-10647.

Demczyk, BG, Wang, YM, Cumings, J, Hetman, M, Han, W, Zettl, A and Ritchie, RO 2002. Direct mechanical measurement of the tensile strength and elastic modulus of multiwalled carbon nanotubes. *Materials Science and Engineering a-Structural Materials Properties Microstructure and Processing,* 334**,** 173-178.

Dresselhaus, MS, Dresselhaus, G and Saito, R 1992. Carbon fibers based on C_{60} and their symmetry. *Physical Review B,* 45**,** 6234-6242.

Ebbesen, TW and Ajayan, PM 1992. Large-Scale Synthesis of Carbon Nanotubes. *Nature,* 358**,** 220-222.

Falvo, MR, Clary, GJ, Taylor, RM, Chi, V, Brooks, FP, Washburn, S and Superfine, R 1997. Bending and buckling of carbon nanotubes under large strain. *Nature,* 389**,** 582-584.

Fam, DWH, Tok, AIY, Palaniappan, A, Nopphawan, P, Lohani, A and Mhaisalkar, SG 2009. Selective sensing of hydrogen sulphide using silver nanoparticle decorated carbon nanotubes. *Sensors and Actuators B: Chemical,* 138**,** 189-192.

Filippov, VI, Vasiliev, AA, Moritz, W and Szeponik, J 2006. Room-temperature hydrogen sensitivity of a MIS-structure based on the Pt/LaF3 interface. *Ieee Sensors Journal,* 6**,** 1250-1255.

Furtado, CA, Kim, UJ, Gutierrez, HR, Pan, L, Dickey, EC and Eklund, PC 2004. Debundling and dissolution of single-walled carbon nanotubes in amide solvents. *Journal of the American Chemical Society,* 126**,** 6095-6105.

Goldoni, A, Larciprete, R, Petaccia, L and Lizzit, S 2003. Single-wall carbon nanotube interaction with gases: Sample contaminants and environmental monitoring. *Journal of the American Chemical Society,* 125**,** 11329-11333.

Goldoni, A, Petaccia, L, Gregoratti, L, Kaulich, B, Barinov, A, Lizzit, S, Laurita, A, Sangaletti, L and Larciprete, R 2004. Spectroscopic characterization of contaminants and interaction with gases in single-walled carbon nanotubes. *Carbon,* 42**,** 2099-2112.

Guo, T, Nikolaev, P, Rinzler, AG, Tomanek, D, Colbert, DT and Smalley, RE 1995a. Self-Assembly of Tubular Fullerenes. *Journal of Physical Chemistry,* 99**,** 10694-10697.

Guo, T, Nikolaev, P, Thess, A, Colbert, DT and Smalley, RE 1995b. Catalytic Growth of Single-Walled Nanotubes by Laser Vaporization. *Chemical Physics Letters,* 243**,** 49-54.

Haridas, D, Sreenivas, K and Gupta, V 2008. Improved response characteristics of SnO2 thin film loaded with nanoscale catalysts for LPG detection. *Sensors and Actuators B: Chemical,* 133**,** 270-275.

Harutyunyan, AR, Pradhan, BK, Chang, JP, Chen, GG and Eklund, PC 2002. Purification of single-wall carbon nanotubes by selective microwave heating of catalyst particles. *Journal of Physical Chemistry B,* 106**,** 8671-8675.

He, L, Jia, Y, Meng, F, Li, M and Liu, J 2009. Gas sensors for ammonia detection based on polyaniline-coated multi-wall carbon nanotubes. *Materials Science and Engineering: B,* 163**,** 76-81.

He, YM, Chen, WJ, Gao, CT, Zhou, JY, Li, XD and Xie, EQ 2013. An overview of carbon materials for flexible electrochemical capacitors. *Nanoscale,* 5**,** 8799-8820.

Hilder, TA, Pace, RJ and Chung, SH 2012. Computational Design of a Carbon Nanotube Fluorofullerene Biosensor. *Sensors,* 12**,** 13720-13735.

Hirsch, A 2002. Funktionalisierung von einwandigen Kohlenstoffnanoröhren. *Angewandte Chemie,* 114**,** 1933-1939.

Hoa, ND, Quy, NV, Suk Cho, Y and Kim, D 2007. Nanocomposite of SWNTs and SnO2 fabricated by soldering process for ammonia gas sensor application. *physica status solidi (a),* 204**,** 1820-1824.

Hofer, LJE, Sterling, E and McCartney, JT 1955. Structure of Carbon Deposited from Carbon Monoxide on Iron, Cobalt and Nickel. *The Journal of Physical Chemistry,* 59**,** 1153-1155.

Huang, CS, Yeh, CY, Yuan, CH, Huang, BR and Hsiao, CH 2009. The study of a carbon nanotube O-2 sensor by field emission treatment. *Diamond and Related Materials,* 18**,** 461-464.

Huang, HJ, Kajiura, H, Tsutsui, S, Hirano, Y, Miyakoshi, M, Yamada, A and Ata, M 2001. Large-scale rooted growth of aligned super bundles of single-walled carbon nanotubes using a directed arc plasma method. *Chemical Physics Letters,* 343**,** 7-14.

Iijima, S 1991. Helical Microtubules of Graphitic Carbon. *Nature,* 354**,** 56-58.

Iijima, S 2002. Carbon nanotubes: past, present, and future. *Physica B: Condensed Matter,* 323**,** 1-5.

Iijima, S and Ichihashi, T 1993. Single-Shell Carbon Nanotubes of 1-Nm Diameter. *Nature,* 363**,** 603-605.

Jennifer, S-O, Hung-Ta, W, Byoung, SK, Zhuangchun, W, Fan, R, Andrew, GR and Stephen, JP 2005. Carbon nanotube films for room temperature hydrogen sensing. *Nanotechnology,* 16**,** 2218.

Jian, JM, Guo, XS, Lin, LW, Cai, Q, Cheng, J and Li, JP 2013. Gas-sensing characteristics of dielectrophoretically assembled composite film of oxygen plasma-treated SWCNTs and PEDOT/PSS polymer. *Sensors and Actuators B-Chemical,* 178**,** 279-288.

Jinesh, KB, Dam, VAT, Swerts, J, de Nooijer, C, van Elshocht, S, Brongersma, SH and Crego-Calama, M 2011. Room-temperature CO2 sensing using metal–insulator–semiconductor capacitors comprising atomic-layer-deposited La2O3 thin films. *Sensors and Actuators B: Chemical,* 156**,** 276-282.

Joseyacaman, M, Mikiyoshida, M, Rendon, L and Santiesteban, JG 1993. Catalytic Growth of Carbon Microtubules with Fullerene Structure (Applied Physics Letter, Vol 62, Pg 202, 1993). *Applied Physics Letters,* 62**,** 657-659.

Journet, C, Maser, WK, Bernier, P, Loiseau, A, delaChapelle, ML, Lefrant, S, Deniard, P, Lee, R and Fischer, JE 1997. Large-scale production of single-walled carbon nanotubes by the electric-arc technique. *Nature,* 388**,** 756-758.

Junya, S, Guangbin, Z and Masanori, H 2003. Fabrication of a carbon nanotube-based gas sensor using dielectrophoresis and its application for ammonia detection by impedance spectroscopy. *Journal of Physics D: Applied Physics,* 36**,** L109.

Kanazawa, E, Sakai, G, Shimanoe, K, Kanmura, Y, Teraoka, Y, Miura, N and Yamazoe, N 2001. Metal oxide semiconductor N2O sensor for medical use. *Sensors and Actuators B: Chemical,* 77**,** 72-77.

Kang, WP and Kim, CK 1994. Performance analysis of a new metal-insulator-semiconductor capacitor incorporated with Pt-SnO[sub x] catalytic layers for the detection of O[sub 2] and CO gases. *Journal of Applied Physics,* 75**,** 4237-4242.

Kaniyoor, A, Imran Jafri, R, Arockiadoss, T and Ramaprabhu, S 2009a. Nanostructured Pt decorated graphene and multi walled carbon nanotube based room temperature hydrogen gas sensor. *Nanoscale,* 1**,** 382-386.

Kaniyoor, A, Jafri, RI, Arockiadoss, T and Ramaprabhu, S 2009b. Nanostructured Pt decorated graphene and multi walled carbon nanotube based room temperature hydrogen gas sensor. *Nanoscale,* 1**,** 382-386.

Kanzow, H, Lenski, C and Ding, A 2001. Single-wall carbon nanotube diameter distributions calculated from experimental parameters. *Physical Review B,* 63**,** -.

Kong, J, Franklin, NR, Zhou, CW, Chapline, MG, Peng, S, Cho, KJ and Dai, HJ 2000. Nanotube molecular wires as chemical sensors. *Science,* 287**,** 622-625.

Krause, S, Krankenhagen, R, Moritz, W, Grohmann, I, Unger, W, Gross, T and Lippitz, A 1993. Influence of the Laf3 Metal Interface on the Properties of a Low-Temperature Oxygen Sensor. *Sensors and Actuators B-Chemical,* 16**,** 252-255.

Krause, S, Moritz, W and Grohmann, I 1992. A Low-Temperature Oxygen Sensor Based on the Si/Laf3/Pt Capacitive Structure. *Sensors and Actuators B-Chemical,* 9**,** 191-196.

Krishnan, A, Dujardin, E, Treacy, MMJ, Hugdahl, J, Lynum, S and Ebbesen, TW 1997. Graphitic cones and the nucleation of curved carbon surfaces. *Nature,* 388**,** 451-454.

Kroto, HW, Heath, JR, Obrien, SC, Curl, RF and Smalley, RE 1985. C-60 - Buckminsterfullerene. *Nature,* 318**,** 162-163.

Kumar, MK and Ramaprabhu, S 2006. Nanostructured Pt Functionlized Multiwalled Carbon Nanotube Based Hydrogen Sensor. *The Journal of Physical Chemistry B,* 110**,** 11291-11298.

La, D-D, Kim, CK, Jun, TS, Jung, Y, Seong, GH, Choo, J and Kim, YS 2011. Pt nanoparticle-supported multiwall carbon nanotube electrodes for amperometric hydrogen detection. *Sensors and Actuators B: Chemical,* 155**,** 191-198.

Lambert, JM, Ajayan, PM, Bernier, P, Planeix, JM, Brotons, V, Coq, B and Castaing, J 1994. Improving Conditions Towards Isolating Single-Shell Carbon Nanotubes. *Chemical Physics Letters,* 226**,** 364-371.

Larciprete, R, Petaccia, L, Lizzit, S and Goldoni, A 2007. The Role of Metal Contact in the Sensitivity of Single-Walled Carbon Nanotubes to NO2. *The Journal of Physical Chemistry C,* 111**,** 12169-12174.

Lee, JH, Kang, WS, Choi, BS, Choi, SW and Kim, JH 2008a. Fabrication of carbon nanotube AFM probes using the Langmuir-Blodgett technique. *Ultramicroscopy,* 108**,** 1163-1167.

Lee, JS, Shin, SM and Park, JW 1997. Surface morphology variation of Pt-Al2O3 thin catalyst films. *Sensors and Materials,* 9**,** 35-45.

Lee, K, Lee, J-W, Dong, K-Y and Ju, B-K 2008b. Gas sensing properties of single-wall carbon nanotubes dispersed with dimethylformamide. *Sensors and Actuators B: Chemical,* 135**,** 214-218.

Lee, K, Scardaci, V, Kim, H-Y, Hallam, T, Nolan, H, Bolf, BE, Maltbie, GS, Abbott, JE and Duesberg, GS 2013. Highly sensitive, transparent, and flexible gas sensors based on gold nanoparticle decorated carbon nanotubes. *Sensors and Actuators B: Chemical,* 188**,** 571-575.

Lee, WH, Kim, SJ, Lee, WJ, Lee, JG, Haddon, RC and Reucroft, PJ 2001. X-ray photoelectron spectroscopic studies of surface modified single-walled carbon nanotube material. *Applied Surface Science,* 181**,** 121-127.

Leghrib, R, Felten, A, Demoisson, F, Reniers, F, Pireaux, J-J and Llobet, E 2010a. Room-temperature, selective detection of benzene at trace levels using plasma-treated metal-decorated multiwalled carbon nanotubes. *Carbon,* 48**,** 3477-3484.

Leghrib, R and Llobet, E 2011. Quantitative trace analysis of benzene using an array of plasma-treated metal-decorated carbon nanotubes and fuzzy adaptive resonant theory techniques. *Analytica Chimica Acta,* 708**,** 19-27.

Leghrib, R, Pavelko, R, Felten, A, Vasiliev, A, Cané, C, Gràcia, I, Pireaux, J-J and Llobet, E 2010b. Gas sensors based on multiwall carbon nanotubes decorated with tin oxide nanoclusters. *Sensors and Actuators B: Chemical,* 145**,** 411-416.

Li, J, Lu, Y, Ye, Q, Cinke, M, Han, J and Meyyappan, M 2003. Carbon Nanotube Sensors for Gas and Organic Vapor Detection. *Nano Letters,* 3**,** 929-933.

Li, S, Yang, XD, Zhu, HY, Liu, Y and Liu, YN 2011. Hydrogen Storage Alloy and Carbon Nanotubes Mixed Catalyst in a Direct Borohydride Fuel Cell. *Journal of Materials Science & Technology,* 27**,** 1089-1093.

Liang, YX, Chen, YJ and Wang, TH 2004. Low-resistance gas sensors fabricated from multiwalled carbon nanotubes coated with a thin tin oxide layer. *Applied Physics Letters,* 85**,** 666-668.

Lin, T, Bajpai, V, Ji, T and Dai, LM 2003. Chemistry of carbon nanotubes. *Australian Journal of Chemistry,* 56**,** 635-651.

Liu, ZF, Shen, ZY, Zhu, T, Hou, SF, Ying, LZ, Shi, ZJ and Gu, ZN 2000. Organizing single-walled carbon nanotubes on gold using a wet chemical self-assembling technique. *Langmuir,* 16**,** 3569-3573.

Llobet, E, Espinosa, EH, Sotter, E, Ionescu, R, Vilanova, X, Torres, J, Felten, A, Pireaux, JJ, Ke, X, Tendeloo, GV, Renaux, F, Paint, Y, Hecq, M and Bittencourt, C 2008. Carbon nanotube–TiO 2 hybrid films for detecting traces of O 2. *Nanotechnology,* 19**,** 375501.

Lofdahl, M, Utaiwasin, C, Carlsson, A, Lundstrom, I and Eriksson, M 2001. Gas response dependence on gate metal morphology of field-effect devices. *Sensors and Actuators B-Chemical,* 80**,** 183-192.

Lu, Y, Li, J, Han, J, Ng, HT, Binder, C, Partridge, C and Meyyappan, M 2004a. Room temperature methane detection using palladium loaded single-walled carbon nanotube sensors. *Chemical Physics Letters,* 391**,** 344-348.

Lu, YJ, Li, J, Han, J, Ng, HT, Binder, C, Partridge, C and Meyyappan, M 2004b. Room temperature methane detection using palladium loaded single-walled carbon nanotube sensors. *Chemical Physics Letters,* 391**,** 344-348.

Lundström, I, Shivaraman, S, Svensson, C and Lundkvist, L 1975. A hydrogen - sensitive MOS field - effect transistor. *Applied Physics Letters,* 26**,** 55-57

Lundstrom, I 1981. Hydrogen Sensitive Mos-Structures .1. Principles and Applications. *Sensors and Actuators,* 1**,** 403-426.

Lundstrom, I, Armgarth, M and Petersson, LG 1989. Physics with Catalytic Metal Gate Chemical Sensors. *Crc Critical Reviews in Solid State and Materials Sciences,* 15**,** 201-278.

Lundstrom, I and Soderberg, D 1981. Hydrogen Sensitive Mos-Structures .2. Characterization. *Sensors and Actuators,* 2**,** 105-138.

Lundstrom, KI, Shivaraman, MS and Svensson, CM 1975. Hydrogen-Sensitive Pd-Gate Mos-Transistor. *Journal of Applied Physics,* 46**,** 3876-3881.

Male, KB, Hrapovic, S, Liu, Y, Wang, D and Luong, JHT 2004. Electrochemical detection of carbohydrates using copper nanoparticles and carbon nanotubes. *Analytica Chimica Acta,* 516**,** 35-41.

Martel, R, Schmidt, T, Shea, HR, Hertel, T and Avouris, P 1998. Single- and multi-wall carbon nanotube field-effect transistors. *Applied Physics Letters,* 73**,** 2447-2449.

Mercuri, F, Sgamellotti, A, Valentini, L, Armentano, I and Kenny, JM 2005. Vacancy-induced chemisorption of NO2 on carbon nanotubes: A combined theoretical and experimental study. *Journal of Physical Chemistry B,* 109**,** 13175-13179.

Miasik, JJ, Hooper, A and Tofield, BC 1986. Conducting polymer gas sensors. *Journal of the Chemical Society, Faraday Transactions 1: Physical Chemistry in Condensed Phases,* 82**,** 1117-1126.

Miura, N, Hisamoto, J, Yamazoe, N, Kuwata, S and Salardenne, J 1989. Solid-state oxygen sensor using sputtered LaF3 film. *Sensors and Actuators,* 16**,** 301-310.

Moritz, W, Fillipov, V, Vasiliev, A, Bartholomaus, L and Terentjev, A 1999. Field-effect sensor for the selective detection of fluorocarbons. *Journal of Fluorine Chemistry,* 93**,** 61-67.

Moritz, W, Krause, S, Roth, U, Klimm, D and Lippitz, A 2001. Re-activation of an all solid state oxygen sensor. *Analytica Chimica Acta,* 437**,** 183-190.

Mubarak, NM, Sahu, JN, Abdullah, EC and Jayakumar, NS 2014. Removal of Heavy Metals from Wastewater Using Carbon Nanotubes. *Separation and Purification Reviews,* 43**,** 311-338.

Mubeen, S, Lai, M, Zhang, T, Lim, J-H, Mulchandani, A, Deshusses, MA and Myung, NV 2013. Hybrid tin oxide-SWNT nanostructures based gas sensor. *Electrochimica Acta,* 92**,** 484-490.

Mubeen, S, Zhang, T, Chartuprayoon, N, Rheem, Y, Mulchandani, A, Myung, NV and Deshusses, MA 2009. Sensitive Detection of H2S Using Gold Nanoparticle Decorated Single-Walled Carbon Nanotubes. *Analytical Chemistry,* 82**,** 250-257.

Mubeen, S, Zhang, T, Yoo, B, Deshusses, MA and Myung, NV 2007. Palladium Nanoparticles Decorated Single-Walled Carbon Nanotube Hydrogen Sensor. *The Journal of Physical Chemistry C,* 111**,** 6321-6327.

Na, PS, Kim, HJ, So, HM, Kong, KJ, Chang, HJ, Ryu, BH, Choi, YM, Lee, JO, Kim, BK, Kim, JJ and Kim, JH 2005. Investigation of the humidity effect on the electrical properties of single-walled carbon nanotube transistors. *Applied Physics Letters,* 87**,** -.

Oberlin, A, Endo, M and Koyama, T 1976. Filamentous growth of carbon through benzene decomposition. *Journal of Crystal Growth,* 32**,** 335-349.

Peng, B, Locascio, M, Zapol, P, Li, S, Mielke, SL, Schatz, GC and Espinosa, HD 2008. Measurements of near-ultimate strength for multiwalled carbon nanotubes and irradiation-induced crosslinking improvements. *Nat Nano,* 3**,** 626-631.

Peng, S and Cho, KJ 2000. Chemical control of nanotube electronics. *Nanotechnology,* 11**,** 57-60.

Peng, S and Cho, KJ 2003. Ab initio study of doped carbon nanotube sensors. *Nano Letters,* 3**,** 513-517.

Penza, M, Alvisi, M, Rossi, R, Serra, E, Paolesse, R, D'Amico, A and Natale, CD 2011a. Carbon nanotube films as a platform to transduce molecular recognition events in metalloporphyrins. *Nanotechnology,* 22**,** 125502.

Penza, M, Cassano, G, Rossi, R, Alvisi, M, Rizzo, A, Signore, MA, Dikonimos, T, Serra, E and Giorgi, R 2007. Enhancement of sensitivity in gas chemiresistors based on carbon nanotube surface functionalized with noble metal (Au, Pt) nanoclusters. *Applied Physics Letters,* 90**,** -.

Penza, M, Rossi, R, Alvisi, M, Signore, MA, Cassano, G, Dimaio, D, Pentassuglia, R, Piscopiello, E, Serra, E and Falconieri, M 2009. Characterization of metal-modified and vertically-aligned carbon nanotube films for functionally enhanced gas sensor applications. *Thin Solid Films,* 517**,** 6211-6216.

Penza, M, Rossi, R, Alvisi, M, Suriano, D and Serra, E 2011b. Pt-modified carbon nanotube networked layers for enhanced gas microsensors. *Thin Solid Films,* 520**,** 959-965.

Picaud, F, Langlet, R, Arab, M, Devel, M, Girardet, C, Natarajan, S, Chopra, S and Rao, AM 2005. Gas-induced variation in the dielectric properties of carbon nanotube bundles for selective sensing. *Journal of Applied Physics,* 97**,** -.

Qi, P, Vermesh, O, Grecu, M, Javey, A, Wang, Q, Dai, H, Peng, S and Cho, KJ 2003. Toward Large Arrays of Multiplex Functionalized Carbon Nanotube Sensors for Highly Sensitive and Selective Molecular Detection. *Nano Letters,* 3**,** 347-351.

Qin, S, Wu, Z, Tang, Z, Song, Y, Zeng, F and Zhao, D 2000. The sensitivity to SO2 of the SAW gas sensor with triethanolamine modified with boric acid. *Sensors and Actuators B: Chemical,* 66**,** 240-242.

Quang, NH, Van Trinh, M, Lee, BH and Huh, JS 2006. Effect of NH3 gas on the electrical properties of single-walled carbon nanotube bundles. *Sensors and Actuators B-Chemical,* 113**,** 341-346.

Rahman, MH, Thakur, JS, Rimai, L, Perooly, S, Naik, R, Zhang, L, Auner, GW and Newaz, G 2008. Dual-mode operation of a Pd/AlN/SiC device for hydrogen sensing. *Sensors and Actuators B: Chemical,* 129**,** 35-39.

Saito, R, Fujita, M, Dresselhaus, G and Dresselhaus, MS 1992. Electronic-Structure of Chiral Graphene Tubules. *Applied Physics Letters,* 60**,** 2204-2206.

Saito, Y, Hamaguchi, K, Uemura, S, Uchida, K, Tasaka, Y, Ikazaki, F, Yumura, M, Kasuya, A and Nishina, Y 1998a. Field emission from multi-walled carbon nanotubes and its application to electron tubes. *Applied Physics a-Materials Science & Processing,* 67**,** 95-100.

Saito, Y, Tani, Y, Miyagawa, N, Mitsushima, K, Kasuya, A and Nishina, Y 1998b. High yield of single-wall carbon nanotubes by arc discharge using Rh-Pt mixed catalysts. *Chemical Physics Letters,* 294**,** 593-598.

Samman, A, Gebremariam, S, Rimai, L, Zhang, X, Hangas, J and Auner, GW 2000. Silicon-carbide MOS capacitors with laser-ablated Pt gate as combustible gas sensors. *Sensors and Actuators B-Chemical,* 63**,** 91-102.

Santucci, S, Picozzi, S, Di Gregorio, F, Lozzi, L, Cantalini, C, Valentini, L, Kenny, JM and Delley, B 2003. NO2 and CO gas adsorption on carbon nanotubes: Experiment and theory. *Journal of Chemical Physics,* 119**,** 10904-10910.

Sayago, I, Terrado, E, Aleixandre, M, Horrillo, MC, Fernández, MJ, Lozano, J, Lafuente, E, Maser, WK, Benito, AM, Martinez, MT, Gutiérrez, J and Muñoz, E 2007. Novel selective sensors based on carbon nanotube films for hydrogen detection. *Sensors and Actuators B: Chemical,* 122**,** 75-80.

Sayago, I, Terrado, E, Lafuente, E, Horrillo, MC, Maser, WK, Benito, AM, Navarro, R, Urriolabeitia, EP, Martinez, MT and Gutierrez, J 2005. Hydrogen sensors based on carbon nanotubes thin films. *Synthetic Metals,* 148**,** 15-19.

Schlecht, U, Balasubramanian, K, Burghard, M and Kern, K 2007. Electrochemically decorated carbon nanotubes for hydrogen sensing. *Applied Surface Science,* 253**,** 8394-8397.

Sharma, A, Tomar, M and Gupta, V 2012. Room temperature trace level detection of NO2 gas using SnO2 modified carbon nanotubes based sensor. *Journal of Materials Chemistry,* 22**,** 23608-23616.

Sharma, RK, Bhatnagar, MC and Sharma, GL 1998. Mechanism in Nb doped titania oxygen gas sensor. *Sensors and Actuators B: Chemical,* 46**,** 194-201.

Shimizu, Y, Matsunaga, N, Hyodo, T and Egashira, M 2001. Improvement of SO2 sensing properties of WO3 by noble metal loading. *Sensors and Actuators B: Chemical,* 77**,** 35-40.

Shivananju, BN, Yamdagni, S, Fazuldeen, R, Kumar, AKS, Hegde, GM, Varma, MM and Asokan, S 2013. CO2 sensing at room temperature using carbon nanotubes coated core fiber Bragg grating. *Review of Scientific Instruments,* 84.

Someya, T, Small, J, Kim, P, Nuckolls, C and Yardley, JT 2003. Alcohol vapor sensors based on single-walled carbon nanotube field effect transistors. *Nano Letters,* 3**,** 877-881.

Spetz, A, Armgarth, M and Lundstrom, I 1988. Hydrogen and Ammonia Response of Metal-Silicon Dioxide-Silicon Structures with Thin Platinum Gates. *Journal of Applied Physics,* 64**,** 1274-1283.

Spetz, AL, Uneus, L, Svenningstorp, H, Tobias, P, Ekedahl, LG, Larsson, O, Goras, A, Savage, S, Harris, C, Martensson, P, Wigren, R, Salomonsson, P, Haggendahl, B, Ljung, P, Mattsson, M and Lundstrom, I 2001. SiC based field effect gas sensors for industrial applications. *Physica Status Solidi a-Applied Research,* 185**,** 15-25.

Star, A, Joshi, V, Skarupo, S, Thomas, D and Gabriel, J-CP 2006a. Gas Sensor Array Based on Metal-Decorated Carbon Nanotubes. *The Journal of Physical Chemistry B,* 110**,** 21014-21020.

Star, A, Joshi, V, Skarupo, S, Thomas, D and Gabriel, JCP 2006b. Gas sensor array based on metal-decorated carbon nanotubes. *Journal of Physical Chemistry B,* 110**,** 21014-21020.

Steele, MC, Hile, JW and MacIver, BA 1976. Hydrogen-sensitive palladium gate MOS capacitors. *Journal of Applied Physics,* 47**,** 2537-2538.

Strano, MS, Moore, VC, Miller, MK, Allen, MJ, Haroz, EH, Kittrell, C, Hauge, RH and Smalley, RE 2003. The role of surfactant adsorption during ultrasonication in the dispersion of single-walled carbon nanotubes. *Journal of Nanoscience and Nanotechnology,* 3**,** 81-86.

Subramoney, S, Ruoff, RS, Lorents, DC and Malhotra, R 1993. Radial Single-Layer Nanotubes. *Nature,* 366**,** 637-637.

Sugie, H, Tanemura, M, Filip, V, Iwata, K, Takahashi, K and Okuyama, F 2001. Carbon nanotubes as electron source in an x-ray tube. *Applied Physics Letters,* 78**,** 2578-2580.

Sumanasekera, GU, Adu, CKW, Fang, S and Eklund, PC 2000. Effects of Gas Adsorption and Collisions on Electrical Transport in Single-Walled Carbon Nanotubes. *Physical Review Letters,* 85**,** 1096-1099.

Sun, Y and Wang, HH 2007a. Electrodeposition of Pd nanoparticles on single-walled carbon nanotubes for flexible hydrogen sensors. *Applied Physics Letters,* 90**,** -.

Sun, YG and Wang, HH 2007b. High-performance, flexible hydrogen sensors that use carbon nanotubes decorated with palladium nanoparticles. *Advanced Materials,* 19**,** 2818-+.

Tans, SJ, Verschueren, ARM and Dekker, C 1998. Room-temperature transistor based on a single carbon nanotube. *Nature,* 393**,** 49-52.

Terrones, M 2003. Science and technology of the twenty-first century: Synthesis, properties and applications of carbon nanotubes. *Annual Review of Materials Research,* 33**,** 419-501.

Thess, A, Lee, R, Nikolaev, P, Dai, HJ, Petit, P, Robert, J, Xu, CH, Lee, YH, Kim, SG, Rinzler, AG, Colbert, DT, Scuseria, GE, Tomanek, D, Fischer, JE and Smalley, RE 1996. Crystalline ropes of metallic carbon nanotubes. *Science,* 273**,** 483-487.

Valentini, L, Armentano, I, Kenny, JM, Cantalini, C, Lozzi, L and Santucci, S 2003. Sensors for sub-ppm NO2 gas detection based on carbon nanotube thin films. *Applied Physics Letters,* 82**,** 961-963.

Valentini, L, Bavastrello, V, Stura, E, Armentano, I, Nicolini, C and Kenny, JM 2004. Sensors for inorganic vapor detection based on carbon nanotubes and poly(o-anisidine) nanocomposite material. *Chemical Physics Letters,* 383**,** 617-622.

Wang, D, Ma, Z, Dai, S, Liu, J, Nie, Z, Engelhard, MH, Huo, Q, Wang, C and Kou, R 2008. Low-Temperature Synthesis of Tunable Mesoporous Crystalline Transition Metal Oxides and Applications as Au Catalyst Supports. *The Journal of Physical Chemistry C,* 112**,** 13499-13509.

Wang, X, Li, Q, Xie, J, Jin, Z, Wang, J, Li, Y, Jiang, K and Fan, S 2009. Fabrication of Ultralong and Electrically Uniform Single-Walled Carbon Nanotubes on Clean Substrates. *Nano Letters,* 9**,** 3137-3141.

Wang, Y and Yeow, JT 2009. A review of carbon nanotubes-based gas sensors. *Journal of Sensors,* 2009.

Watson, KA, Ghose, S, Delozier, DM, Smith Jr, JG and Connell, JW 2005. Transparent, flexible, conductive carbon nanotube coatings for electrostatic charge mitigation. *Polymer,* 46**,** 2076-2085.

Watts, PCP, Mureau, N, Tang, ZN, Miyajima, Y, Carey, JD and Silva, SRP 2007. The importance of oxygen-containing defects on carbon nanotubes for the detection of polar and non-polar vapours through hydrogen bond formation. *Nanotechnology,* 18**,** -.

Wei, BY, Hsu, MC, Su, PG, Lin, HM, Wu, RJ and Lai, HJ 2004. A novel SnO2 gas sensor doped with carbon nanotubes operating at room temperature. *Sensors and Actuators B-Chemical,* 101**,** 81-89.

Winquist, F, Spetz, A, Armgarth, M, Nylander, C and Lundstrom, I 1983. Modified Palladium Metal-Oxide-Semiconductor Structures with Increased Ammonia Gas Sensitivity. *Applied Physics Letters,* 43**,** 839-841.

Winquist, F, Spetz, A, Lundström, I and Danielsson, B 1984. Determination of ammonia in air and aqueous samples with a gas-sensitive semiconductor capacitor. *Analytica Chimica Acta,* 164**,** 127-138.

Wong, EW, Sheehan, PE and Lieber, CM 1997. Nanobeam mechanics: Elasticity, strength, and toughness of nanorods and nanotubes. *Science,* 277**,** 1971-1975.

Wong, SS, Joselevich, E, Woolley, AT, Cheung, CL and Lieber, CM 1998. Covalently functionalized nanotubes as nanometre-sized probes in chemistry and biology. *Nature,* 394**,** 52-55.

Wong, YM, Kang, WP, Davidson, JL, Wisitsora-at, A and Soh, KL 2003a. A novel microelectronic gas sensor utilizing carbon nanotubes for hydrogen gas detection. *Sensors and Actuators B: Chemical,* 93**,** 327-332.

Wong, YM, Kang, WP, Davidson, JL, Wisitsora-at, A and Soh, KL 2003b. A novel microelectronic gas sensor utilizing carbon nanotubes for hydrogen gas detection. *Sensors and Actuators B-Chemical,* 93**,** 327-332.

Yeung, CS, Liu, LV and Wang, YA 2008a. Adsorption of small gas molecules onto Pt-doped single-walled carbon nanotubes. *Journal of Physical Chemistry C,* 112**,** 7401-7411.

Yeung, CS, Liu, LV and Wang, YA 2008b. Adsorption of Small Gas Molecules onto Pt-Doped Single-Walled Carbon Nanotubes. *The Journal of Physical Chemistry C,* 112**,** 7401-7411.

Yoo, K-P, Kwon, K-H, Min, N-K, Lee, MJ and Lee, CJ 2009. Effects of O2 plasma treatment on NH3 sensing characteristics of multiwall carbon nanotube/polyaniline composite films. *Sensors and Actuators B: Chemical,* 143**,** 333-340.

Yoon, TH and Park, YJ 2013. Polydopamine-assisted carbon nanotubes/Co3O4 composites for rechargeable Li-air batteries. *Journal of Power Sources,* 244**,** 344-353.

Young, P, Lu, Y, Terrill, R and Li, J 2005. High-Sensitivity NO₂ Detection with Carbon Nanotube–Gold Nanoparticle Composite Films. *Journal of Nanoscience and Nanotechnology,* 5**,** 1509-1513.

Yue, GZ, Qiu, Q, Gao, B, Cheng, Y, Zhang, J, Shimoda, H, Chang, S, Lu, JP and Zhou, O 2002. Generation of continuous and pulsed diagnostic imaging x-ray radiation using a carbon-nanotube-based field-emission cathode. *Applied Physics Letters,* 81**,** 355-357.

Zahab, A, Spina, L, Poncharal, P and Marlière, C 2000. Water-vapor effect on the electrical conductivity of a single-walled carbon nanotube mat. *Physical Review B,* 62**,** 10000-10003.

Zamani, C, Shimanoe, K and Yamazoe, N 2005. A new capacitive-type NO2 gas sensor combining an MIS with a solid electrolyte. *Sensors and Actuators B: Chemical,* 109**,** 216-220.

Zhang, J, Boyd, A, Tselev, A, Paranjape, M and Barbara, P 2006a. Mechanism of NO2 detection in carbon nanotube field effect transistor chemical sensors. *Applied Physics Letters,* 88.

Zhang, T, Nix, MB, Yoo, BY, Deshusses, MA and Myung, NV 2006b. Electrochemically functionalized single-walled carbon nanotube gas sensor. *Electroanalysis,* 18**,** 1153-1158.

Zhao, J, Su, YJ, Yang, Z, Wei, LM, Wang, Y and Zhang, YF 2013. Arc synthesis of double-walled carbon nanotubes in low pressure air and their superior field emission properties. *Carbon,* 58**,** 92-98.

Zhao, JJ, Wen, B, Zhou, Z, Chen, ZF and Schleyer, PV 2005a. Reduced Li diffusion barriers in composite BC3 nanotubes. *Chemical Physics Letters,* 416**,** 323-326.

Zhao, Q, Buongiorno Nardelli, M, Lu, W and Bernholc, J 2005b. Carbon Nanotube−Metal Cluster Composites: A New Road to Chemical Sensors? *Nano Letters,* 5**,** 847-851.

Zubkans, J, Spetz, AL, Sundgren, H, Winquist, F, Kleperis, J, Lusis, A and Lundstrom, I 1995. In-situ modification of the NOx sensitivity of thin discontinuous platinum films as gates of chemical sensors. *Thin Solid Films,* 268**,** 140-143.